Diagenetic imprints on magnetic mineral assemblages in marine sediments

With a summary in Dutch and German

Dissertation
zur Erlangung des
Doktorgrades in den Naturwissenschaften
am Fachbereich Geowissenschaften
der Universität Bremen

Vorgelegt von

Johanna Fredrika Lukina Garming

Bremen, 2006

Tag des Kolloquiums:

24 März 2006

Gutachter:

Prof. Dr. U. Bleil
(Universität Bremen)

Prof. Dr. C.G. Langereis
(Utrecht University)

Prüfer:

Prof. Dr. H.D. Schulz
(Universität Bremen)

Prof. Dr. T. von Dobeneck
(Universität Bremen)

A man who owned a needle made of octiron would never lose his way, since it always pointed to the Hub of the Discworld, being acutely sensitive to the disc's magical field; it would also miraculously darn his socks.

The Color of Magic

by Terry Pratchett

Contents

Bibliography

Chapter 2.1   J.F.L. Garming, G.J. de Lange, M.J. Dekkers and H.F. Passier, 2004. Changes in magnetic parameters after sequential iron phase extraction of eastern Mediterranean sapropel S1 sediments. *Studia Geophysica et Geodaetica*, **48**, 345-362.

Chapter 2.2   N. Riedinger, K. Pfeifer, S. Kasten, J.F.L. Garming, C. Vogt and C. Hensen, 2005. Influence of sedimentation rate on diagenetic alteration of geophysical signals by anaerobic oxidation of methane. *Geochimica et Cosmochimica Acta*, **69**, 4117-4126.

Chapter 2.3   J.F.L. Garming, U. Bleil and N. Riedinger, 2005. Alteration of magnetic mineralogy at the sulfate methane transition: analysis of sediments from the Argentine continental slope. *Physics of the Earth and Planetary Interiors*, **151**, 290-308.

Chapter 2.4   J.F.L. Garming, U. Bleil, C. Franke, and T. Von Dobeneck, in review. Low-temperature partial magnetic self-reversal in marine sediments. *Geophysical Journal International*.

Chapter 2.5   C. Franke, M. Drury, G. Pennock, R. Engelmann, D. Lattard, J.F.L. Garming, T. von Dobeneck and M.J. Dekkers, subm. Identification of magnetic Fe-Ti-oxides by electron backscatter diffraction (EBSD) in scanning electron microscopy. *Submitted to Journal of Geophysical Research.*

Summary

Sediments and sedimentary rocks are important sources for paleomagnetic studies of the geomagnetic field behaviour and of environmental changes. These studies are greatly dependent on the reliable extraction of the detrital magnetic signal. Overprinting of this signal by reductive diagenetic processes, where iron-bearing minerals are dissolved and secondary (magnetic) sulphide minerals form, jeopardizes the validity of such investigations. It is therefore necessary to be aware of the possible presence of diagenetic/authigenic magnetic phases, i.e. greigite, and their influence on the paleomagnetic signal. A chemical remanent magnetisation (CRM) due to these phases can obscure the detrital magnetic signal. It remains to be shown how primary detrital minerals may survive dissolution under these conditions, and by which mechanisms secondary (magnetic) sulphide minerals are formed.

Geochemical, environmental magnetic and optical methods, or combinations thereof may be applied to marine sediments in order to establish which magnetic minerals are present and in the ideal situation if they are of primary or secondary origin.

The application of sequential chemical extraction of mineral phases has been frequently applied in the pursuit of this question (Hounslow and Maher, 1996; van Oorschot and Dekkers, 1999; Rutten and de Lange, 2002a; 2002b). The destructive nature of the method renders it less useful in studies where the specific mineral compositions of the magnetic fraction is of central importance.

Environmental or mineral magnetic methods are non-destructive but like the chemical extraction provide only bulk sample information. Ratios of various magnetic properties are specific for grain size, mineralogy and/or concentration, whereas coercive force distributions can be used to discriminate between magnetic minerals (Robertson and France, 1994; Kruiver *et al.*, 2001). Comparison of properties between various studies should not be attempted where different measurement criteria have been used.

Scanning and transmission electron microscopy have also been frequently applied in (magnetic) mineral studies. SEM in combination with energy dispersive spectroscopy (EDS) is a powerful tool in identifying minerals. To facilitate the identification process physical separation techniques may be applied. Next to heavy liquid separation magnetic mineral extraction can be applied. Conventional mineral magnetic separation techniques extract relatively coarse magnetic grains (>20μm). However bacterial magnetites have been shown to significantly contribute to the sedimentary NRM and thus a new way of extraction was developed by Petersen *et al.* (1986) and von Dobeneck *et al.* (1987).

In the manuscripts produced during this Ph.D., various combinations of these methods and their results are discussed related to the scientific question(s) posed. In the following sections these manuscripts together with some additional background information of the recovery area of the sediments investigated are summarized.

The alteration of magnetic parameters in sapropel S1 sediments from the eastern Mediterranean after sequential iron phase extraction is investigated in **chapter 2.1**. The occurrence of sapropels is related to increased accumulation/preservation of organic material (OM) in eastern Mediterranean sediments. Several theories have been postulated by various authors: e.g. an improved preservation by Bradley (1938) and Olausson (1961), a sluggish circulation by Rossignol-Strick *et al.* (1982), and a reversed ciculation by Calvert (1983), Sarmento *et al.* (1988) and Rohling and Gieskes (1989).

The sequence of alternating organic rich layers (sapropels) and organic poor sediments, provides a unique setting to study the diagenetic interactions that take place when (anoxic) organic rich layers overlie (sub)oxic organic poor sediments and vice versa. The most recent sapropel (S1, 8-10 ka) in the eastern Mediterranean has been intensively investigated in the last decade with geochemical and mineral magnetic techniques. Through time, different redox conditions prevail in the sediments giving rise to the formation of authigenic magnetic minerals. The sequential iron phase extraction showed that in the oxidised S1 sediments iron is mainly incorporated into silicates and 'amorphous' oxides, whereas pyrite is the major iron-bearing mineral in the reduced sediments next to silicates. Component analysis of IRM acquisition curves obtained from S1 sediments revealed three minerals, respectively 'detrital' magnetite, biogenic magnetite and hematite. The formation of in-situ magnetite as a result of the activity of magnetotactic bacteria confirms previous results that the high coercivities observed in sediments near the active oxidation front are most likely of diagenetic origin.

Sediments from the continental margin near the Rio de la Plata estuary have been investigated with geochemical and mineral magnetic methods. In the subtropical South Atlantic significant amounts of terrigenous eolian (Patagonian plain) and fluvial (Rio de la Plata) material is supplied to the marine environment. A plausible model developed by Frenz *et al.* (2004) showed the recent sedimentation patterns in the western South Atlantic. The sediments of the continental slope can be divided into two areas, a coarse grained and carbonate depleted southwestern area, and a finer grained and carbonate rich north-eastern area. The division is located at the Brazil Malvinas Confluence (BMC), where the northward flowing Malvinas current meets the southward flowing Brazil current near the Rio de la Plata estuary. The BMC is characterised by high concentrations of

organic carbon (OC), low carbonate content and high proportions of intermediate sized sediments. The fluvial discharge by the Rio de la Plata in this model is clearly recognizable by a down slope tongue of coarse grained sands. The fine grained fluvial fraction is transported northwards at greater depths.

Geochemical and mineral magnetic investigations with the aim of studying the diagenetic processes at three sites on the continental margin near the Rio de la Plata estuary are described in **chapter 2.2**. The occurrence of anaerobic oxidation of methane (AOM) in a few meters depth is a typical feature of the sediments near the Rio de la Plata estuary. The process of AOM causes a strong reducing (sulphidic) environment, enhancing the dissolution of oxic magnetic carriers and the precipitation of iron sulphides, mainly pyrite. This ultimately results in a distinct minimum in susceptibility at around the sulphate methane transition (SMT). Numerical modelling of the geochemical data showed that drastic changes in sedimentation rates are needed to fix the SMT at a certain depth interval for longer periods of time and cause the observed susceptibility minimum. It is assumed that the strong decrease in sedimentation rate encountered at the glacial/interglacial transition is responsible for the fixation of the SMT in the investigated sediments.

The results of a more detailed study of the mineral magnetic parameters of one of the sites are reported in **chapter 2.3**. It is observed that less then 10% of the low coercivity ferrimagnetic (titano-)magnetite fraction remains after encountering the sulphidic conditions surrounding the SMT. At the iron redox boundary, in the upper meter of the sedimentary sequence, approximately 60% of the finer magnetic grain fraction is already dissolved. The high coercivity minerals are relatively unaffected by this, however in the sulphidic zone large portions (>40%) are diagenetically dissolved. In contrast to other studies magnetic grain size appears to be reduced in the sulphidic zone. Different factors can contribute to this effect. SEM in combination with EDS analyses have identified fine grained (titano-)magnetite in the sulphidic zone, preserved as inclusions in a silicate matrix and between high Ti bearing titanohematite lamellae. Another possibility, probably of great importance, is the comprehensive fragmentation of larger grains during maghemitization. The only secondary iron sulphide mineral identified by thermomagnetic analysis and SEM is pyrite. It is present as clusters of euhedral crystals or is directly replacing (titano-)magnetite.

Low-temperature magnetic properties of minerals, which survive the two stage diagenetic processes described in **chapter 2.3**, are discussed in **chapter 2.4**. Investigation of the room temperature saturation isothermal remanent magnetisation (RT-SIRM; 5 T), on magnetic extracts, cycled to low-temperatures and back again revealed a sharp reduction of the remanent magnetisation around ~210 K, next to the

Verwey transition, which is indicative of magnetite. The titanohematite lamellae observed by SEM analyses, most likely originate from high temperature oxidation (deuteric oxidation), and have an approximate composition of TH85 to ilmenite. Below approximately 210 K the mineral would become ferrimagnetic, but the moment is ordered antiparallel to the magnetic moment of the (titano-)magnetite, which most likely carries the remanence at room temperature. Consequently, the mechanism responsible for this self-reversal is sought in magnetostatic interaction. This would also explain the absence of an anomaly in the heating of a LT-SIRM (5 T) to ambient temperatures.

A further investigation of sedimentary magnetic with the aid of electron backscatter diffraction (EBSD) is documented in **chapter 2.5**. This method allows discrimination between chemically identical but mineralogically different phases. In the sediments of the Rio de la Plata estuary it confirmed the presence of high Ti bearing titanohematites as well as ilmenite and titanomagnetite. The application of this technique on sediments and on magnetic extracts is new, but has already proven itself to be valuable in the identification of magnetic intergrowths.

Chapter 1

Introduction

1   The aim of this study

Magnetic minerals, mainly iron oxides, iron oxyhydroxides and some iron sulphides, occur in minor or trace amounts in igneous and sedimentary rocks, soils, dusts and even in living organisms. Depending on their grain size, magnetic minerals are able to carry a stable natural remanent magnetisation (NRM) and act as recorders of the ancient Earth's magnetic (or geomagnetic) field. Paleomagnetic and geomagnetic studies investigate this NRM history for plate tectonic reconstructions, magnetostratigraphy and short-term variations in the Earth's magnetic field. In the discipline of environmental magnetism, properties of magnetic minerals are used as proxies for paleoclimatic and paleoenvironmental change. Secondary magnetisations acquired in the period between formation and the present time are generally considered as a bias on the primary magnetisation, but can also in some cases be used when studying the nature and timing of geological and geochemical events.

In considerably (chemically) altered sedimentary assemblages plausible magnetic polarity information has often been retained, although the primary magnetic mineral assemblage has been almost completely transformed. The mechanisms, which permit oxic magnetic minerals to survive in strong reducing environments, are to be identified. The NRM carried by the primary magnetic minerals can also be replaced by or passed onto secondary minerals. By comparing the magnetic minerals present in distinct layers, and under various sedimentary conditions, different preservation mechanisms may be identified. An integrated geochemical and mineral magnetic approach is aimed at establishing the primary or secondary nature of the magnetic signal. This will aid the development of models that describe and explain reaction kinetics and past redox conditions.

In the next sections a brief introduction is given of environmental magnetism and some characteristics of magnetic minerals, encountered in this study, are described. In addition, the main diagenetic processes occurring in marine sediments studied are introduced.

2   Environmental magnetism

Paleoclimatic and paleoenvironmental changes are recorded in sedimentary sequences by magnetic minerals, the study thereof is called environmental magnetism. The most important terrestrial record is arguably the wind-blown silt deposit of the Chinese loess plateau, which spans approximately 2.6 Ma (e.g., Ding *et al.*, 1998; Sun *et al.*, 2005). Water-laid lake sediments on the other hand, also have long been used for obtaining climatic and environmental information (Thompson *et al.*, 1975). However, the

time period that could be investigated was generally relatively short, at around 10.000 years. Longer records have been found in the French lake 'Lac du Bouchet' (Thouveny *et al.*, 1994) and in the Siberian Lake 'Ozero Baykal' (Peck *et al.*, 1994), respectively 140.000 and 5 million years. In contrast, marine sediments provide short high-resolution records as well as long records (i.e. obtained by the Ocean Drilling Program (ODP)), and have become an important archive of mineral magnetism related to environmental variability.

There are many other applications for magnetism and magnetic particles in environmental studies. They can be used as tracers of pollutants, as indicators of the provenance and distance of transport of soils during erosion, as an aid to determine sediment load and velocity in streams, etc. (Dunlop and Özdemir, 1997; Evans and Heller, 2003). In this study only marine sediments were investigated, therefore the principles and applications discussed further in this chapter will only be related to this type of record. A more complete overview of environmental magnetism and its methods has been published by Thompson and Oldfield (1986), Dekkers (1997), Maher and Thompson (1999) and Evans and Heller (2003).

2.1   Mineral magnetic properties

Similar techniques and principles are used in environmental magnetic studies, for the identification of the mineralogy, grain size and concentration, as in paleomagnetic studies. Mineral magnetic techniques have the advantage that they are sensitive, require little sample preparation and are generally non-destructive. They complement geochemical analyses of the same material by giving bulk magnetic mineral information.

In paleomagnetic studies the natural remanent magnetisation (NRM) in samples is investigated. Iron oxides, iron oxyhydroxides and some iron sulphides, which occur in minor and trace amounts in sedimentary rocks/sequences, mainly carry this stable magnetisation (i.e., the NRM). How the NRM becomes recorded at the time of mineral formation and retained over geological times, is fascinating, however beyond the scope of this thesis. Nevertheless some knowledge is required of iron (titanium) oxide phases encountered in igneous rocks and sediments derived thereof. They are discussed in the next paragraph, followed by some information of other magnetic minerals encountered in sedimentary studies.

2.1.1   Iron (titanium) oxides

Magnetically, three naturally occurring iron oxide minerals are important; magnetite, hematite and maghemite. Some properties of these minerals and several others are given in table 1. Magnetite is found in rocks and sediments and can also be produced by certain types of bacteria, known as magnetotactic bacteria, which use it for navigational purposes. Magnetite is characterised a high spontaneous magnetic moment and by two important temperatures, i.e., the Curie point at 580 ^{o}C and the Verwey transition at about -150 ^{o}C (e.g., Dunlop and Özdemir, 1997). These temperatures and the respective changes in observed magnetisation are frequently used in diagnostic tests.

Table 1. Properties of some common magnetic minerals

| Mineral	Formula	M_s (kA/m)	T_C (^{o}C)	magnetic structure
Magnetite	Fe_3O_4	480	580	ferrimagnetic
Hematite	α-Fe_2O_3	~2.5	675	canted antiferromagnetic
Maghemite	γ-Fe_2O_3	380	590-675	ferrimagnetic
Goethite	α-FeOOH	~2	120	antiferromagnetic
Greigite	Fe_3S_4	~125	~330	ferrimagnetic
Pyrrhotite	Fe_7S_8	~80	320	ferrimagnetic

A more detailed description is given by Hunt et al. (1995), Dekkers (1997) and Dunlop and Özdemir (1997).

Hematite is common in soils and sediments, and is the main carrier of the magnetisation of 'red beds', a major source of information in classic paleomagentism (Evans and Heller, 2003). The mineral is like magnetite characterized by two temperatures (e.g., Dunlop and Özdemir, 1997), the Néel temperature at 675 ^{o}C and the Morin transition at approximately -15 ^{o}C (Morin, 1950).

Maghemite, the fully oxidised form of magnetite, is also frequently encountered in soils. It has a Curie temperature at around 645 ^{o}C, that is unfortunately difficult to measure, there the mineral is metastable, i.e. it transforms to hematite with a loss of magnetisation (e.g., Dunlop and Özdemir, 1997). This so-called inversion temperature can be used in identification, however it is very variable and many different values have been reported.

In nature varying compositions for the above-mentioned minerals are observed, in most cases some iron has been replaced by titanium. In Fig. 1 a ternary diagram illustrates the solid solution series in which iron titanium minerals can occur. Two main

groups of iron titanium oxides are important, respectively the titanomagnetite and the titanohematite groups. The amount of titanium substitution in magnetites is denoted by x ($Fe_{3-x}Ti_xO_4$), whereas the titanium substitution on hematites is denoted by y ($Fe_{2-y}Ti_yO_3$). Titanomagnetites are cubic minerals with an inverse spinel structure, and titanohematites are characterised by rhombohedral symmetry (e.g., Dunlop and Özdemir, 1997; Evans and Heller, 2003). Note that minerals of the same composition but of different structure, e.g. maghemite and hematite, occupy the same position in the diagram.
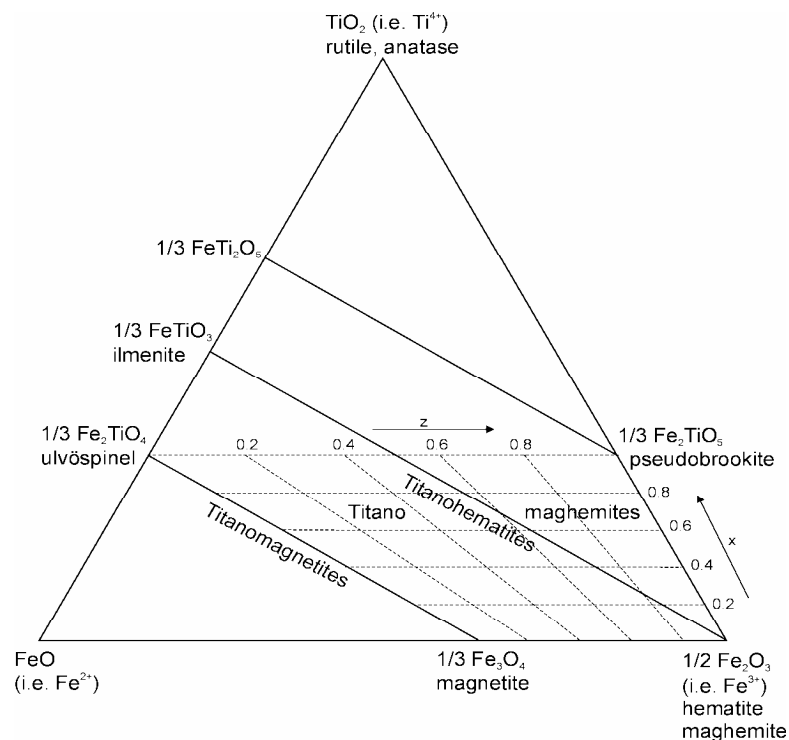
Fig. 1. The TiO_2-FeO-Fe_2O_3 ternary diagram after Dunlop and Özdemir (1997). The solid solution line of titanomagnetite and titanohematite are indicated as well as the titanomaghemite field. During either low-temperature or high-temperature oxidation of titanomagnetites the bulk compositions follow the horizontal dashed lines (oxidation parameter indicated by z).

The composition of titanomagnetites is strongly depended on the cooling temperatures. At ordinary temperatures titanomagnetites of intermediate composition are only preserved if the original material cooled very rapidly, for example in submarine lavas. If cooling is slower, the primary oxides will exsolve into intergrowths of near magnetite and ulvöspinel cubic minerals. Titanohematites of intermediate composition also tend to exsolve into near hematite and ilmenite intergrowths.

Magnetic intergrowths of ulvöspinel composition are relatively rare in nature, there is usually enough oxygen present to oxidise the titanomagnetite completely. Low-temperature oxidation converts a single-phase spinel into another single-phase spinel with a different lattice parameter, whereas high-temperature oxidation (deuteric oxidation), during the initial cooling, results in intergrowths of spinel (near magnetite) and rhombohedral (near ilmenite) phases. This process is also known as oxyexsolution.

In **chapter 2.4**, low-temperature magnetic properties of exsolved titanomagnetite and titanohematite, which have been found in the sediments near the Rio de la Plata estuary, are discussed in more detail.

2.1.2   Iron oxyhydroxides

The only magnetically significant oxyhydroxide is goethite. It has a slightly lower spontaneous magnetic moment than hematite and its Néel point lies at about 120 ^{o}C (Table 1, e.g., Dunlop and Özdemir, 1997). Recent studies have showed the wide spread occurrence of goethite in soils and sediments (France and Oldfield, 2000).

Two other oxyhydroxides, i.e. ferrihydrite and lepidocrocite, are worth mentioning, as they may undergo chemical changes and produce hematite and magnetite in soils (Schwertmann, 1988) and sediments.

2.1.3   Sulphides

The ferromagnetic magnetic iron sulphide, greigite was formerly thought to be rare in nature, but commonly occurs in sediments formed under anoxic, i.e. sulphate reducing, conditions (Roberts, 1995) and may also be bio-mineralised by magnetotactic bacteria (Mann *et al.*, 1990). Greigite is the sulphide equivalent of magnetite, and has a saturation remanent magnetisation, that is approximately a quarter of that of magnetite (Table 1). Thermomagnetically it may be identified by its Curie temperature, which lies at approximately 330 ^{o}C (e.g., Dunlop and Özdemir, 1997).

Pyrrhotite is found in igneous, metamorphic and sedimentary rocks, as well as in sulphide ores, but it seldom dominates the remanent magnetic signal. It has a Curie point close to that of greigite, ~320°C (e.g., Dunlop and Özdemir, 1997). Differently from greigite pyrrhotite displays a low-temperature transition at ~34 K (Dekkers, 1989; Rochette *et al.*, 1990), which can be used to distinguish between the two sulphidic phases. Grain-size dependent parameters of pyrrhotite have been studied by Clark (1984) and Dekkers (1988; 1989).

The significance of the iron sulphides in environmental magnetic studies is discussed in more detail by Snowball and Torii (1999).

2.1.4   Other magnetic minerals

A common carbonate in sediments and rocks is siderite ($FeCO_3$). It is paramagnetic at ordinary temperatures. A chemical remanent magnetisation (CRM) is acquired by oxidation at room temperature, this can occur within weeks to months. On heating, above 300 ^{o}C it rapidly oxidises to magnetite, maghemite and finally hematite (Dunlop and Özdemir, 1997). At low temperatures siderite undergoes a transition at its Néel temperature (T_N) at about 38 K (e.g., Frederichs *et al.*, 2003). However, in sulphidic environments siderite is not stable, and the lack of this mineral can be used in geochemical classification of the sediments (Berner, 1981).

A related carbonate mineral is rhodochrosite ($MnCO_3^{2-}$) that like siderite is paramagnetic at room temperature. Its Néel temperature lies at about 34 K (Frederichs *et al.*, 2003). The two phases may be distinguished from each other by their different temperature dependence below their Néel temperatures. However, the occurrence of other strongly magnetic minerals exhibiting transitions in this temperature range (i.e., pyrrhotite, Dekkers, 1989) may mask their presence.
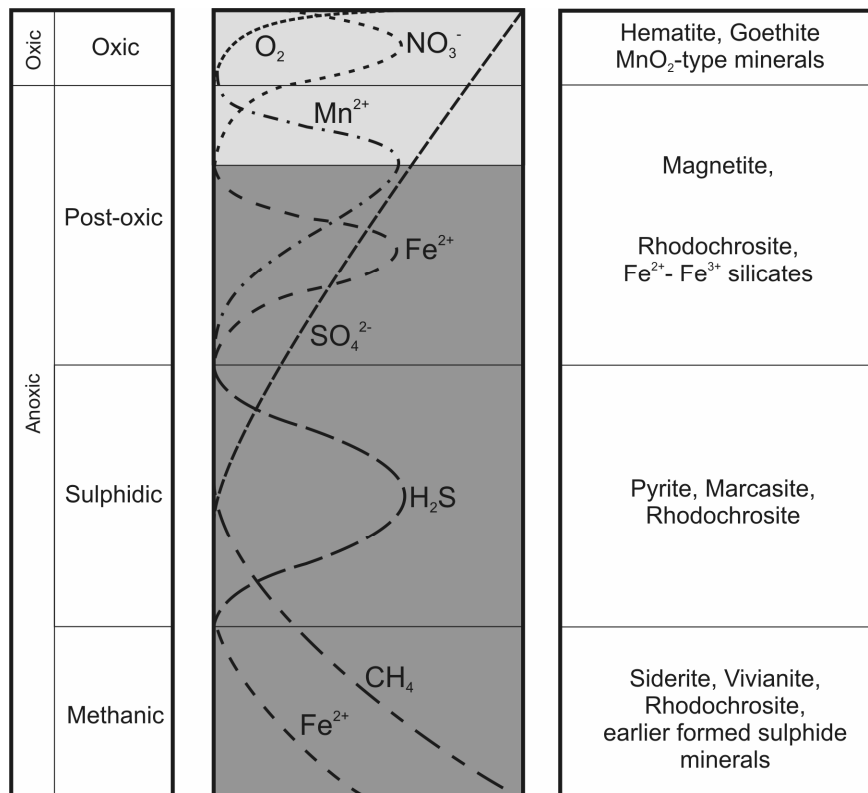
Paramagnetic behaviour is observed in many silicates, because of the iron or manganese they contain. Some silicates exhibit ferrimagnetic behaviour, and that has been traced in a number of cases to magnetite inclusions (Dunlop and Özdemir, 1997). In biotites, magnetite fills cracks and planar voids between the mica sheets, and can thus be quite abundant. Exsolved magnetite needles are also observed in plagioclases and pyroxenes. They are capable of carrying an extremely stable remanent magnetisation.

3   Diagenesis in marine sediments

Biochemical processes occurring in relation to the mineralisation of organic matter (OM), are summarised under the name of early diagenesis. The work of Froelich et al. (1979) is the classic model of early diagenesis. Herein the degradation of OM by micro-organisms and the simultaneous reduction of electron acceptors is described. Under the assumption that the composition of marine OM is described by the Redfield-ratio: $(CH_2O)_{106}(NH_3)_{16}(H_3PO_4)$ (Redfield *et al.*, 1963), and that the degradation takes place under controlled circumstances, i.e. neutral pH and 25°C, a sequence of reactions can be formulated based on the free energy production of the individual reactions. First oxygen is used as electron acceptor, followed by nitrate, manganese and iron oxides and sulphate.

In the last stage of reduction the OM is fermented producing methane and carbon dioxide. The extent of theses reactions greatly depends on the amount of OM added to the sediments, the sedimentation rate and the bio-availability of the reactants (Evans and Heller, 2003).

A new geochemical classification model was presented by Berner in (1981). It is based on the presence or absence of oxygen and dissolved hydrogen sulphide (i.e. HS⁻ and H_2S), at the time of authigenic mineral formation in marine sediments. The environments identified occur in the following order: oxic, post-oxic, sulphidic and methanic. In Fig. 2 a schematic representation is given, together with some characteristic pore water profiles and authigenic minerals.

Oxic	Oxic	O_2 NO_3^- Mn^{2+}	Hematite, Goethite MnO_2-type minerals
Anoxic	Post-oxic	Fe^{2+} SO_4^{2-}	Magnetite, Rhodochrosite, Fe^{2+}- Fe^{3+} silicates
	Sulphidic	H_2S	Pyrite, Marcasite, Rhodochrosite
	Methanic	CH_4 Fe^{2+}	Siderite, Vivianite, Rhodochrosite, earlier formed sulphide minerals

Fig. 2. Classification of the different early diagenetic environments and some stable authigenic iron and manganese minerals characteristic for the corresponding environment (Froelich *et al.*, 1979; Berner, 1981).

Knowledge about the chemical stability of the (authigenically formed) magnetic minerals is essential when trying to understand the sediment geochemistry or to reconstruct the paleoenvironment.

In marine sediments (titano-)magnetite is the most important carrier of the magnetic signal. It is mainly present as detrital particles or as inclusions in siliceous matrices. However magnetotactic bacteria may also form magnetite in-situ at the transition where nitrate is reduced and iron is oxidised (Fig. 2, Karlin *et al.*, 1987; Karlin, 1990). Authigenic magnetite is either present as extra-cellular extremely fine grained magnetite (super-paramagnetic grain size: 6 - 20 nm) or as intra-cellular single domain (35 - 130 nm) magnetite particles. Macroscopically this transition is reflected by a colour change of the sediments, from reddish brown to green (Lyle, 1983).

Sulphate is the least favoured electron acceptor, but the most commonly available. Bacterial reduction of sulphate results in the establishment of sulphidic pore water conditions (Fig. 2). As soon as the amount of hydrogen sulphide exceeds the reduced iron concentration, dissolution of magnetite begins (Evans and Heller, 2003). High pore water concentrations of hydrogen sulphide over a prolonged period of time (several hundred years) will result in complete pyritisation of magnetite (Canfield and Berner, 1987). Magnetite will be preserved if hydrogen sulphide formation is absent, or if insufficient hydrogen sulphide can build up due to reaction with other more reactive iron oxide minerals (Goldhaber and Kaplan, 1974; Canfield and Berner, 1987). Recent studies by Emiroglu *et al.* (2004) in Spanish Ría environments and by Liu *et al.* (2004) in continental shelf sediments from the Korea Strait, showed the opposite. Hematite and goethite are more resistant to reductive dissolution under sulphidic conditions than magnetite, but eventually they will be completely reduced.

(Mono)sulphidic phases (i.e. mackinawite, greigite and pyrrhotite) are the first to be formed when reduced iron reacts with hydrogen sulphide (e.g., Berner, 1984; Roberts and Turner, 1993). As long as excess hydrogen sulphide is present in the pore water these minerals are unstable and will be transformed to pyrite. But when preserved in the sediments a secondary remanent magnetisation will be acquired by the ferrimagnetic minerals greigite and pyrrhotite, jeopardizing the paleoclimatic and/or paleoenvironmental interpretation.

Only under strong reducing conditions, where all electron acceptors have been used (i.e. no sulphate is present) and hydrogen sulphide has been depleted, siderite and vivianite form. Consequently these minerals are encountered more often in non-marine sediments than in marine sediments, and suggestions have been made to use these minerals as paleosalinity indicators (Berner, 1981, and references cited therein). Rhodochrosite is a manganese carbonate formed under anoxic conditions. It is however not as indicative as siderite or pyrite. In order to identify the environment in which the rhodochrosite was formed, other co-existing minerals have to be investigated.

Chapter 2

Manuscripts and publications

Synopsis of manuscripts and publications

During my PhD five manuscripts were produced, of which three already have been published in international peer reviewed journals. The brief contents of these manuscripts and publications are provided in the following section.

The results of sequential iron phase extraction from Sapropel S1 sediments from the eastern Mediterranean and rock magnetic parameters measured prior and after are discussed in the first manuscript. From the results it could be concluded that next to silicates, iron is mainly incorporated into amorphous oxides in the oxidised part of the sapropel, whereas pyrite is the main constituent in the still reduced part. Component analysis of isothermal remanent magnetisation (IRM) identified three phases interpreted as 'detrital' magnetite, hematite and biogenic magnetite.

In manuscript two, geochemical analysis of the pore waters recovered from cores from the continental slope of the Argentine Basin identified strong reducing conditions, i.e. sulphidic conditions, in a few meters depth. These are related to the anaerobic oxidation of methane (AOM). A typical feature of these sediments is the formation of authigenic sulphides accompanied by a nearly complete loss of magnetic susceptibility. Modelling of the data revealed that a drastic change in sedimentation rate, which occurred during the Pleistocene/Holocene transition, is needed to produce the features observed.

Detailed rock magnetic analysis, described in manuscript three, revealed that at the iron redox boundary 40% of the fine grained magnetic fraction is already dissolved. Only 10% survives the strong reducing environment surrounding the sulphate methane transition (SMT). Scanning electron microscope analysis in combination with X-ray microanalysis showed that the magnetic particles survive either as inclusions in a siliceous matrix or as intergrowths with titanohematite. Pyrite was the only secondary sulphidic mineral found, unlike other studies investigating magnetic properties at around the SMT.

Low-temperature properties of intergrown titanomagnetite and titanohematite are discussed in the fourth manuscript. Warming a low-temperature saturation isothermal remanent magnetisation (LT-SIRM) only shows a Verwey transition indicative for magnetite, whereas cooling of a room temperature saturation isothermal remanent magnetisation (RT-SIRM) shows a market drop in remanence at around 210 K,

corresponding to the Curie temperature of the titanohematite. The mechanism responsible for apparent magnetic self-reversal is sought in magnetostatic interaction.

In the fifth manuscript the viability of using electron backscatter diffraction (EBSD) in combination with energy dispersive spectroscopy (EDS) is investigated, in order to successfully differentiate between titanomagnetite and titanohematite, which are frequently observed in mineral magnetic investigations.

Chapter 2.1   Changes in magnetic parameters after sequential iron phase extraction of eastern Mediterranean sapropel S1 sediments

Abstract

Iron is distributed over different minerals (i.e. silicates, pyrite, and detrital oxides) that are present in a sediment sequence that formed under anoxic conditions. After post-depositional re-oxidation of the sediments pyrite is no longer present and diagenetic iron phases constitute an important portion of the iron in the oxidised part of the sapropel. They are very fine-grained making them amenable to analysis by means of sequential extraction and mineral-magnetic methods. The sequential extraction shows that besides iron in silicates, iron mainly occurs in 'amorphous' oxides in the oxidised part of the S1 sapropel. Pyrite constitutes an important fraction in the still reduced part of the S1 sapropel. Some silicon is dissolved during the extraction for the 'amorphous' oxides, suggesting that 'amorphous' iron also occurs as ferro-silicate coatings. Mineral-magnetic analysis involved component analysis of the isothermal remanent magnetisation (IRM) and hysteresis loop measurements. Three coercivity phases could be identified in the IRM component analysis; these were interpreted as 'detrital' magnetite, hematite, and biogenic magnetite. The diagenetically formed iron phases influence the parameters of the IRM components. Hysteresis measurements together with the IRM component analysis, indicate the importance of bacterial magnetite in the oxidised sapropel, particularly in the lower part of the active oxidation zone.

1   Introduction

The sediments of the Mediterranean consist of alternating organic-rich and organic-poor sediments. The organic-rich intervals, named sapropels, with formally more than 2% of organic matter (Sigl et al., 1978; Kidd et al., 1978), were deposited under anoxic sedimentary conditions. Times of sapropel formation can be correlated to minima in the precession index (Rossignol-Strick, 1983, 1985; Thunell et al., 1984; Hilgen, 1991). Increased seasonal contrasts and a changed monsoon regime altered the overall water budget of the Mediterranean (Rohling and Hilgen, 1991; Béthoux and Pierre, 1999). Enhanced input of fresh water caused a decrease in bottom water circulation resulting in a depletion of oxygen in the deeper basins of the Mediterranean (Olausson, 1961; Cita et al., 1977; Vergnaud-Grazzini et al., 1977; Nolet and Corliss, 1990). Passier (1998) and Passier et al. (1999) concluded that almost the entire water column may have been sulphidic during deposition of some sapropels. Primary production is enhanced by the increased addition of terrigenic nutrients, consequently an increased amount of organic matter is raining down to the sediments. Anoxic bottom water conditions can contribute to the increased preservation of the organic matter. Sapropels are thus thought to be the consequence of increased production and increased preservation.

In hemipelagic sediments 'detrital' magnetite grains are subject to reductive dissolution and pyritisation during suboxic and anoxic diagenesis of organic matter (e.g. Canfield and Berner, 1987). During anoxic diagenesis, the fine (super-paramagnetic and single-domain) magnetite grains would be totally dissolved, while the coarser (pseudo-single-domain and multi-domain) grains may develop pyrite overgrowths, thus protecting their inner parts from further dissolution (Canfield and Berner, 1987).

Upon re-establishment of oxygenated bottom water conditions and cessation of sapropel deposition, oxidants diffuse from the water column into the sediment. The secondary oxidative diagenesis causes cations to migrate, following an Eh/pH gradient (Colley et al., 1984, Thomson et al., 1998). This may lead to precipitation (mineral authigenesis or bio-authigenesis) of secondary oxides or oxyhydroxides in the oxidised zone of the sediment (Pruysers et al, 1993). Such secondary, authigenic phases of iron (and some manganese) compounds are magnetic (e.g. Karlin et al., 1987), and thus will lead to the acquisition by the sediment of a secondary, chemical remanent magnetisation (CRM), and potentially, a characteristic rock-magnetic signature of early diagenesis (Robinson et al., 2000; Passier et al., 2001; Passier and Dekkers, 2002; Larrasoaña et al., 2003).

Magnetotactic bacteria constitute a special carrier of remanent magnetisation. They utilise magnetosomes (crystalline magnetite) to control their locomotion in the chemically

stratified pore space of unconsolidated sedimentary deposits, just below the oxidation front (Gorby et al., 1988Bleil, 2000). Biogeochemical processes at redox boundaries affect remanent magnetisations. They may cause significant smoothing of paleomagnetic records (e.g. Tarduno et al., 1998).

Here, we discuss how diagenesis of iron phases influences magnetic hysteresis parameters and magnetic coercivity components. To this end, we incorporate the results of a recently evaluated nine-step sequential extraction procedure (Rutten and De Lange 2002a, 2002b) into the recentlynewly developed IRM component analysis (Kruiver et al., 2001; Heslop et al., 2002). The merits of these two techniques may be enhanced by their combination because dissolution puts constraints on the mineral-magnetic analysis, while the sensitive magnetic techniques simultaneously allow validation of the sequential extraction.

2   Material and Methods

Boxcore PSO36BC was recovered by the R/V Pelagia in May 2000 at 36°15.85'N; 21°48.38'E, in a water depth of 3286 meters. The 41 cm long boxcore contains the partially oxidised sapropel S1, as found in large parts of the eastern Mediterranean (Fig. 1). In the overlying mud, a tephra layer occurs, tentatively interpreted as being originating from the Minoan eruption of Santorini, 3.6 ka BP (de Rijk et al., 1999). At a sediment depth of 26 centimetres (cmsbd) the sapropel starts, indicated by the darker sediments of the markerbed (van Santvoort et al., 1996), continuing until the bottom of the boxcore. The upper part of the sapropel has been altered by oxic diagenesis. This oxidised part can be divided in two segments, the upper part being the oxidised sapropel and the lower part the active oxidation zone, starting at a depth of 30 cmsbd. Below the active oxidation zone the sapropel is still unchanged. In the present boxcore, sapropel S1 is interrupted near the bottom of the core by a thin zone (3 cm thickness) of muddy sediment. The position concurs with the interruption in S1 that was shown to be a distinct cooling event around 7 ka BP by de Rijk et al. (1999).

Six subcores were taken from the boxcore. The sediments from the subcores, #2, #4, #5 and #6 were subsampled, whereby the core was divided into 32 intervals according to the colour of the sediment. An overview of the sampled intervals is given in table 1. The sample intervals range from a few millimetres in the (oxidised) sapropel to two centimetres in the oxic sediments overlying the sapropel. The samples were freeze-dried and gently ground in an agate mortar. Coinciding intervals were mixed prior to analysis.
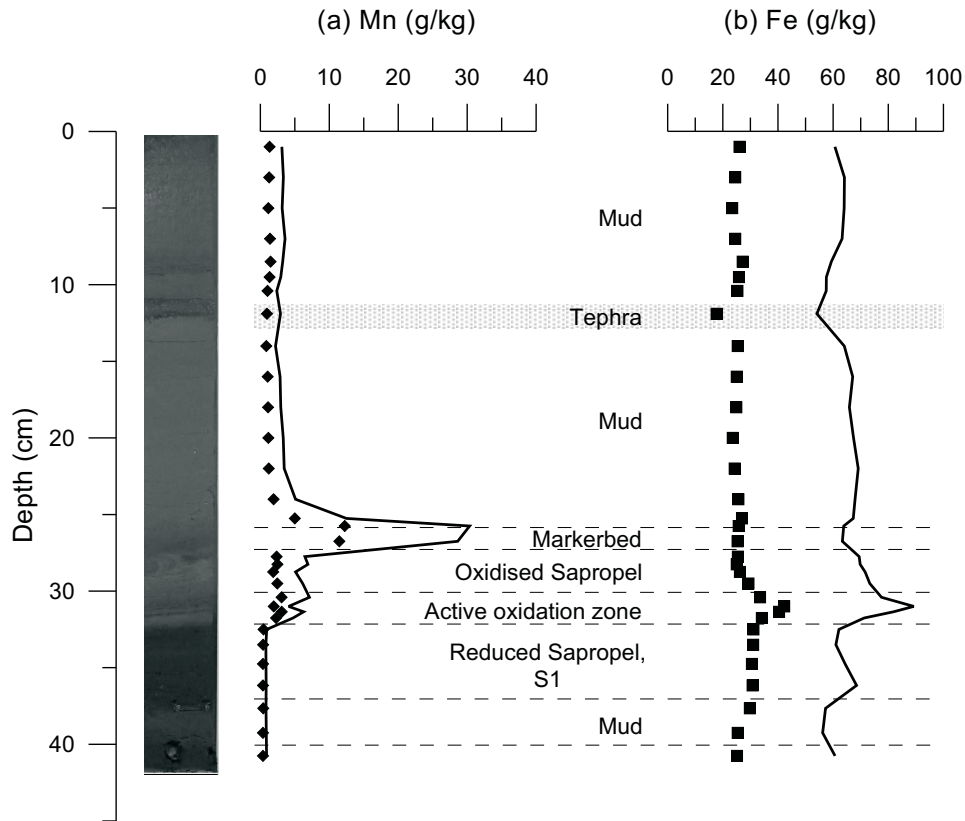
Fig. 1. (a) Down-core manganese concentration in sediment in g/kg (filled diamonds). (b) Down-core iron concentration in sediment in g/kg (filled squares). The solid lines represent the down-core concentrations calculated on a carbonate free basis. Dashed horizontal lines indicate the approximate boundaries of different geochemical zones in the core. The concentration of the elements on a carbonate free basis is calculated by assuming that the amount of calcium extracted in the different steps of the sequential extraction is solely related to carbonates.

2.1   Geochemical analyses

For the analysis of total element contents, 125 mg of all 32 samples were accurately weighed and digested in a mixture of hydrofluoric, nitric and perchloric acids. Final solutions were made in 1M HCl and measured with an Inductively Coupled Plasma Optical Emission Spectrometer (ICP-OES; Perkin Elmer Optima 3000). The quality of the measurements was monitored by the inclusion of blanks, duplicate measurements and in-house standards (MMIN and MM91). The reproducibility of the duplicate measurements was better than 2% for each element, and the reproducibility of the standards was better than 3% for the major elements.

Table 1. Sample intervals of core PS036BC with their Munsell colour coding. The cores were opened using a core-cutter and the samples were scooped out in a cool-container at 15°C. Before storage the samples were rinsed three times with nitrogen gas.

Sample no.	Begin Depth (cm)	End Depth (cm)	Average Depth (cm)	Munsell colour coding and description
1	0	2	1	10YR4/4 (Dark yellowish brown)
2	2	4	3	10YR5/3 (Brown)
3	4	6	5	10YR5/3 (Brown)
4	6	8	7	10YR5/3 (Brown)
5	8	9	8.5	10YR5/3 + 2 (Brown)
6	9	10	9.5	10YR5/3 + 2 (Brown)
7	10	10.8	10.4	10YR5/3 (Brown)
8	10.8	13	11.9	10YR4/3 Tephra
9	13	15	14	10YR5/4 (Beige)
10	15	17	16	10YR5/4 (Beige)
11	17	19	18	10YR5/4 (Beige)
12	19	21	20	10YR5/4 (Beige)
13	21	23	22	10YR5/4 (Beige)
14	23	25	24	10YR5/4 (Beige)
15	25	25.5	25.25	10YR5/4 (Beige) + 10YR5/2 (Grey)
16	25.5	26	25.75	10YR5/2 Markerbed
17	26	27.5	26.75	10YR5/2 Markerbed
18	27.5	28	27.75	10YR6/3 (Pale brown i.e. whitish beige)
19	28	28.5	28.25	10YR6/3 (Pale brown i.e. whitish beige)
20	28.5	29	28.75	10YR5/4 (Beige)
21	29	30	29.5	10YR5/5
22	30	30.8	30.4	10YR4/4 (Dark yellowish brown)
23	30.8	31.2	31	10YR5/6 (Yellowish brown i.e. orange)
24	31.2	31.5	31.35	10YR5/6 (Yellowish brown i.e. orange)
25	31.5	32	31.75	5Y3/1 (Very dark grey)
26	32	33	32.5	5Y4/1 (Dark grey)
27	33	35	33.5	5Y4/1 (Dark grey)
28	35	35.5	34.75	5Y3/1 (Very dark grey)
29	35.5	36.8	36.15	5Y3/1 (Very dark grey)
30	36.8	38.5	37.65	5Y5/1 (Grey)
31	38.5	40	39.25	5Y5/1 (Grey)
32	40	41.5	40.75	5Y3/1 (Very dark grey)

Sedimentary constituents were chemically extracted using the nine-step sequential extraction scheme of Rutten and De Lange (2002a, 2000b, Table 2). It differentiates between coatings and carbonates (dissolving agents: NH_4Cl, and acetate), 'amorphous' oxides (ascorbate), 'crystalline' oxides (dithionite), silicates (HF), pyrite and organically bound minerals (HNO_3), and residual minerals ($HF/HNO_3/HClO_4$). The carbonates are removed in several steps (at pH 9, 8, 7, and 5). 'Amorphous' oxides are dissolved in a step between the carbonate steps of pH 7 and pH 5. 'Amorphous' oxides and carbonates dissolve both in 1M Na-Acetate, (Chester and Hughes, 1967), therefore the 'amorphous' oxides are removed separately, prior to the last carbonate dissolution step. The distinction between 'amorphous' and 'crystalline' oxides is based on the solubility of iron and manganese in manganese nodules on the one hand, and that of hematite, goethite, ilmenite, and magnetite on the other (Rutten and De Lange, 2002b).

Table 2. Sequential extraction scheme used (after Rutten and de Lange, 2002a,b).

Step	Solution	Mineral(s) aimed at to dissolve
1 a+b	2M NH_4Cl at pH 9	Carbonates and coatings
2 a+b	2M NH_4Cl at pH 8	Carbonates and coatings
3 a+b	2M NH_4Cl at pH 7	Carbonates and coatings
4	Ascorbate solution	'Amorphous' oxides
5	1M Acetate solution at pH 5	Carbonates
6	Dithionite solution at pH 4.6	'Crystalline' oxides
7	20% HF	Clay minerals
8	Conc. HNO_3	Pyrite and organically bound minerals
9	Mixture $HNO_3/HF/HClO_4$	Residual minerals

For the sequential extraction approximately 250 mg of sediment from ten different levels in the boxcore were accurately weighed in. This was done six times for each level to facilitate the taking of subsamples for rock-magnetic measurements. The samples were taken in the interval from 26 to 35 cmsbd. The subsamples for mineral-magnetic analysis were taken after the initial removal of the carbonates (steps 1-3), the removal of the 'amorphous' oxides (step 4), the removal of the remaining carbonates (step 5) and after the removal of the 'crystalline' oxides (step 6) (see Table 2). After performing the extraction of the clay minerals not enough material was left to obtain accurate magnetic data.

2.2 Magnetic measurements

For magnetic measurements, the untreated samples and the samples taken after the different extraction steps were dried in a desiccator and lightly ground in an agate mortar before further sample preparation. Magnetic measurements included IRM component analysis (Kruiver et al., 2001; Heslop et al., 2002) and hysteresis loop measurements.

For the IRM acquisition measurements, c. 100 mg of sample were accurately weighed-in in plastic vials of 8 cm^3 and moulded into epoxy raisin (Ciba-Geigi Araldite D/Hardener HY926; mixing ratio 5:1) until a homogeneous dispersion was obtained. Hardening took 24 hours at room temperature, and was done in a low-field environment (< 100 nT). IRM was induced with a PM4 pulse magnetiser, after AF demagnetisation, in 29 steps. IRM intensities were measured with a 2G Enterprises RF SQUID (Super Conducting Quantum Interference Device) magnetometer, model 740R. The noise level of the instrument is $\sim 10^{-11}$ Am^2, corresponding to $1.25*10^{-6}$ Am^{-1} for a 8 cm^3 sample.

The IRM acquired data were used to perform, what is referred to as IRM component analysis. The program that is used to separate the individual mineral contributions (Irmunmix), was developed by Heslop et al. (2002). The IRM values are plotted against the logarithm of the applied field, this results in a simple sigmoid shaped curve (Fig. 2).

This is essentially a cumulative log Gaussian curve (or a combination of such curves) for the coercive force distribution of the constituent magnetic mineral(s) (Robertson and France, 1994; Kruiver et al., 2001). The Irmunmix software automatically fits the IRM acquisition curve with respect to the [10]log field using an expectation-maximisation algorithm to effectively separate the IRM acquisition curves of individual components (typically two or three). Before the IRM component analysis was executed, a correction was made for the vial and the epoxy resin.

For the hysteresis measurements, c. 10 mg of sample were accurately weighed-in to pieces of drinking straws with a diameter of 3 mm and a length of 3 - 4 mm, glued to a piece of paper on one end. After the straws were filled with sample powder, they were sealed with a drop of glue. The hysteresis measurements were performed on an Alternating Gradient Magnetometer (MicroMag, Princeton) with a so-called 'P1 phenolic' probe. The accuracy of the measurements is 2%; the repeatability is 1% standard deviation, if the sample is not removed. The P1 phenolic probe displays a $\leq 2*10^{-9}$ Am^2 ferromagnetic background superposed on a $\leq -0.13*10^{-9}$ m^3 diamagnetic background. Corrections are made for the vial and the probe.
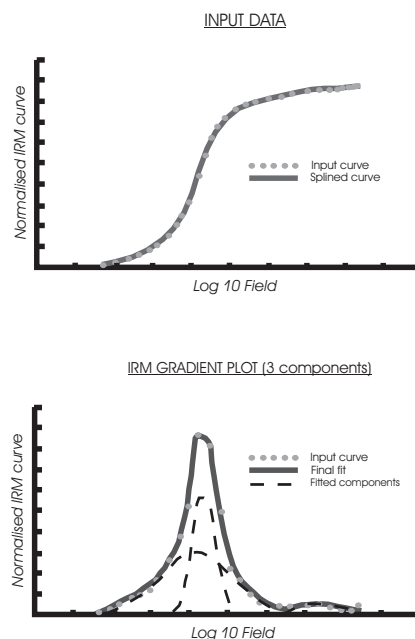
Fig. 2. Upper panel: redrawn example of the input IRM acquisition curve as given by the program Irmunmix2_2 (Heslop et al., 2002) for a sample from the oxidised part of the sapropel. The lower panel: redrawn gradient acquisition plot fitted with three components for the same sample. The total SIRM is $1.85*10^{-3}$ Am^2/kg; Comp. 1 ('detrital' magnetite), SIRM $1.10*10^{-3}$ Am^2/kg, ^{10}logB$_{1/2}$ is 1.63 (log mT) with a DP of 0.39 (log mT); Comp. 2 (hematite), SIRM $0.10*10^{-3}$ Am2/kg, ^{10}logB$_{1/2}$ is 2.91 (log mT) with a DP of 0.31 (log mT); Comp. 3 (biogenic magnetite), SIRM $0.65*10^{-3}$ Am^2/kg, ^{10}logB$_{1/2}$ is 1.74 (log mT) with a DP of 0.11 (log mT).

3   Results

3.1   Geochemistry

The down core variations of the elements manganese and iron are represented in Fig. 1. The manganese concentration (Fig. 1a) displays a distinct peak at the depth of the markerbed, approximately 26 cmsbd. In the oxidised upper part of the sapropel the amount of manganese is slightly elevated compared to the overlying sediments in which 3 g/kg of manganese is present, whereas that of iron (Fig. 1b) shows a pronounced downward increase, culminating in a maximum around 31 cmsbd. Below the transition from oxidised to reduced sediments in the sapropel the iron content of the sediments is slightly elevated compared to the background values of the overlying sediments (~ 25 g/kg). No significant amount of manganese is present below this transition. These profiles agree with previous findings, e.g. Passier et al. (2001).
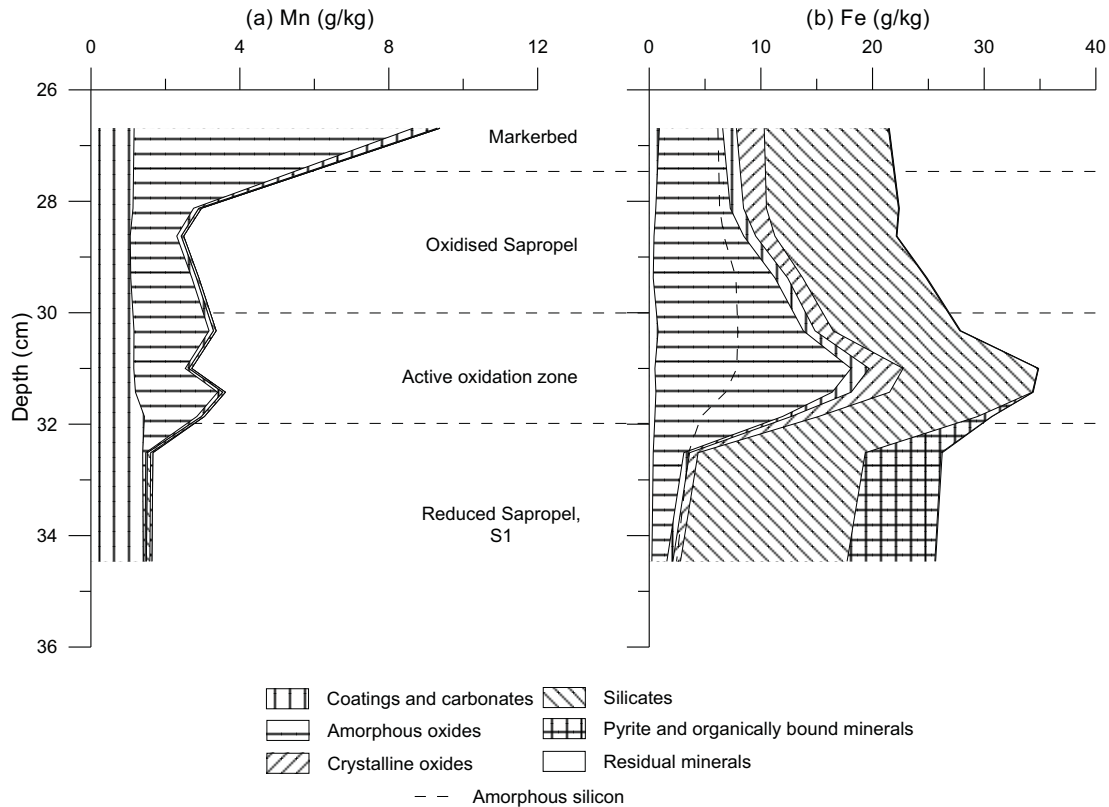
3.2   Sequential extraction

Approximately 80% of the carbonates was removed during the first three steps of the sequential extraction, assuming that all the calcium extracted is related to carbonates. Manganese associated with carbonates was largely extracted in the first step (pH=9, Table 2; Fig. 3a); almost no iron was extracted at this pH. During steps two and three some iron was extracted. The total amount of iron extracted in these steps did not surpass 5% of the total amount. The manganese remaining after step 1 through 3 is almost completely removed during the extraction of the 'amorphous' oxides.

Approximately 30% of the total amount of iron present in the sediments of the oxidised sapropel is extracted during the removal of the 'amorphous' oxides (step 4, Table 2; Fig. 3b). In the zone of active oxidation this increases to about 45% of total iron content. A small amount of iron can be assigned to the 'crystalline' oxides fraction throughout the core. The amount decreases with depth in the oxidised sapropel. Higher values appear again in the active oxidation zone to decrease again in the reduced sapropel.

During the dissolution of the 'amorphous' oxides, also a distinct amount of silicon was dissolved, as indicated by the dashed line in Fig. 3a. During the removal of the remaining carbonates (step 5, Table 2) some iron and silicon were extracted as well. This could be the result of the dissolution in the previous step 4, removal of the 'amorphous' oxides. The largest amount of iron found in the sediments, approximately 50%, appears to be incorporated into silicates (step 7). In step 8, the extraction of pyrite, iron was only

extracted in the reduced part of the sapropel. The residual minerals (step 9) were mainly composed of aluminium, iron, and titanium.


Fig. 3. (a) The amount of manganese (g/kg), and (b) the amount of iron (g/kg) extracted in the different steps of the sequential extraction. The vertical hatched lines represent the amount removed during the removal of the coatings and carbonates (step 1 – 3, Table 2). Horizontal hatched lines indicate the removal of the 'amorphous' oxides (step 4). The dashed line represents the amount of silicon also extracted in step 4. The diagonally hatched lines indicate the removal of the crystalline oxides and the silicates. The tiles refer to the removed pyrite and organically bound minerals. No filling was applied for the amount removed from the remaining fraction. Dashed horizontal lines indicate the approximate boundaries of different geochemical zones in the core.

3.3   Magnetic parameters

The IRM_{cfb} (calculated on a carbonate free basis, suffix cfb) acquired by the sediments after the different extraction steps is given in Fig. 4a, the remanent coercivity (H_{cr}) is presented in Fig. 4b. The IRM_{cfb} is calculated with the assumption that the calcium extracted in the different steps of the sequential extraction is solely related to carbonates. The IRM_{cfb} acquired by the untreated samples displays values ranging from $6.8*10^{-3}$ Am^2/kg in the markerbed, via $\sim4.5*10^{-3}$ Am^2/kg in the oxidised part of the

sapropel, and up to 5.8×10^{-3} Am^2/kg in the active oxidation zone. In the reduced part of the sapropel the IRM$_{cfb}$ is ~1.3×10^{-3} Am^2/kg directly under the active oxidation zone, and 4.7×10^{-3} Am^2/kg further down. After the removal of the coatings and carbonates (step 1 through 3) the IRM$_{cfb}$ decreases, on average with 25%. This indicates that magnetic material is dissolved and that the extraction of the carbonates is not completely specific. The removal of the 'amorphous' oxides further decreases the magnetisation measured. The peak at the lower boundary of the active oxidation zone becomes more perceptible. After the second removal of the carbonates the observed magnetisation is slightly higher then that of the previous measurements, this can be attributed to the concentration of the magnetic signal. The removal of the 'crystalline' oxides results in a total decrease of magnetisation to approximately 0.6×10^{-3} Am^2/kg.
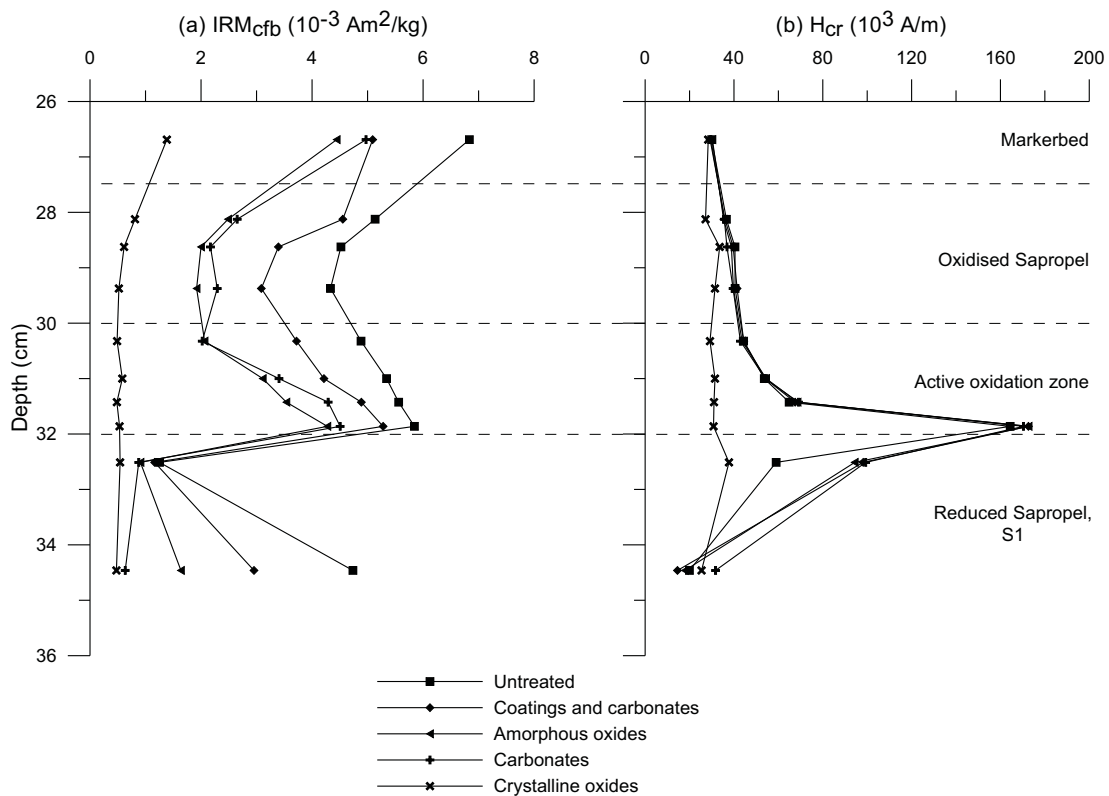
Fig. 4. (a) IRM$_{cfb}$ acquisition (suffix, carbonate free basis), and (b) the remanent coercive force (B$_{cr}$) measured during backfield curves (hysteresis measurements) of the untreated sediment (squares) and after several steps of the sequential extraction. The IRM$_{cfb}$ is calculated by assuming that the amount of calcium extracted in the different steps of the sequential extraction is solely related to carbonates. Diamonds: the removal of the coatings and carbonates, step 1-3 in the extraction scheme (Table 1). Triangles: the removal of the 'amorphous' oxides, step 4. Plusses: the removal of the remaining carbonates, step (5). Crosses: the removal of 'crystalline' oxides (step 6). Dashed horizontal lines indicate the approximate boundaries of different geochemical zones in the core.

A large peak is present in the remanent coercivity (H_{cr}, Fig. 4b), located at the lower boundary of the active oxidation zone. After the removal of the carbonates, the 'amorphous' oxides and the remaining carbonates, the down-core shape of the coercivity profile remains unchanged. The peak in coercivity disappears after the removal of the 'crystalline' oxides: a constant remanent coercivity of approximately $30*10^3$ A/m is observed.

3.4 IRM component analysis

The results of the IRM component analysis are summarised in table 3. In the untreated sediments, three components could be identified in the oxidised sapropel and the active oxidation zone. These are a relatively strong low-coercivity component (component 1) and a relatively weak high coercivity component (component 2), identified in the studies of Passier et al. (2001), and Kruiver and Passier (2001), as respectively 'detrital' magnetite and hematite. Component 3 was interpreted along similar lines as Kruiver and Passier (2001) as biogenic magnetite. It displays a characteristic low dispersion (DP) in the coercivity, indicating a narrow grain-size range distribution. In the sediments of the reduced sapropel component 3 could not be identified.

The removal of the 'amorphous' oxides changes the distribution of the components in the sapropel. A relative increase to the SIRM contribution of component 1, 'detrital' magnetite is observed. Consequently, the other components, biogenic magnetite and hematite, display a decrease in their magnetic contribution. The contribution of component 2 (hematite) decreases strongly in the reduced part of the sapropel. After the removal of the 'crystalline' oxides, component 3 (biogenic magnetite) disappears from the sediments. The components 1 and 2, respectively 'detrital' magnetite and hematite remain detectable.

4 Discussion

4.1 Diagenetic interpretation

The identification of the diagenetic zones in the sediments of boxcore PS036BC is mainly based on the colour transitions observed in the sediments. The geochemical analyses confirmed the presence and location of the zones (Fig. 1 and 3). The markerbed, indicated by darker sediments and a manganese peak, is located at 26 cmsbd. It also marks the original upper boundary of sapropel S1 (van Santvoort et al., 1996). The transition from pale brown to slightly yellow/orange sediments occurs at a depth of approximately 30 cm, and marks the upper boundary of the active oxidation zone, in

which the maximum concentrations of iron are observed. However no second manganese peak could be observed in this zone, as in previous studies by e.g. van Santvoort et al. (1996) and Passier et al. (2001). The transition of oxidised to reduced sediments is located at a depth of 32 cm as evidenced by the presence of pyrite below this depth.

Table 3. Average fitted IRM components, for the different geochemical zones in the core as specified in Fig.s 3 and 4 (Ox. Sap: Oxidised Sapropel; AOZ: Active Oxidation Zone; Red. Sap: Reduced Sapropel). The SIRM is given in 10^{-3} Am^2/kg, units for relative contribution are percentages, units for mean ^{10}log $B_{1/2}$: ^{10}log(mT) and DP: ^{10}log(mT). Section A, untreated sediments. Section B, after coating and carbonate extraction. Section C, after extraction of the 'amorphous' oxides. Section D, after extraction of the remaining carbonates. Section E, after extraction of the 'crystalline' oxides.

			Component 1			Component 2			Component 3		
		SIRM	Rel. contr. SIRM	Mean (^{10}log $B_{1/2}$)	DP	Rel. contr. SIRM	Mean (^{10}log $B_{1/2}$)	DP	Rel. contr. SIRM	Mean (^{10}log $B_{1/2}$)	DP
A	Ox. Sap	1.767	0.457	1.649	0.364	0.076	2.553	0.409	0.467	1.747	0.128
	AOZ	2.576	0.309	1.801	0.465	0.296	2.254	0.279	0.395	1.858	0.171
	Red. Sap	1.454	0.703	1.569	0.397	0.297	2.242	0.429			
B	Ox. Sap	3.090	0.326	1.417	0.336	0.049	2.631	0.347	0.624	1.736	0.174
	AOZ	4.163	0.310	1.748	0.420	0.311	2.154	0.309	0.379	1.871	0.184
	Red. Sap	1.739	0.683	1.452	0.357	0.317	2.217	0.429			
C	Ox. Sap	1.859	0.579	1.719	0.430	0.034	3.053	0.223	0.386	1.731	0.150
	AOZ	3.097	0.332	1.796	0.393	0.364	2.149	0.281	0.304	1.862	0.181
	Red. Sap	1.137	0.856	1.669	0.418	0.144	2.356	0.371			
D	Ox. Sap	2.366	0.596	1.704	0.445	0.040	3.068	0.198	0.364	1.737	0164
	AOZ	3.545	0.363	1.844	0.455	0.289	2.429	0.186	0.348	1.851	0.191
	Red. Sap	0.753	0.777	1.712	0.426	0.223	2.717	0.265			
E	Ox. Sap	0.649	0.965	1.726	0.444	0.035	3.172	0.145			
	AOZ	0.524	0.939	1.736	0.444	0.061	3.200	0.102			
	Red. Sap	0.512	0.827	1.749	0.426	0.169	2.890	0.283			

In the different diagenetic zones different proportions of iron species are found. This not only pertains to the magnetic iron oxides but to fine-grained super-paramagnetic iron oxides as well. Earlier mineral-magnetic analysis (Passier et al., 2001; Passier and Dekkers 2002) pointed in this direction, but firm validation is obtained in the present research.

The results of the sequential extraction allocate circa 35% 'amorphous' iron, 10% 'crystalline' iron, and 55% 'other' iron (mainly silicate-related iron), to the total iron content

of the oxidised sapropel (Fig.s 1 and 3). In the peak of the active oxidation zone the iron is allocated over the same species but in different proportions, 45% 'amorphous' iron, 10% 'crystalline' iron, and 45% 'other' iron. In the reduced part of the sapropel the proportions are: approximately 20% iron incorporated into oxides, 25% pyrite-related iron, and 55% 'other' iron. Manganese is incorporated into carbonates and 'amorphous' oxides. In the markerbed the oxides are the dominant species, whereas in the oxidised part of the sapropel and the active oxidation zone and approximately equal amount of carbonate related manganese is present. In the reduced part of the sapropel mainly carbonate-related manganese is present.

In this study, in the dissolution step with ascorbate (step 4, Table 2), a significant amount of silicon was dissolved together with aluminium and potassium, whereas in the dithionite step (step 6, Table 2), little dissolution was observed of the latter two elements. The extraction of silicon and related elements occurs in the oxidised sapropel and in the zone of active oxidation. A plausible explanation could be given by the reaction of ferrous iron with dissolved oxygen to initially form abiological ferrihydrite, that with time transforms into goethite or hematite depending on the pH conditions (cf. Konhauser, 1998 and references cited herein). Ferrihydrite can sorb a wide variety of elements and anionic groups including silicon as $Si(OH)_4$ groups and phosphate (Carlson and Schwertmann, 1981; Schwertmann, 1988). Although both refer to pedogenic conditions, the underlying principles may be extended toward a marine setting: electrical double layers are smaller in the marine environment but the pH in the pore waters is often slightly acidic as well, i.e. ~6–7. Sorption of silicate, that is a bidendate inner-sphere complex, distinctly reduces crystallinity. It may favour a ferrihydrite aging mechanism toward more stable iron oxides via dissolution and precipitation from solution. This would yield goethite and would explain the extreme magnetic hardness in the active oxidation zone that was found by Passier et al. (2001) and Kruiver and Passier (2001). Note that a yellowish brown colour occurs within the active oxidation zone (cf. Table 1). This would point to goethite rather than to hematite. It is unclear, however, why it would 'disappear' higher up in the oxidised sapropel. A reason could be that the disappearance is only apparent: one could speculate that in the oxidised sapropel more hematite-like ferric oxide is added so that the colour that is ascribed to a goethite phase would no longer be traceable because hematite is known to be a strong pigment. In addition to inorganically precipitated ferric oxides also bacterially induced precipitation occurs often yielding ferrihydrite. This ferrihydrite is also a precursor of more stable iron oxides, as goethite and hematite. These iron-phases are by-products of bacterial metabolism, and may be formed in large quantities (cf. Konhauser, 1998 and references cited herein). With time and depth the downward progression of the oxidation front retards, due to continuing (oxic) sedimentation, which

increases the distance between the front and the sediment-water interface. Thus, at deeper levels more time is available for the formation of bacterially induced iron phases. Moreover, magnetotactic bacteria can form magnetite. Hence we end up with a 'bimodal' iron oxide precipitate: amorphous iron oxides that age higher up in the oxidised sapropel (they become older with decreasing depth) and highly crystalline magnetotactic magnetite that may partially maghematise higher up (Passier and Dekkers, 2002).

4.2   Magnetic parameters and sequential extraction

4.2.1   IRM component analysis

The diagenetic zones – the oxidised sapropel, the active oxidation zone, and the reduced sapropel – display different IRM properties pointing to a chemically different environment. Three coercivity phases could be identified in the IRM component analysis: Component 1 is interpreted as 'detrital' magnetite, component 2 as hematite, and component 3 as biogenic magnetite (Table 3).

The first component, 'detrital' magnetite, is the main component remaining in the sediment samples after the extraction of carbonates and amorphous (iron) oxides. In the active oxidation zone this component displays higher coercivities compared to the surrounding diagenetic zones, until the removal of the 'crystalline' oxides. Coatings on the mineral surface, most likely composed of iron-silicates, could be responsible. The difference between the active oxidation zone and the other zonations is reduced after the extraction of the 'amorphous' oxides. After this step the majority of the iron-silica precipitates is removed as discussed in the previous section. It remains to be shown whether the part of IRM component 1, remaining after the first six steps of the sequential extraction, is a pure mineral surviving in the sediments after reductive diagenesis, or whether it is present as inclusions in other mineral-phases as proposed by Canfield and Berner (1987).

Component 2, identified as hematite by Kruiver and Passier (2001), is strongly affected by the sequential extraction. Its coercivity increases from ^{10}log $B_{1/2}$ ~2.6 (log mT) to ~3.1 (log mT) after the removal of the 'amorphous' oxides in the oxidised part of the sapropel. Simultaneously, the dispersion parameter (DP) decreases from 0.35 (log mT) to 0.22 (log mT). This indicates a poorly crystalline hematite-like phase that is preferentially dissolved over the goethite phase, which is magnetically harder. This would imply the presence of both goethite and hematite in the oxidised sapropel, concurring with colour observations. After extraction of the 'crystalline' oxides ~2% of component 2 remains, indicating that not has been completely dissolved. In the zone of active oxidation the

coercivity remains relatively constant, until the removal of the 'crystalline' oxides. The coercivity then increases to approximately $^{10}\log B_{\frac{1}{2}}$ of 3.2 (log mT) with a dispersion (DP) of 0.12 (log mT). Apparently goethite is present and is more resistant to dissolution than hematite.

The third IRM component, biogenic magnetite, is only present in the oxidised sapropel and the active oxidation zone. Like IRM component 1, it is harder in the active oxidation zone than in the other zonations. Its contribution to the SIRM decreases after the removal of the 'amorphous' oxides, indicating some dissolution of biogenic magnetite during this step. The effect is more pronounced in the oxidised sapropel than in the zone of active oxidation. A plausible explanation is that the magnetosome chains become disintegrated upon cell lyses after the oxidation front has moved further down in the sediment. Therefore they are more amenable to dissolution. Component 3 has disappeared completely after the extraction of 'crystalline' oxides.

4.2.2 Hysteresis parameters

The coercivity pattern found in the present study (Fig. 4b) with peak values at the lower boundary of the active oxidation zone was also observed in sapropel S1 by Passier et al. (2001) and Kruiver and Passier (2001) and in other sediments by e.g. Tarduno et al. (1998). They concluded that an unusually abundant population of bacterial magnetite produces the peak at the iron-redox boundary. This coincides with the findings of the IRM component analysis. The peak disappears after the removal of the 'crystalline' oxides, after which 'biogenic' magnetite is absent in the IRM component analysis.

It is common to summarize hysteresis parameters by plotting M_{rs}/M_s versus H_{cr}/H_c (i.e. Day plot), because different domain states plot in different areas (Day et al., 1977). Fig. 5 shows the Day plot for the ten samples analysed after the different extraction steps. The sample positions on the Day plot have to be viewed with some caution because the domain state areas refer to monomineralic (titano-)magnetite assemblages in the absence of superparamagnetic (SP) grains. SP grains tend to displace values for the hysteresis ratios to the right of the experimentally calibrated band of Day et al. (1977) as a recent study by Dunlop (2002) shows. The theoretical Day-plot curves as calculated by Dunlop (2002) are added to Fig. 5. Compared to the calculated mixing curves of single domain (SD) and multidomain (MD) grains and the experimentally calibrated band, all data points are displaced to the right. The position of the samples conforms rather closely to the trend line for unremagnetised limestones as found by Channell and McCabe (1994). This indicates an assemblage of magnetic minerals dominated by 'primary' magnetite concurring with results of the IRM component analysis. Surface oxidation and the

presence of moderate amounts of hematite and /or goethite, as indicated by the IRM component analysis, play a role in explaining the observed displacement to the right. Extreme displacement to the right as observed in the samples taken in and near the active oxidation zone invokes the presence of very fine-grained SP magnetic minerals. Most SP grains occur in the sample from the active oxidation zone. The sample directly above it needs much less SP grains to explain its position on the Day plot. Note that the position does not change so much after removal of the 'amorphous' oxides: this indicates hematite
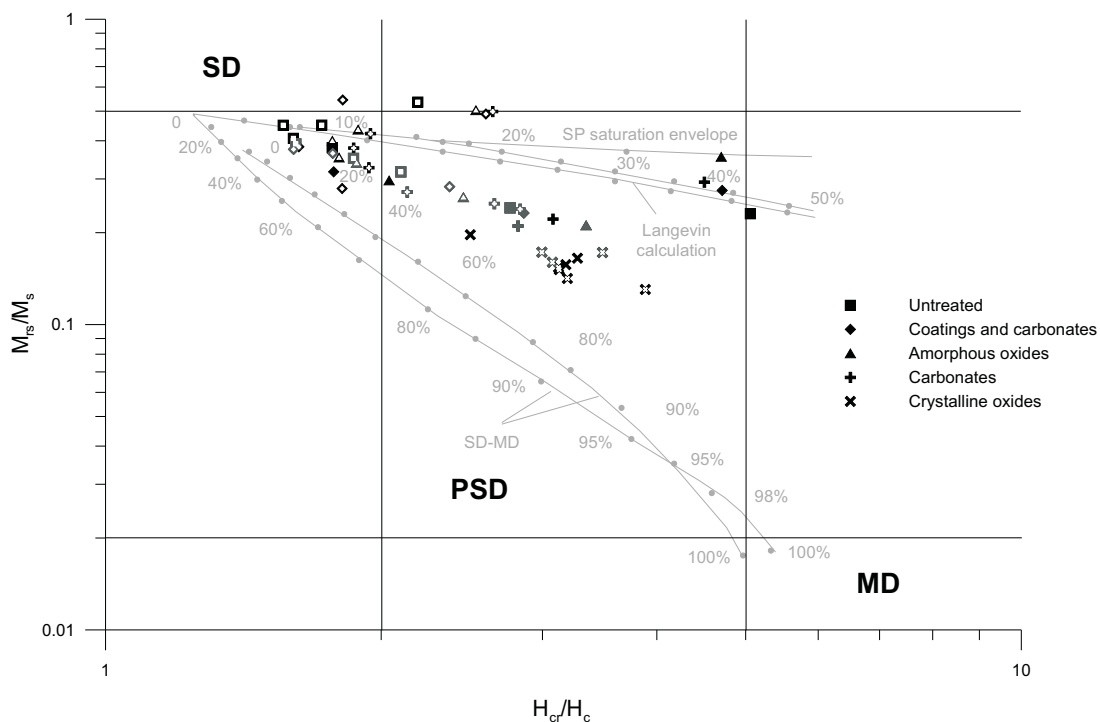
Fig. 5. Classification of magnetic minerals in terms of magnetisation and coercivity ratios *(after Day et al., 1977)*. The grey curves in the background are theoretical Day plot curves calculated for magnetite by *Dunlop (2002)*. Numbers along the curves are volume fractions of the soft component (SP or MD) in mixtures with SD grains. Squares: represent the measured data of the untreated sediment of this study. Diamonds: after the removal of the coatings and carbonates (step 1 – 3). Triangles: after the removal of the 'amorphous' oxides (step 4). Plusses, after the removal of the remaining carbonates (step 5). Crosses: after the removal of the 'crystalline' oxides (step 6). Colour coding of the symbols: Markerbed, grey; Oxidised Sapropel, filled grey; Active oxidation zone, filled white; Reduced Sapropel, black. Note that after extraction of the 'crystalline' oxides the initial scattering of the samples is strongly reduced.

and goethite are present as well in those samples. After the removal of the 'crystalline' oxides in step 6 of the sequential extraction this extreme displacement disappears. The difference in M_{rs}/M_s and H_{cr}/H_c ratios between the samples has almost disappeared: all samples plot closely together in the pseudo single domain (PSD) field. A tendency towards the calculated SD-MD curves is observed for the samples as well. Deviations

from the experimentally calibrated band are related to the presence of a mixture of magnetic-minerals as indicated by the IRM components. It could be that the remaining magnetic minerals occur as inclusions in silicates. Electron microscopic analysis could be used to verify this.

5   Conclusion and implications

The sequential extraction clearly separates different phases of iron that occur in oxic and in anoxic sediment conditions. However, the separation between the 'amorphous' and 'crystalline' oxides seems to be grain-size selective. The dissolution of silicon during the extraction of the 'amorphous' oxides implies the presence of a relatively easily soluble ferro-silicate, which is most likely to be a by-product of bacterial metabolism.

IRM acquisition followed by IRM component analysis could identify three components, e.g. different species of iron oxides. The magnetites found in the sapropelic sediments can be subdivided into two categories: 1) 'Detrital' magnetite with a relatively low mean coercivity, 2) Biogenic magnetite, formed by magnetotactic bacteria living in the lower part of the active oxidation zone. The grains display single domain to super-paramagnetic behaviour. The other component identified is a mixture of hematite and goethite.

The sequential extraction together with the magnetic parameters of the sediments identified also two other iron phases of diagenetic origin: a) Coatings on mineral surfaces mainly composed of ferro-silicates; b) 'Amorphous' iron oxides (hematite and/or goethite) which are likely to have the same microbially induced origin as the coatings.

The hysteresis measurements and the IRM component analysis, verify earlier findings that the coercivity peak observed in the sediments is of diagenetic origin. It is most likely the result of the activity of magnetotactic bacteria forming in-situ magnetite (Tarduno et al., 1998; Passier et al., 2001, Kruiver and Passier, 2001).

Acknowledgements

Chapter 2.2 Diagenetic alteration of magnetic signals by anaerobic oxidation of methane related to a change in sedimentation rate

Abstract

Geochemical and rock magnetic investigations of sediments from three sites on the continental margin off Argentina and Uruguay were carried out to study diagenetic alteration of iron minerals driven by anaerobic oxidation of methane (AOM). The western Argentine Basin represents a suitable sedimentary environment to study nonsteady-state processes because it is characterized by highly dynamic depositional conditions. Mineralogic and bulk solid phase data document that the sediment mainly consists of terrigeneous material with high contents of iron minerals. As a typical feature of these deposits, distinct minima in magnetic susceptibility (κ) are observed. Pore water data reveal that these minima in susceptibility coincide with the current depth of the sulfate/methane transition (SMT) where HS^- is generated by the process of AOM. The released HS^- reacts with the abundant iron (oxyhydr)oxides resulting in the precipitation of iron sulfides accompanied by a nearly complete loss of magnetic susceptibility. Modeling of geochemical data suggests that the magnetic record in this area is highly influenced by a drastic change in mean sedimentation rate (SR) which occurred during the Pleistocene/Holocene transition. We assume that the strong decrease in mean SR encountered during this glacial/interglacial transition induced a fixation of the SMT at a specific depth. The stagnation has obviously enhanced diagenetic dissolution of iron (oxyhydr)oxides within a distinct sediment interval. This assumption was further substantiated by numerical modeling in which the mean SR was decreased from 100 cm kyr^{-1} during glacial times to 5 cm kyr^{-1} in the Holocene and the methane flux from below was fixed to a constant value. To obtain the observed geochemical and magnetic patterns, the SMT must remain at a fixed position for ~9000 yrs. This calculated value closely correlates to the timing of the Pleistocene/Holocene transition. The results of the model show additionally that a constant high mean SR would cause a concave-up profile of pore water sulfate under steady state conditions.

1   Introduction

Iron (oxyhydr)oxides are a common component of marine sediments (e.g. Canfield, 1989; Haese et al., 2000) and are important carriers of magnetostratigraphic and paleomagnetic information (Frederichs et al., 1999; Bleil, 2000). After deposition primary iron mineral assemblages pass through a sequence of early diagenetic zones in which the minerals undergo alterations. Strong modifications of iron (oxyhydr)oxides and rock magnetic properties during the early stages of diagenesis across the Fe redox boundary have been documented by numerous studies (Wilson, 1986; Tarduno and Wilkison, 1996; Funk et al., 2003a, 2003b; Reitz et al., 2004). The early diagenetic transformation of iron (oxyhydr)oxides in marine sediments is linked to different pathways. One important process is the reaction with hydrogen sulfide via sulfate reduction (Berner, 1970; Froelich et al., 1979; Canfield, 1989; Lovley, 1991; Haese et al., 1998). Besides sulfate reduction driven by the bacterial degradation of organic matter, which typically occurs at high rates in the upper layers of the sediment (Jørgensen, 1982; Ferdelman et al., 1999), the process which ultimately leads to the complete consumption of interstitial sulfate in marine sediments is the anaerobic oxidation of methane (AOM). This important biogeochemical process finds its geochemical expression in a characteristic sulfate/methane transition (SMT) typically located one to a few meters below the sediment surface. Sulfate reduction driven by AOM releases adequate amounts of hydrogen sulfide into the pore water (Barnes and Goldberg, 1976; Bernard, 1979; Blair and Aller, 1995; Borowski et al., 1996; Niewöhner et al., 1998; Jørgensen et al., 2004). The liberated hydrogen sulfide leads to diagenetic alteration of primary geochemical and geophysical properties and the formation of distinct secondary signals in the zone of AOM (Passier et al., 1998; Kasten et al., 2003; Neretin et al., 2004).

The extent of geochemical and magnetic overprint occurring at geochemical boundaries and reaction fronts, particularly in deeper sediments is poorly understood. An important geochemical process in the zone of AOM is the transformation of magnetic iron minerals (Kasten et al., 1998; Passier et al., 1998). One of the major minerals to carry remanent magnetism in sediments is the ferrimagnetic mineral (titano)magnetite. The conversion of magnetite to iron sulfides during sediment diagenesis is a major cause of the loss of the magnetostratigraphic record in marine sediments (Karlin and Levi, 1983, 1985; Channell and Hawthorne, 1990; Karlin, 1990; Passier et al., 1998; Channell and Stoner, 2002). Ferrimagnetic iron oxides can be altered to paramagnetic iron sulfides (Berner, 1970; Canfield et al., 1992) and the magnetic signal can change dramatically (Canfield and Berner, 1987; Channell and Hawthorne, 1990; Channell and Stoner, 2002). An often cited mechanism is the formation of the iron sulfide pyrite via an intermediate

sulfide mineral such as greigite (Berner, 1967; Roberts and Turner, 1993). These latter minerals are ferrimagnetic and their preservation would lead to the formation of a strong secondary magnetic signal (Roberts and Turner, 1993; Kasten et al., 1998; Jiang et al., 2001; Neretin et al., 2004). Intermediate iron sulfides are metastable, but they can persist for a considerable period of time if hydrogen sulfide is entirely consumed (Berner, 1982; Kao et al., 2004). Pyrite is thermodynamically more stable and thus will be the end-member of the transformation from iron (oxyhydr)oxides to iron sulfides (Berner, 1970; Coleman and Raiswell, 1995). However, if hydrogen sulfide is present in pore water, the oxidation of iron monosulfides by hydrogen sulfide can form pyrite directly without a greigite intermediate (Morse and Cornwell, 1987; Rickard et al., 1995; Butler and Rickard, 2000). Therefore, the diagenetic formation of iron sulfides in aquatic sediments has a strong effect on the interpretation of paleomagnetic data (Roberts and Turner, 1993; Furukawa and Barnes, 1995; Neretin et al., 2004).

The continental margin off Argentina and Uruguay represents a suitable sedimentary environment to study nonsteady-state processes because it is characterized by highly dynamic depositional conditions (Ewing et al., 1971; Biscay and Dasch, 1971; Ledbetter and Klaus, 1987; Hensen et al., 2000, 2003). The sediment has a high content of ferric iron minerals and specific variations in magnetic signals (Sachs and Ellwood, 1988). Extensive geochemical and geophysical studies were carried out by Hensen et al. (2003) on sediments from the western Argentine Basin. Focusing on the reconstruction of mainly modern sedimentary history, especially gravity-driven mass flows, gravity cores with nonsteady-state sulfate pore water profiles (concave, kink-, and s-type) were investigated.

In this study, we present geochemical, magnetic, and mineralogical data for three sediment cores from the continental margin off Argentina and Uruguay. These coring sites are characterized by a rather homogenous recent sedimentation and linear sulfate pore water profiles. We investigate the influence of depositional settings and AOM on the diagenetic overprint of iron (oxyhydr)oxides and the resulting change in the magnetic record, and present results of numerical modeling of the processes involved.

2   Materials and Methods

2.1   Location and Geological Settings

The study area is located in the western South Atlantic on the continental margin off Argentina and Uruguay (Fig. 1). The investigated gravity cores (Table 1) were taken during expeditions M46/2 and M46/3 of the RV *Meteor* (Bleil et al., 2001; Schulz et al., 2001). The gravity cores were retrieved east of the Rio de la Plata at the western

boundary of the Argentine Basin. Sedimentation in this area is controlled by two main processes: gravity-controlled sediment transport and strong current circulation (Ewing and Leonardi, 1971; Klaus and Ledbetter, 1988). Terrigenous input originates from the numerous fluvial tributaries along the coast of Argentina and Uruguay (Iriondo, 1984; Piccolo and Perillo, 1999). The sediments are transported directly down-slope along the western margin of the Argentine Basin by gravity-controlled processes (Ewing et al., 1971; Biscay and Dasch, 1971; Klaus and Ledbetter, 1988; Sachs and Ellwood, 1988; Romero and Hensen, 2002; Hensen et al., 2003). These gravity-driven mass transports, such as debris flows and turbidity currents, are the main pathways of sediment supply into the deeper basin. The second important process controlling the sedimentation in this area is the action of strong currents along the continental margin. The currents in the upper water
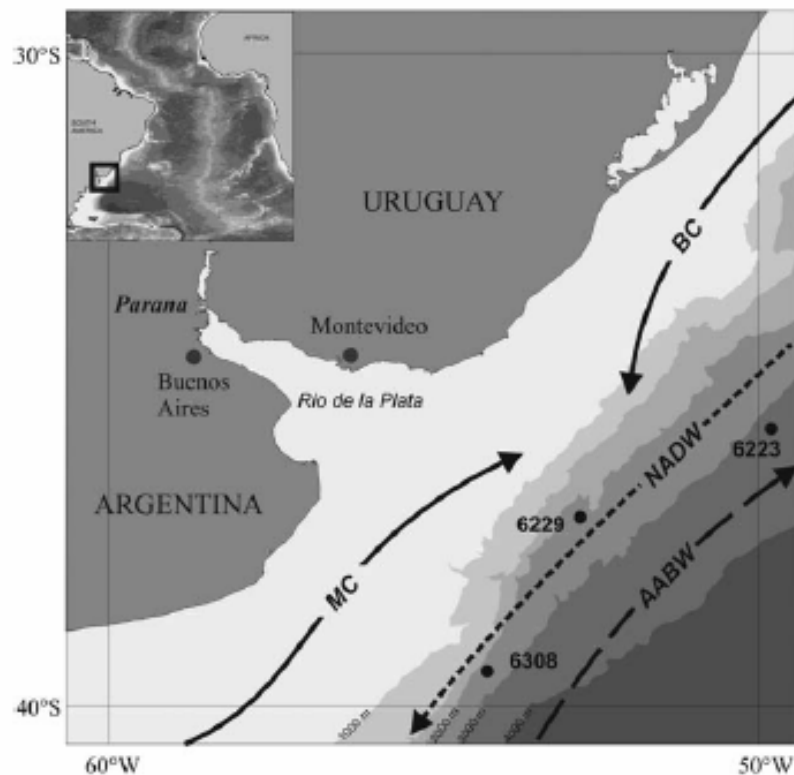
Fig. 1. Location map of the study area offshore of the Rio de la Plata. Arrows indicate simplified pathways of the main currents (solid line presents the surface-water currents MC (Malvinas Current) and BC (Brazil Current), and the lower-level and bottom-water currents are marked by dashed lines: NADW = North Atlantic Depth Water; AABW = Antarctic Bottom Water.

column are the southward flowing Brazil Current and the northward flowing Malvinas (Falkland) Current (Peterson and Stramma, 1991). These two currents meet in the Brazil Malvinas Confluence (BMC), located in front of the Rio de la Plata. The confluence of the

two different water masses leads to an increase in primary production over a large area (Antoine et al., 1996; Behrenfeld and Falkowski, 1997), which results in relatively high inputs of organic carbon into the sediment.

The suspended load of the Rio de la Plata is carried by northerly currents and thus forms a tongue of fine-grained sediment which is deposited parallel to the shore line off the coast of Uruguay (Ewing and Lonardo, 1971; Ledbetter and Klaus, 1987; Frenz et al., 2003). Between depths of 2000 and 4000 m, the water column is governed by the southward-flowing North Atlantic Deep Water (NADW). Below 4000 m, the strong currents carry Antarctic Bottom Water (AABW) to the North. These currents flow parallel to the continental margin, supplying benthic diatoms from higher latitudes (Romero and Hensen, 2002). The AABW dominates the transport of predominantly fine-grained sediment below 4000 m water depth. The currents winnow and entrain sediments deposited by gravity-controlled mass flows, and the fine material is transported into the deep basin (Groot et al., 1967; Ewing et al., 1971; Ledbetter and Klaus, 1987; Sachs and Ellwood, 1988).

Table 1. Studied gravity cores with the location and water depth.

Station	Longitude [W]	Latitude [S]	Water Depth [m]	Core Length [m]
GeoB 6223-6	49°40.86'	35°44.42'	4280	8.67
GeoB 6223-5[a]	49°40.86'	35°44.43'	4280	8.15
GeoB 6229-6	52°39.00'	37°12.41'	3446	9.50
GeoB 6308-4	53°08.70'	39°10.00'	3620	11.66

[a] Core GeoB 6223-5 is the parallel core at site GeoB 6223 subjected to magnetic analysis.

The composition of the sediments in the study area is characterized by low calcium carbonate concentrations, but with relatively high amounts of organic carbon, biogenic opal, and iron (oxyhydr)oxides. Due to the sediment composition and the highly dynamic sedimentary conditions, few to no reliable stratigraphic information for this region exists (Romero and Hensen, 2002; Hensen et al., 2003).

2.2 Sampling

To prevent warming of the sediments after retrieval on board, all cores were immediately placed in a cooling laboratory and were maintained at a temperature of ~4°C. Gravity cores were cut into 1-m segments on deck, and syringe samples were taken from

the bottom of every segment for methane analysis. Higher-resolution sampling for methane was carried out in the cooling room by sawing 4x4 cm rectangles into the PVC liner. Syringe samples of 5 ml sediment were taken every 20 to 25 cm. For hydrogen sulfide analyses at higher concentrations, 1 mL subsamples of the pore water were added to a ZnAc-solutions to fix all hydrogen sulfide present as ZnS (see also Hensen et al., 2003).

Within the first two days after recovery, gravity cores were cut lengthwise into two halves and processed within a glove box under argon atmosphere. Conductivity and temperature were measured on the archive halves. On the working halves, pH and E_H were determined by punch-in electrodes, and sediment samples were taken every 25 cm for pressure filtration. Solid phase samples for total digestions, sequential extractions and mineralogical analyses were taken at 10 cm intervals and kept in gas-tight glass bottles under argon atmosphere. The storage temperature for all sediments was -20°C to avoid dissimilatory oxidation of reduced species. Teflon-squeezers were used for pressure filtration. The squeezers were operated with argon at a pressure that was gradually increased up to 5 bar. The pore water was retrieved through 0.2 μm cellulose acetate membrane filters.

2.3   Pore Water Analysis

The parameters hydrogen sulfide, sulfate, alkalinity, phosphate, and iron (Fe^{2+}) were determined by standard methods, as described in detail by Schulz (2000), within a few hours after retrieval of the pore water. All further analyses were carried out at the University of Bremen. Methane was measured with a gas chromatograph (Varian 3400), equipped with a split less injector, by injecting 20 μL of the headspace gas. The concentrations were subsequently corrected for sediment porosity. Aliquots of the remaining pore water were diluted and acidified with HNO_3 for determination of cations using atomic absorption spectrometry (AAS; Unicam Solaar 989 QZ) and inductively coupled plasma atomic emission spectrometry (ICP-AES; Perkin Elmer Optima 3000 RL). For further information regarding analytical methods and devices, we refer to the homepage of the University of Bremen geochemistry group at http://www.geochemie.uni-bremen.de.

2.4   Solid Phase Analysis

All solid phase analyses were performed on anoxic subsamples. For total digestion, the samples were freeze-dried and homogenized in an agate mortar. About 50 mg of the

sediment was digested in a microwave system (MLS - MEGA II and MLS – ETHOS 1600) and was treated with a mixture of 3 mL HNO_3, 2 mL HF, and 2 mL HCl. Dissolution of the sediments was performed at 200 ℃ and a pressure of 30 bar. The solution was fully evaporated, redissolved with 0.5 mL HNO_3 and 4.5 mL deionised water (MilliQ) and homogenized. Finally, the solution was filled up to 50 mL with MilliQ. Major and minor elements were measured by ICP-AES. The accuracy of the measurements was verified using standard reference material USGS-MAG-1. The reference material element concentrations were within certified ranges. The precision of ICP-AES analyses was better than 3%.

The concentrations of reactive Fe phases were determined following the method described by Haese et al. (2000). In the first step, 150-250 mg of the wet sample were treated with 20 mL of an ascorbate solution (a weak reducing agent) containing sodium citrate, sodium carbonate, and ascorbate acid and extracted over 24 hours. In the second step, the ascorbate residuum was treated with 20 mL of a dithionite solution consisting of acetic acid, sodium citrate, and sodium dithionite and kept in suspension for one hour. The extractions of ascorbate and dithionite were diluted 1:10 and measured by ICP-AES. Standards were prepared using the corresponding matrix.

For the determination of inorganic carbon (IC) and total organic carbon (TOC) contents, freeze-dried and homogenized samples of cores GeoB 6229-6 and GeoB 6308-4 were measured using a LECO CS-300 carbon sulfur analyzer. For organic carbon, the samples were treated with 12.5% HCl, washed two times with MilliQ and dried at 60 ℃. The accuracy, checked by marble standards, was ± 3%. The samples of core GeoB 6223-6 were measured using a Shimadzu TOC with SSM 5000A carbon analyzer. Inorganic carbon was measured by adding 35% phosphoric acid to the sample and heating up to 250 ℃. The accuracy is ± 3%, and the limit of detection is below 0.05% for a 100 mg sample.

The data set of pore water and solid phase measurements is available via the geological data network Pangaea (http://www.pangaea.de).

2.5   Mineral Analysis

Mineral identification was carried out by X-ray diffraction (XRD), which was performed at a few selected depths of core GeoB 6229-6 (75, 375, 545, 675, and 725 cm) using Philips X´Change (Cu-tube) with fixed divergence slit. The measurement was carried out with a first angle of 3° 2Θ and a last angle of 100° 2Θ. The step size was 0.02° 2Θ, with measurement time of 12 s/step. Samples of core GeoB 6223-6 (255, 525, 655 cm) and core GeoB 6308-4 (555 and 655 cm) were measured by X'Pert Pro MD, X'Celerator

detector system, with a step size of 0.033° 2Θ, and the calculated time per step was 219.71 seconds. Quantification of the mineral content quantification was carried out with QUAX (for further information see Vogt et al., 2002). Scanning electron microscope (SEM) analysis was performed on selected samples.

2.6   Magnetic Susceptibility Measurement

The magnetic susceptibility data for site GeoB 6223 were obtained on the parallel core GeoB 6223-5 on board the RV *Meteor*. Determination of susceptibility on the archive halves of the gravity cores GeoB 6229-6 and GeoB 6308-4 took place at the University of Bremen. The susceptibility measurements were performed using a non-magnetic automated core conveyor system equipped with a commercial BARTINGTON MS2 susceptibility meter and a 'BARTINGTON F-type' spot sensor. The measurement interval was 2 cm and 1 cm, respectively.

2.7   Geochemical Modeling

AOM and the associated diagenetic processes were simulated with the non-steady state transport and reaction model CoTReM. A detailed description of this computer software is given in the CoTReM User's Guide (Adler et al., 2000; http://www.geochemie.uni-bremen.de/cotrem.html) and by Adler et al. (2001). The upper 20 m of the sediment (model area) was subdivided into cells of 5 cm thickness. The time-step to fulfill numerical stability was set to 10^{-1} yr, and the porosity of the sediment was set to 75%. Transport mechanisms were molecular diffusion (D_s) for all solutes in the pore water and the sedimentation rate (SR) for the solid phase and pore water. Diffusion coefficients were corrected for tortuosity (Boudreau, 1997) and a temperature of 2°C. The bottom water concentration of species defines the upper boundary condition. The lower boundary is defined as an open/transmissive boundary, which means that the gradient of the last two cells is extrapolated to allow diffusion across the boundary. For methane, a fixed concentration was defined at the lower boundary that creates the gradient necessary to simulate the measured influx of methane into the model area from below. For geochemical reactions, 0th-order kinetics were used by defining maximum reaction rates. These rates are used as long as the reduct species are available in sufficient amounts. If the amount decreases, the rates were automatically reduced to the available amount of reactants in each cell to avoid negative concentrations (for further details see Hensen et al., 2003). All input parameters are given in the respective section below.
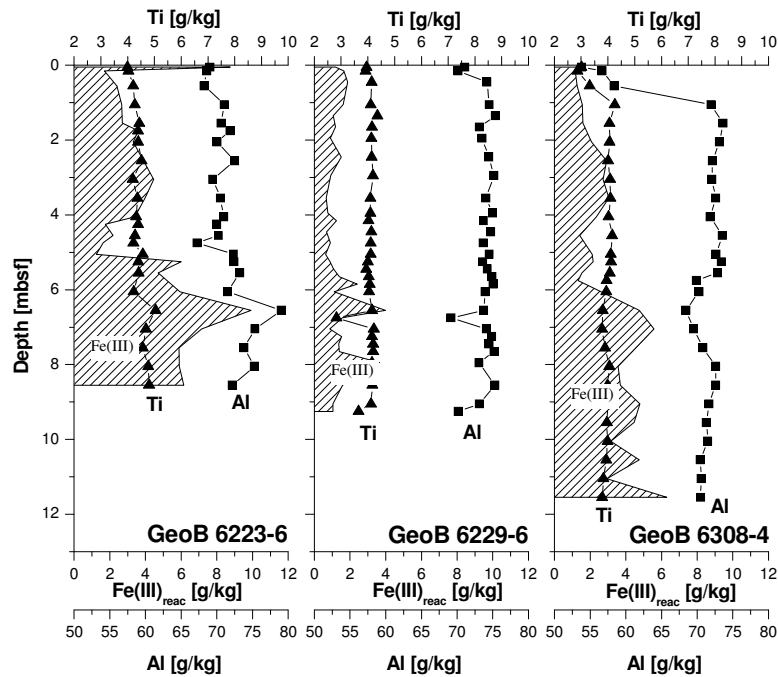
Fig. 2. Solid phase data of Al (solid squares) and Ti (solid triangles) indicating the dominance of terrigenous input. The cross-hatched area indicates the amount of reactive Fe(III) phases.

3 Results and Discussion

3.1 Sediment composition

Sediment composition and grain size are two important parameters that affect diagenetic processes (Roberts and Turner, 1993). These attributes vary in all three cores. Whereas the sediment of core GeoB 6229 and GeoB 6308 is quite variable in grain size, the sediment in core GeoB 6223-6 is rather fine-grained, as identified macroscopically and by SEM. At all sites, the composition of the sediment is dominated by lithogenic components, as indicated by the major mineral assemblages of selected samples from all three cores (20-28 wt% quartz, 18-35 wt% feldspar, and 23-44 wt% phyllosilicates). The lowest amounts of phyllosilicates were found at site GeoB 6308. Additionally, the solid phase concentrations of Al and Ti indicate a high terrigenous input (Fig. 2). Total concentrations of Al and Ti positively correlate in sediments of the southern-most site GeoB 6308-4 ($R^2 = 0.93$), which is not the case for the other two sites (GeoB 6229-6: $R^2 = 0.60$ and GeoB 6223-6: $R^2 = 0.75$). We attribute this finding to variable depositional processes. The comparatively high content of glauconite (3-17 wt%) detected by XRD in the sediment from all three cores gives evidence for mass flow deposition events. In

general, glauconite in recent sediment is an indicator of rather slow rates of clastic deposition in shallow marine environments (Odin and Matter, 1981; Harris and Whiting, 2000). The presence of this mineral at all three sites suggests erosion of near-shore/shelf sediments and redeposition at greater water depths on the continental slope. A further characteristic component of the sediments of this area is the relatively high amount (up to 1 wt%) of reactive iron (oxyhydr)oxides (Fig. 2).
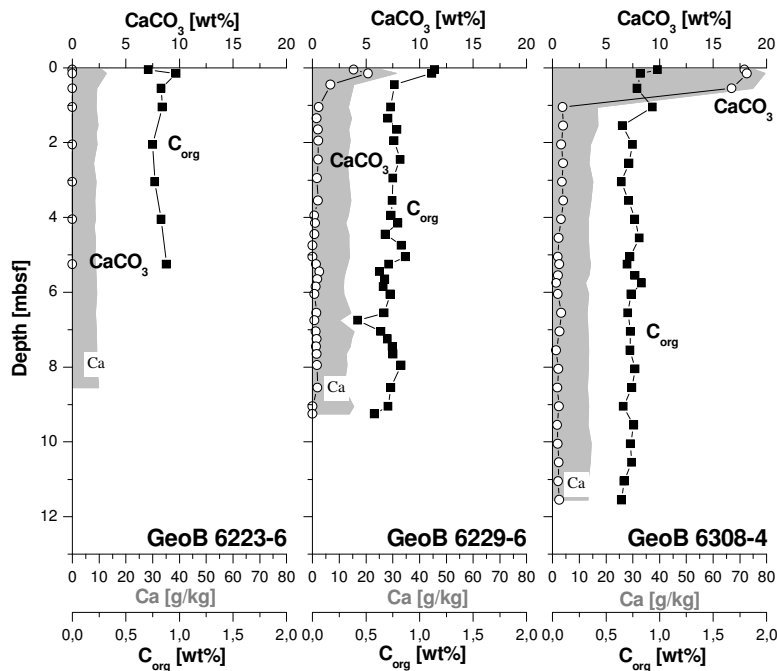
Fig. 3. Solid phase concentrations of total Ca (cross-hatched area), calcium carbonate (open circles), and total organic carbon (TOC, solid squares). The TOC in the upper layer of core GeoB 6308-4 is diluted by the higher amount of $CaCO_3$. There is no measurable carbonate in the sediment of core GeoB 6323-6, but there is a higher organic carbon content in the uppermost centimeters before it decreases toward the sediment surface.

All three cores display a distinct change in sediment composition in the uppermost section. Total organic carbon (TOC) reaches values of up to 1.1 wt% close to the sediment surface, while the mean content for the deeper sediment is ~0.7 wt% (Fig 3). Correspondingly, calcium carbonate also has the highest overall concentrations in the uppermost sediments. The calcium carbonate contents are generally low and well correlated with the total concentration of calcium obtained from acid digestion. The lack of carbonate in the deepest core GeoB 6223-6 can be due to the depositional system, e.g., dilution by terrigenous input, or due to its depth lying below the lysocline resulting in dissolution of carbonate (Archer, 1996; Frenz et al., 2003). At site GeoB 6229, $CaCO_3$ concentrations of up to 5 wt% were determined, and, at the southernmost site GeoB 6308,

high $CaCO_3$ contents of up to 18 wt% are found in the uppermost layer (Fig. 3). A similar transition from terrigenous-dominated to carbonate-enriched sediments in the upper sediment layers is also found in sediments of the Amazon Fan (e.g., core GeoB 1514-6 of Kasten et al., 1998). In these sediments, a sedimentation change is found at ~60 cm, with $CaCO_3$ gradually increasing upwards. While the glacial sedimentation rate for the Amazon Fan area amounts to a few meters per kyr (Flood et al., 1995), stratigraphic data for the upper 35 cm of core GeoB 1514 indicate a Holocene age with an SR of 3.5 cm/kyr (Schneider et al., 1991). A similar transition from terrigenous-dominated to more calcareous sediments in the upper sediment layers for the investigated sites would suggest a Holocene SR of ~3 to ~7 cm kyr^{-1}. This is in good agreement with unpublished stratigraphic data by O. Romero (personal communication) from Argentine Basin sites (e.g., GeoB 6340 at 44°54.95'S, 58°05.78'W, water depth 2785 m), which reveal an SR of a few cm per kyr in the Holocene. Although the mean SR in the investigated area is not the same as for the Amazon Fan, similar patterns in sediment composition are consistent with a comparable decrease in mean SR during the glacial/interglacial transition.
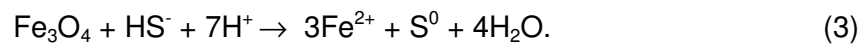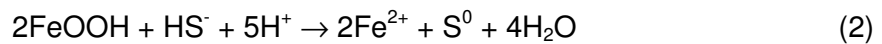
3.2   Diagenetic Alteration

The sulfate pore water profiles of all three studied cores show a linear decrease with depth, which indicates a currently steady-state situation (Fig. 4). The SMT is located between 5 and 5.5 mbsf (meters below seafloor) in each case. In cores GeoB 6229-6 and GeoB 6308-4, excess hydrogen sulfide could be detected between 4-7 and 4-6 mbsf, respectively. The sulfidic sediment intervals are characterized by distinct minima in magnetic susceptibility (Fig. 4). Based on the pore water data, we suggest that the characteristic decrease in magnetic susceptibility (κ), which is a widespread phenomenon in sediments of the continental margin off Argentina and Uruguay, is caused by diagenetic processes within the zone of AOM. Except for the decrease in magnetic susceptibility in the uppermost centimeters of core GeoB 6308-4, which is due to dilution by $CaCO_3$, we attribute the decrease in magnetic susceptibility to the reduction of iron (oxyhydr)oxides by hydrogen sulfide and subsequent formation of iron sulfides as described by Karlin and Levi (1983) and Channell and Hawthorne (1990).

Because of the current relatively high fluxes of methane and sulfate into the SMT at all three sites (Fig. 4), we suggest that deep sulfate reduction is primarily driven by AOM (Niewöhner et al., 1998). Thus, hydrogen sulfide is produced by a reaction of sulfate and methane (e.g., Barnes and Goldberg, 1976).

$$CH_4 + SO_4^{2-} \rightarrow + HCO_3^- + H_2O + HS^- \qquad . \tag{1}$$
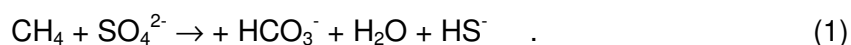
The species distribution of hydrogen sulfide is pH dependent (Pyzik and Sommer, 1981). Based on the measured pH values (7.2 to 8.0), we conclude that HS^- is the predominant hydrogen sulfide species in the sediment of the studied cores.

The concentration of measured reactive iron (oxyhydr)oxides for cores GeoB 6223-6 and GeoB 6308-4 is low (Fig. 2) in the interval where magnetic susceptibility data show a minimum (Fig 4). In this zone, the iron (oxyhydr)oxides are almost completely reduced and only a relict concentrations are left. For the process of iron (oxyhydr)oxide reduction, the assumed reactions for lepidocrocite (Eqn. 2) (as an example for iron (oxyhydr)oxides) and for magnetite (Eqn. 3) are

$$2FeOOH + HS^- + 5H^+ \rightarrow 2Fe^{2+} + S^0 + 4H_2O \qquad (2)$$

$$Fe_3O_4 + HS^- + 7H^+ \rightarrow 3Fe^{2+} + S^0 + 4H_2O. \qquad (3)$$

The available dissolved ferrous iron reacts directly with HS^- (Berner, 1970; Pyzik and Sommer, 1981) according to the following equation

$$Fe^{2+} + HS^- \rightarrow FeS_{(s)} + H^+ \qquad (4)$$
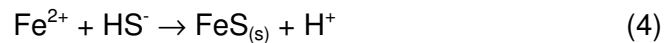
The precipitated amorphous iron sulfide is highly unstable and transformed rapidly to other iron sulfide phases (Schoonen and Barnes, 1991). Morse (2002) discussed that the oxidation of FeS by hydrogen sulfide (Eqn. 5) is the faster process compared to the oxidation by elemental sulfur as discussed by Berner (1970). In addition, Rickard (1997) pointed out that pyrite formation through the oxidation by HS^- is thermodynamically favored:

$$FeS_{(s)} + HS^-_{(aq)} + H^+_{(aq)} \rightarrow FeS_{2(s)} + H_{2(g)} \qquad (5)$$

In contrast to the intermediate iron sulfides pyrrhotite ($Fe_{x-1}S$) and greigite (Fe_3S_4), the iron disulfide pyrite is paramagnetic and therefore has a low magnetic susceptibility and does not contribute to the remanent magnetization of a sediment. Because both pyrite and marcasite are paramagnetic, we term all iron disulfides as pyrite for simplicity. Thus, the dissolution of magnetite and the precipitation of pyrite would cause a strong decrease in magnetic susceptibility. Such a decrease of the magnetic signal can be observed in the susceptibility (κ) at all three sites (Fig. 4).

3.3   Magnetic Susceptibility Profiles

We have explained the mechanisms of alteration of iron (oxyhydr)oxides to iron sulfides within the zone of AOM, but we still have to explain the occurrence of iron (oxyhydr)oxides below the SMT. We assume that there are only a few possible processes that can cause a decrease of iron (oxyhydr)oxides limited to the zone of AOM and that leads to a localized minimum in magnetic susceptibility.

One process would be the reoxidation of ferrous iron below the sulfidic zone. The oxidation could be driven by Mn(II) released during reduction of Mn-oxides (Aller and Rude, 1988; Postma and Appelo, 2000; Schippers and Jørgensen, 2001). This process could explain the existence of iron (oxyhydr)oxides below the SMT where no hydrogen sulfide is present. Detailed rockmagnetic and SEM analyses performed on magnetic minerals of samples from core GeoB 6229-6 by Garming et al. (2005) reveal that the magnetic mineral assemblages above and below the zone of AOM are similar and that the authigenic formation of iron oxides can therefore be excluded.
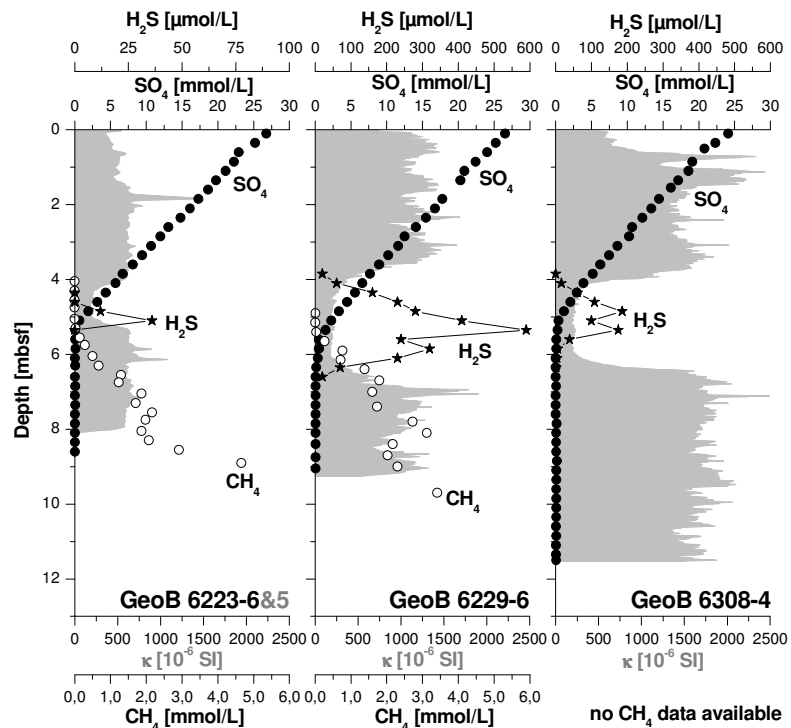
Fig. 4. Sulfate (solid circles), methane (open squares) and sulfide (solid stars) pore water profiles (pore water data of methane, sulfate and sulfide of core GeoB 6223-6 and of sulfate of core GeoB 6229-6 taken from Hensen et al., 2003) and the magnetic susceptibility (gray area) (note that the offset in GeoB 6223-5 is probably due to the measurements coming from a parallel core). Except for the primary decrease in the magnetic susceptibility at the top of the core GeoB 6308-4, due to the dilution by higher carbonate concentrations, the decrease in susceptibility is restricted to the sulfidic zone.

Another process that could potentially cause a distinct loss in magnetic susceptibility in the zone of AOM is a variation in the parameters controlling the position of the SMT. The depth at which the SMT established is driven mainly by the upward flux of methane and the downward diffusion of sulfate, which is directly influenced by the SR. We simulated different scenarios with the numerical model CoTReM to investigate whether a constant SR alone can lead to the observed profiles of magnetic susceptibility. Under steady-state conditions prevailing over a long period of time, with continuous sedimentation and no change in the upward flux of methane, the zone of AOM would keep a fixed offset to the sediment surface (Borowski et al., 1996; Kasten et al., 2003). This process would lead to a continuous reduction of iron (oxyhydr)oxides within the SMT and below. The degree of reduction to which every sediment layer is subject would thereby be coupled to the rate at which the zone of AOM moves upward as a function of SR. The dissolution rate is dependent on the reactivity of the iron (oxyhydr)oxides and their grain size, and the time period over which they are in contact with hydrogen sulfide (Pyzik and Sommer, 1981; Karlin and Levi, 1983, 1985; Canfield and Berner, 1987; Canfield, 1992; Roberts and Turner, 1993).

Table 2. Parameters used in the modeling of magnetic susceptibility profiles for different sedimentation rates.

Parameters		
Model area[a]:	20 m	
Cell discretization:	5 cm	
Time step:	1×10^{-1} yr	
Sediment porosity:	75%	
Temperature:	2 °C	
Input concentration		
Magnetite (Fe_3O_4):	1 wt%	
	Upper boundary	Lower boundary
Sulfate (SO_4^{2-}):	26 mmol L^{-1}	0 mmol L^{-1}
Methane (CH_4):	0 mmol L^{-1}	45 mmol L^{-1}

[a] The model area is the sediment column incorporated in the approach

Hensen et al. (2003) give a detailed description for reaction kinetics of hydrogen sulfide with a continuum of different Fe(III)-phases. The reaction rates are sensitive to dissolved Fe and HS⁻ in the model approach because HS⁻ is involved in two reactions

(Eqns. 3 and 4). For simplicity, we consider only magnetite (Fe_3O_4) and adapt a maximum reaction rate of 3×10^{-5} mol L^{-1} yr^{-1} to account for the measured hydrogen sulfide concentration compared to rates between 5.5×10^{-6} mol L^{-1} yr^{-1} and 1.2×10^{-4} mol L^{-1} yr^{-1} in Hensen et al. (2003). The initial concentration of Fe_3O_4 is set to 1 wt%, which is reduced to iron monosulfide (FeS) in the sulfidic zone. A compilation of input parameters for all simulation runs is given in Table 2, where the lower boundary is defined at a model depth of 20 m (whereas the figures are only displayed to a depth of 13 m). During simulation of a relatively low mean SR of 5 cm kyr^{-1} (Fig. 5a), the SMT moves slowly upward, resulting in a complete transformation of the initially present magnetite into iron sulfides (Fig. 5b). In contrast, more rapid sedimentation can lead to the preservation of a considerable amount of magnetic iron oxides and therefore to a preservation of the magnetic record, as also discussed by Canfield and Berner (1987). Model runs with a high SR of 200 cm kyr^{-1} result in a fast burial of magnetite (Fig. 6a), with reduction of only a small amount (~1/5) of Fe_3O_4 (Fig. 6b). These model runs demonstrate that the observed patterns cannot be formed under conditions of constant mean SR.
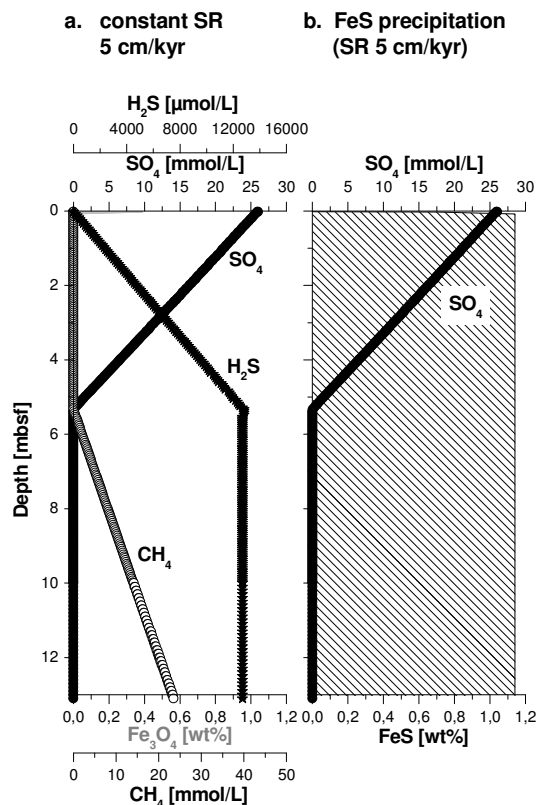
Fig. 5. Modeling results for diagenetic alteration of magnetite to iron monosulfide. (a) Sulfate, methane and sulfide profiles at a constant SR of 5 cm kyr^{-1}. (b) All iron (oxyhydr)oxides are altered into iron monosulfides.

Different scenarios were modelled to assess the influence of variations in depositional and/or geochemical conditions on the position of the SMT. A sudden increase in the upward methane flux would push up the SMT and result in a concave-up sulfate pore water profile (Hensen et al., 2003; Kasten et al., 2003). At a constant high mean SR, this concave-up profile would remain and the observed linear sulfate profile would not be seen. At low mean SR, the SMT would move rapidly upwards owing to the increased methane flux until a new steady state with a linear sulfate pore water profile is regained. But, as shown in the simulation of constant mean SR (Fig. 5a), at a low SR all available reactive iron (oxyhydr)oxide would be altered and thus the increased methane flux would not produce the observed localized magnetic susceptibility minimum.
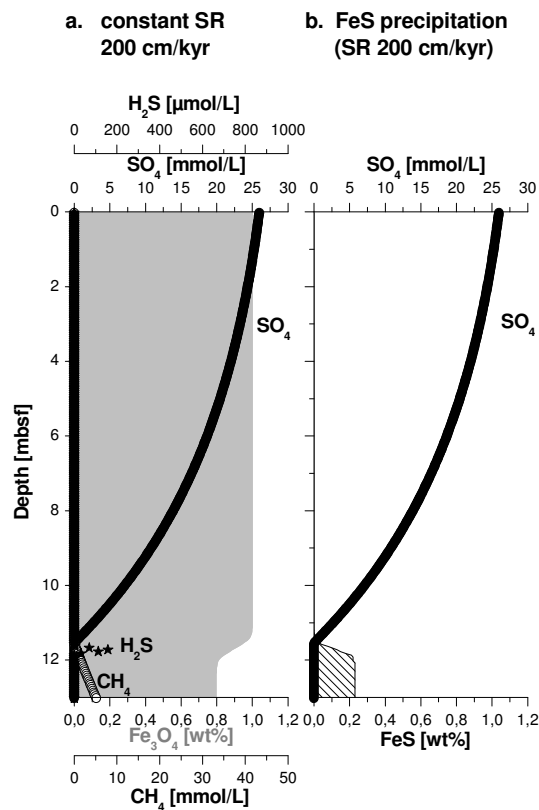
Fig. 6. Model results for a constant mean SR of 200 cm kyr^{-1}. (a) The high mean SR leads to a good preservation of magnetite below the SMT. The pore water profile of sulfate shows a concave-up shape. (b) Only a small amount of iron sulfide is precipitated in this scenario.

After demonstrating that variations in the upward methane flux alone cannot produce the observed patterns, we simulated the effect of changing mean SR. Kasten et al. (1998) demonstrated that the strong decrease in SR for the Amazon Fan sediments as a consequence of the glacial/interglacial transition was responsible for the fixation of the

SMT for a prolonged period of time. To test whether the observed profile of magnetic susceptibility could be explained by a drastic decrease in mean SR, we modeled scenarios of different mean SR with a constant flux of methane over time. The history of sedimentary events for the three studied sites are not known in detail. We therefore assume, as the starting condition for the model, a high mean SR of 100 cm kyr^{-1}. This mean SR includes all possible mechanisms of sediment deposition. This mean SR is sufficiently high to limit the contact time between the iron oxides and the sulfidic pore water, and thus to alter only one third of the initially present iron oxides into iron sulfides. With a subsequent decrease in the rate of sedimentation to ~5 cm kyr^{-1}, estimated from CaCO$_3$ concentrations in the solid phase (see section 3.1), the SMT moves upwards until a steady-state is regained (Fig. 7b). In this scenario, there is a complete transformation of all available iron oxides to iron monosulfides in the SMT and subsequently in the expending zone of excess hydrogen sulfide (Fig. 7c). This process causes a pronounced loss in magnetic susceptibility in a particular sediment interval. The time needed for the complete conversion of magnetite into iron sulfides in an interval of 2 m (e.g., GeoB 6308-4) is ~8,000 yrs. Although the results of our approach are strongly dependent on the boundary parameters, the estimation correlates well with a change in mean SR at the glacial/interglacial transition.

A further interesting finding of the simulation is the concave-up sulfate profile at high constant mean SR. This shape of sulfate profile has previously been described for nonsteady-state conditions such as an increased methane flux (Kasten et al., 2003), upward-directed advective flow (e.g., Aloisi et al., 2004) and transient diagenesis after a sedimentary event has occurred (Hensen et al., 2003). An example of a transient event is a single slide event, which results in a kink-type profile (de Lange, 1983; Zabel and Schulz, 2001) that is smoothed to a concave-up profile by diffusion. As shown by our model outcome, the concave-up sulfate profile can also result from high mean SR under steady-state conditions. This could be explained by the high sulfate accumulation compared with the diffusion flux of sulfate.

3.4   Solid Phase Enrichment of Iron and Sulfur

For core GeoB 6308-4, the solid phase profiles of total iron and total sulfur (Fig. 8) indicate an enrichment of iron sulfides between 6 and 7 mbsf. Similar solid phase peaks of total iron and sulfur are found at site GeoB 6223, where XRD analyses of the sample taken at 525 cm prove the presence of pyrite (2.5 wt%). The accumulation of authigenic iron sulfides within the distinct interval could be explained by diffusion of ferrous iron from below reacting with hydrogen sulfide (e.g., Kasten et al., 1998). At site GeoB 6223,

ferrous iron is detected in pore water directly below the solid phase iron enrichment (Fig. 8). Another explanation for the enrichment of iron in the solid phase could be the consequence of an initial enrichment of iron (oxyhydr)oxides at this particular layer due to a sedimentary event. The iron (oxyhydr)oxides will be reduced and the ferrous iron can be transformed directly into iron sulfide. As the enrichment of total iron and sulfur in core GeoB 6308-4 is located below the distinct susceptibility minimum, we suggest that the reduction of the magnetic minerals ((titano-)magnetite) has not yet taken place and only the more reactive iron phases have been reduced.
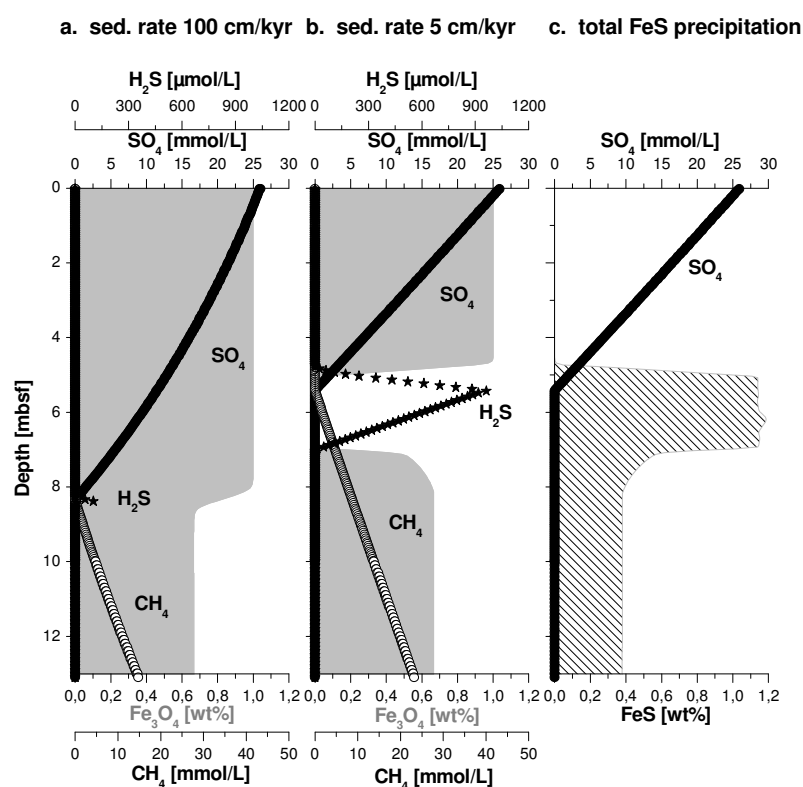
Fig. 7. Modeling results for diagenetic alteration of magnetite to iron monosulfide with a major change in mean SR (for sediment porosity of 75%). (a) A mean SR of 100 cm kyr^{-1} leads to reduction of only about one third of the Fe_3O_4. (b) If the mean SR is decreased down to 5 cm kyr^{-1}, a time interval of ~8,000 years is needed to reduce the total amount of magnetite for an interval of 2 m. (c) The cross-hatched area indicates the total amount of precipitated monosulfides for the modeled scenario with change in mean SR.

Under the premise of a decrease in mean SR, and hence a fixation of the zone of AOM for a specific length of time, we calculated the time needed to produce the total amount of solid phase sulfur in sediments of site GeoB 6223 at 525 cm and site GeoB 6308 at 625 cm. The calculation is described in detail by Kasten et al. (1998). We

simulated the enrichment of solid phase sulfur by downward diffusion of sulfate, assuming that the sulfur contained in the solid phase was fixed owing to the precipitation of iron sulfide as a result of hydrogen sulfide liberated by AOM. Assuming a linear sulfate pore water profile over the whole time of iron sulfide formation, the flux of pore water sulfate is calculated using Fick's first law, with a diffusion coefficient in free solution (D_0) for sulfate of 165 cm^2 yr^{-1} (after Iversen and Jørgensen, 1993). The sediment dry density averages 2.2 g cm^{-3}, and the temperature is 2°C. The presumed mean Holocene SR amounts to 5.0 cm kyr^{-1}. If we assume a porosity of 70% for the sediment of core GeoB 6223-6 and 75% for core GeoB 6308-4, the time needed to produce the measured sulfur peak would be ~9,000 yrs. This calculated result is in good agreement with the outcome of the model above.
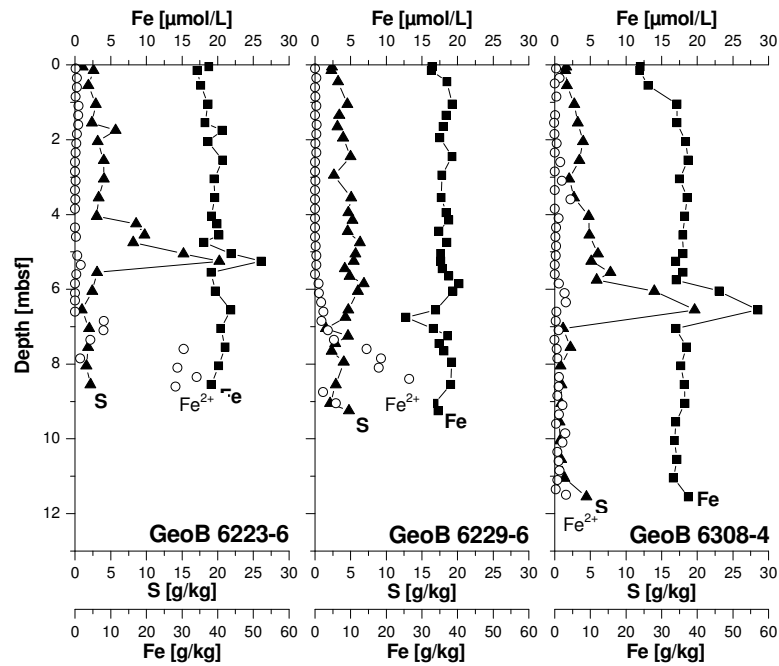
Fig. 8. Total sulfur (solid triangles) and total iron (solid squares) concentrations of the solid phase. Correlation of the iron and sulfur peak at site GeoB 6223 and GeoB 6308 indicates an iron sulfide enrichment. The iron minimum in the sediment of core GeoB 6229-6 correlates with a turbidite sequence. Open circles indicate the ferrous iron in the pore water.

Based on the model results, we suggest that the only scenario that produces the observed localized loss in magnetic susceptibility is a nonsteady-state diagenetic scenario involving a drastic decrease in mean SR, from a few hundred cm to ~5 cm per 1000 yrs, during the Pleistocene/Holocene transition leading to a fixation of the SMT for a period of 8000 to 9000 yrs.

4   Conclusions

A marked localized minimum in magnetic susceptibility in distinct sediment intervals of Argentine Basin deposits is observed, which correlates with the current position of the SMT. To explain the diagenetic impact of AOM on magnetic susceptibility, we modeled different geochemical and depositional scenarios. The model results indicate that the depletion of iron (oxyhydr)oxides and the resulting strong decrease in magnetic susceptibility within the sulfidic zone around the current depth of the SMT is an effect of the rather low and constant mean SR since the beginning of the Holocene, compared with the high mean SR of one to several meters per kyr during the last Glacial. The drastic change in mean SR results in a fixed or slow-moving SMT, which increases the time of contact between iron (oxyhydr)oxides and the liberated hydrogen sulfide, leading to enhanced dissolution of iron (oxyhydr)oxides and formation of the paramagnetic iron sulfide pyrite in this particular sediment layer. Furthermore, the results of the model indicate that a constant high mean SR is able to cause a concave-up pore water sulfate profile. Such concave-up sulfate profiles have been previously interpreted to result from either nonsteady-state depositional conditions or upward-directed advective flow. In the scenarios we have modeled, the concave-up sulfate profile would be a steady-state case. A low mean SR with a fixation of the SMT is necessary to produce an enrichment of iron and sulfur in the solid phase, as can be found in the sediment at site GeoB 6223 and site GeoB 6308. We calculated the time needed to produce the total amount of sulfur in the solid phase to be ~9,000 yrs, which corresponds very well with the estimation of the model and the Pleistocene/Holocene transition.

However, the stagnation of the SMT caused a loss of magnetic signal by diagenetic destruction of magnetite due to AOM. Another influence of AOM on sediment magnetism can be, e.g., a magnetic enhancement via growth of greigite. This important but different magnetic effect was described by Neretin et al. (2004). The two effects are both results of similar processes, except that pyritization seems to have been arrested in the study by Neretin et al. (2004), which has led to preservation of greigite nodules with magnetizations 10-100 times greater than surrounding sediments. The net result is that nonsteady-state diagenesis can have varying effects on the magnetic record. Thus, diagenentic transformation of iron oxides to iron sulfides in the zone of AOM that corresponds to a loss and new formation of magnetic signals should be considered in the interpretation of magnetic records.

Acknowledgements

Chapter 2.3   Alteration of Magnetic Mineralogy at the Sulfate Methane Transition: Analysis of Sediments from the Argentine Continental Slope

Abstract

On the Argentine continental slope off the Rio de la Plata estuary, the sulfate-methane transition (SMT) has been encountered at shallow depths of a few meters below the seafloor. At around this horizon, where sulfate diffusing downward from the bottom water is met and reduced by methane rising from deeper in the sediment column, intense alteration affects the detrital magnetic mineral assemblage. Less than 10% of the dominant primary low coercivity ferrimagnetic (titano-)magnetite remains after alteration. In the upper part of the suboxic environment, underlying the iron redox boundary, which is located at a depth of ~0.1 m, approximately 60% of the finer grained detrital fraction is already dissolved. While the high coercivity minerals are relatively unaffected in the suboxic environment, large portions (> 40%) are diagenetically dissolved in the sulfidic SMT zone. Nevertheless, the characteristics of the magnetic residue are entirely controlled by a high coercivity mineral assemblage. Unlike common observations, that diagenetic alteration produces coarser magnetic grain-sizes in suboxic milieus, a distinct overall fining is found in the sulfidic zone. Different factors should contribute to this effect. Scanning electron microscope analysis, combined with X-ray microanalysis, identified fine grained (titano-)magnetite preserved as inclusions in silicates and between high Ti titanohematite lamellae, and possibly of prime importance, a comprehensive fragmentation of larger grains in the course of maghemitization. The only secondary iron sulfide mineral detected is pyrite, which is present as clusters of euhedral crystals or directly replaces (titano-)magnetite. The thermomagnetic measurements did not provide evidence for the presence of ferrimagnetic sulfides such as greigite. Different from other studies reporting a marked magnetic enhancement at around the SMT due to the precipitation and preservation of such metastable ferrimagnetic sulfides, a complete pyritization process will cause a distinct magnetic depletion, like in the present case.

1   Introduction

Microbially mediated degradation of particulate organic matter drives both the iron and sulfur cycles in marine sediments (Goldhaber and Kaplan, 1974; Froelich et al., 1979). In suboxic milieus, the diagenetic dissolution of primarily ferrimagnetic (titano-)magnetite iron oxides around the iron redox boundary is a common phenomenon that has been intensively studied (e.g., Karlin and Levi, 1983; Canfield and Berner, 1987; Karlin, 1990a; Karlin, 1990b; Canfield et al., 1992; Dekkers et al., 1994; Tarduno and Wilkison, 1996; Robinson et al., 2000; Passier et al., 2001; Larrasoaña et al., 2003; Reitz et al., 2004). This process affects the paleomagnetic signal with varying intensity and may jeopardize the validity of paleofield directional and intensity data (e.g., Channell and Hawthorne, 1990; Channell and Stoner, 2002).

In anoxic environments, which are typical of deeper strata, the hydrogen sulfide $\left(H_2S\right)$ needed for the formation of (iron) sulfides is produced by the biogenic reduction of sulfate $\left(SO_4^{2-}\right)$, either by degradation of organic matter or by oxidation of methane $\left(CH_4\right)$. Boetius et al. (2000) found that in sediments containing gas hydrates, sulfate reducing bacteria form aggregates with archaea that oxidize methane. The coupled sulfate-methane reaction is proposed to proceed according to the following equation assuming a one-to-one stoichiometry (Niewöhner et al., 1998):

$$CH_4 + SO_4^{2-} \rightarrow HCO_3^- + HS^- + H_2O \,.$$

The depth of this sulfate-methane reaction, called the sulfate-methane transition (SMT), depends on the penetration depth of seawater sulfate into the sediments and on the intensity of the methane flux from deeper sediment layers. Borowski et al. (1996) proposed that sulfate pore water profiles with constant gradients above the transition zone are indicative of anaerobic oxidation of methane (AOM) controlling the sulfate reduction.

Numerous pore water profiles from the Argentine continental slope show approximately linear sulfate gradients to unusually shallow penetration depths of about 4 to 6 m (Bleil et al., 1994; Schulz et al., 2001; Hensen et al., 2003; Riedinger et al., 2005). At around the SMT, magnetic susceptibility, which is routinely measured directly after core recovery on board the research vessel, exhibits pronounced minima. Susceptibility is characteristically reduced by 80% or more over depth intervals of several meters relative to the sedimentary layers above and below, indicating large-scale alteration of the magnetic mineral assemblage. In Fig. 1, the shaded area in front of the Rio de la Plata estuary, ranging from about 1500 to 4000 m water depth, outlines the region where such

'susceptibility gaps' have been observed (Bleil et al., 1994; Bleil et al., 2001; Schulz et al., 2001). They are thought to ultimately result from a depth fixation of the SMT for a prolonged period of time, with intense magnetic iron oxide dissolution occurring at around the SMT (Riedinger et al., 2005). A marked change from high sedimentation rates during the last glacial period to low Holocene accumulation has been proposed to be the cause of a rapid rise of the SMT from deeper positions and its stagnation at the present horizon, after which steady state conditions for the sulfate-methane reaction were established (Kasten et al., 1998; Riedinger et al., 2005).

Sparse information is currently available about diagenetic alteration of magnetic oxides/hydroxides and the potential formation of magnetic iron sulfide minerals in SMT environments. This topic will be discussed here on the basis of comprehensive rock magnetic analyses and scanning electron microscope (SEM) analysis combined with X-ray microanalyses for sediments from the Argentine continental slope.
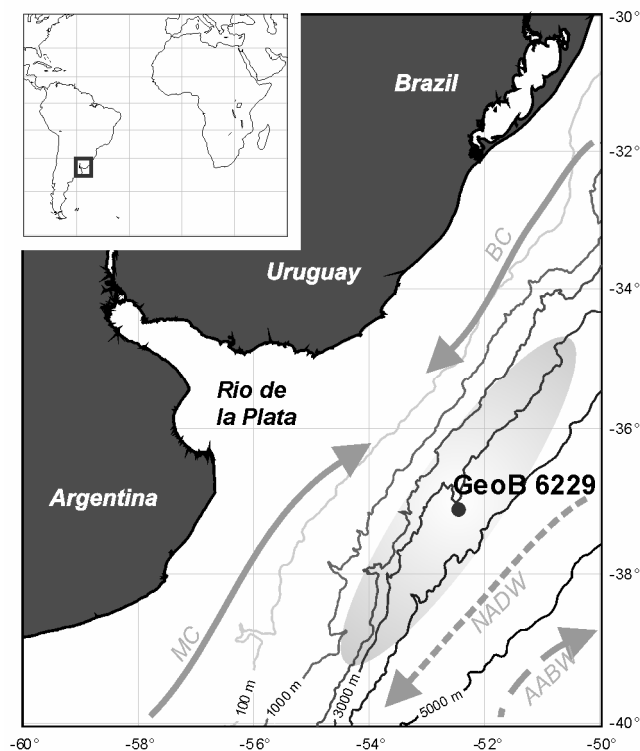
Fig. 1. Map of the South American continental margin off the Rio de la Plata estuary. Arrows indicate simplified main flow paths of surface (MC - Malvinas Current, BC - Brazil Current), deep (NADW - North Atlantic Deep Water) and bottom (AABW - Antarctic Bottom Water) water masses. Shading around the core site GeoB 6229 outlines the area where distinct 'susceptibility gaps' were found in the sedimentary deposits (see text). Isobaths at 1000 m intervals, including the 100 m isobath, are according to GEBCO. (redrawn after Frenz et al., 2004).

2   Study Area

The highly dynamic sedimentation processes along the Argentine continental margin are controlled by strong surface and bottom water currents as well as gravity driven mass flows. The fluvial load discharged by a number of large and small rivers is generally not deposited near the coast, but is transported to deeper water by offshore currents and turbidites (Ewing et al., 1964). Post-glacial sedimentation rates of around 25 to 50 cm/kyr on the shelf and continental slope (Haese, 1997) and 0.5 to 5 cm/kyr in the western abyssal plain region (Stevenson and Cheng, 1969; Ewing et al., 1971) have been reported. Fine grained sediment components are known to be transported far into the central basin by bottom currents, which produce massive nepheloid layers, drift deposits and mudwaves (Ewing et al., 1971; Ledbetter and Klaus, 1987; Manley and Flood, 1993; Richardson et al., 1993).

Modern oceanographic studies differentiate more than eight individual water masses along the western boundary of the South Atlantic (e.g., Memery et al., 2000; Frenz et al., 2004). Sub-Antarctic waters (SAW) and subtropical waters (STW) are present in the upper 500 m of the water column. Combined with Antarctic Intermediate Water (AAIW), which flows in the depth interval from about 500 to 1500 m, SAW forms the Malvinas (Falkland) Current (MC), and STW forms the Brazilian Current (BC). In the area of the Rio de la Plata estuary, these currents merge in the Malvinas-Brazil Confluence (MBC) and are deflected to the southeast. In the depth range from 2000 to 4000 m, North Atlantic Deep water (NADW) flows southward as far as 45ºS. Below, northward directed Antarctic Bottom water (AABW) forms a strong contour current (Fig. 1).

The sediments investigated were recovered in a gravity core at station GeoB 6229 (37°12.4'S / 52°39.0'W) during R/V Meteor Cruise M46/2 (Schulz et al., 2001) from a water depth of 3446 m in front of the Rio de la Plata estuary (Fig. 1). The suspended load of its two major tributaries, the Uruguay and Paraná rivers, is dominated by clays. These loads are carried away to the north, forming a sedimentary tongue parallel to the coast of Uruguay (Ewing et al., 1964; Frenz et al., 2004), whilst the coarser fraction is transported directly down slope. Relatively coarse grained sediments were therefore retrieved at station
GeoB 6229, which predominately consist of lithogenic components. XRD analyses (Riedinger et al., 2005) indicate that some 90% of the deposits are composed of quartz, feldspar and phyllosilicates. Considering the drainage areas of the Uruguay and Paraná rivers, the detrital magnetic mineral component of the sediment should primarily originate from the Paraná volcanic province. While calcium carbonate concentration is low (< 5 wt%), relatively high amounts of organic carbon, about 1.1 wt% in the top layers and

overall on average 0.7 wt%, provide evidence for elevated regional marine biologic productivity.

3   Laboratory Procedures

4.1   Sampling

Sediments from the 9.27 m core GeoB 6229 mostly consist of uniform olive green-gray mud with increasing numbers of black spots at greater depths. Upon recovery, the sediments smelled strongly of H_2S.

For shipboard pore water analysis and subsequent shore-based geochemical and rock magnetic investigations, the sediments were sampled at 10 to 20 cm intervals. A supplementary series of cube specimens (6.2 cm^3) was taken exclusively for rock magnetic purposes.

4.1   Geochemical and Rock Magnetic Analyses

Shipboard pore water measurements comprised quantification of SO_4^{2-}, CH_4, H_2S and Fe^{2+}. Solid phase analyses and sequential iron extraction were subsequently performed in the University of Bremen laboratories. An overview of the experimental methods is available at http://www.geochemie.uni-bremen.de/links.html (for more detailed information see: Schulz et al., 1994; Haese et al., 1997; Niewöhner et al., 1998; Hensen et al., 2003; Riedinger et al., 2005).

Hysteresis and thermomagnetic cycling experiments, as well as magnetic mineral separation extracts, were made on freeze-dried splits of the geochemical samples. Miniature specimens for hysteresis measurements were prepared with a technique described by von Dobeneck (1996), while the routine of Petersen et al. (1986) was applied for magnetic mineral extraction.

Magnetic hysteresis measurements limited to a maximum field of 0.3 T were performed with a *PMC* M2900 alternating-gradient force magnetometer. For data processing, the program 'Hystear' (von Dobeneck, 1996) was used to determine mass specific saturation magnetization σ_S and remanent saturation magnetization σ_{rs}, coercive force B_c and remanent coercivity B_{cr}, all of which specify characteristics of the ferrimagnetic (titano-)magnetite mineral components. Additionally, the non-ferromagnetic susceptibility χ_{nf}, which quantifies paramagnetic and diamagnetic contributions of the

sedimentary matrix to susceptibility, has been inferred from these measurements with an approach-to-saturation analysis (von Dobeneck, 1996).

For 10 selected samples, thermomagnetic runs to maximum temperatures of 720°C were performed with a modified horizontal translation type Curie balance (Mullender et al., 1993) on 20 to 30 mg of bulk sediment weighed into a quartz glass sample holder open to air and held in place by quartz wool. Heating rates were 10°C per minute, while cooling rates were 15°C per minute.

Magnetic extracts of the same 10 selected samples were molded into epoxy resin for SEM analysis. Thin sections were examined and photographed with a XL30 *SFEG* instrument. X-ray microanalysis was performed with an Energy Dispersive Spectroscopy (EDS) detector unit.
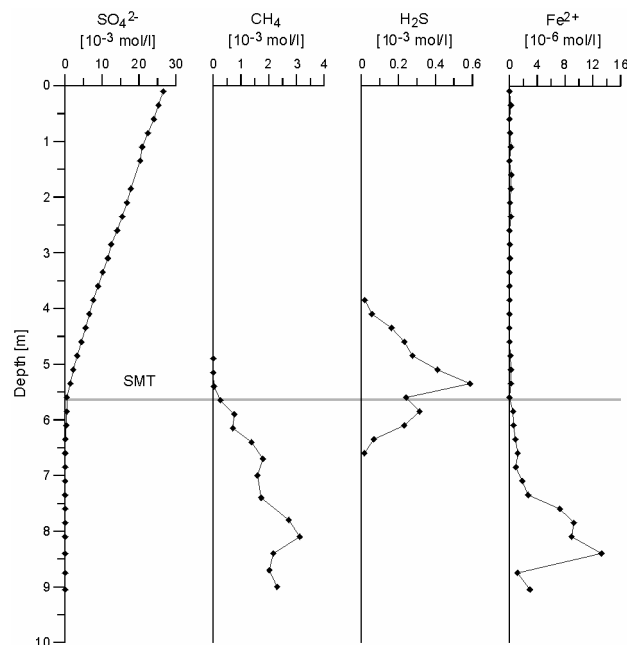
Fig. 2.   Sulfate, methane, sulfide, and iron pore water profiles as measured directly after recovery of the sediments. The horizontal line indicates the approximate position of the sulfate-methane transition (SMT). Data are taken from Riedinger et al. (2005).

Magnetic susceptibility per volume κ was determined at 1 cm spacing on the split sediment surface of core GeoB 6229 archive halves using a *Bartington Instruments* MS2 F sensor. Bulk rock magnetic measurements were accomplished on cube specimens taken at an average of 5 cm depth intervals. Incremental acquisition of isothermal remanent magnetization (M_{IR}) to 0.3 T and incremental acquisition of anhysteretic remanent magnetization (M_{AR}), imparted by superimposing a gradually decaying

alternating field (AF) of 0.3 T maximum amplitude to a constant bias field of 40 T was followed by systematic (18 steps) AF demagnetization to a maximum field of 0.3 T. All remanences were measured on a *2G Enterprises* 755R DC SQUID cryogenic magnetometer system. The various applied fields were generated with its built-in facilities. A number of specific rock magnetic parameters that characterize the ferrimagnetic (titano-)magnetite mineral fraction were deduced from these data sets, including the median acquisition field, $B_{1/2}$ M_{IRA}, and the median destructive fields $B_{1/2}$ M_{AR} and $B_{1/2}$ M_{IR}.

To estimate high coercivity hematite/goethite concentrations from the hard isothermal remanent magnetization M_{HIR} (Stoner et al., 1996), detailed M_{IR} acquisition was continued to 2.5 T, the maximum field available for an external *2G Enterprises* 660 pulse magnetizer. At this stage, a 0.3 T backfield was applied. M_{IR} acquisition data were also used to perform a component analysis with a modified version of the *Irmunmix 2_2* program developed by Heslop et al. (2002). Plotted against the logarithm of the acquisition field, incremental M_{IR} results in a simple sigmoid shaped curve, which is essentially a cumulative log Gaussian curve (or a combination of such curves) representing the coercivity distribution of the constituent magnetic mineral (Robertson and France, 1994; Kruiver et al., 2001). The *Irmunmix* software utilizes an expectation maximization algorithm to automatically separate M_{IR} contributions of (typically two or three) individual components.

4   Results

4.1   Geochemistry

Pore water analyses have identified the SMT at a depth of approximately 5.5 meters (Riedinger et al., 2005). The virtually linear decrease of sulfate from the top layers to this level (Fig. 2) indicates a dynamic equilibrium between downward sulfate diffusion and the methane flux rising from deeper sources (Borowski et al., 1996; Niewöhner et al., 1998; Hensen et al., 2003). Around the SMT, free sulfide generated by AOM is observed in the pore water. Gas hydrates were not encountered in the sediment sequence, but are likely to exist in deeper strata of the Argentine continental margin (Gornitz and Fung, 1994).

The presence of sulfide in the pore waters gave reason for subdividing the sediment sequence into three sections, (1) an upper part, from the top to 3.9 m, (2) a sulfidic zone ranging from 3.9 to 6.6 m and (3) a lower part, from 6.6 m to the bottom of the core at 9.27 m depth. In the upper part of the core and in the sulfidic zone, little to no iron $\left(Fe^{2+}\right)$ was

detected in the pore waters, whereas this redox sensitive element is present in the pore waters of the lower part of the core (Fig. 2). Solid phase analyses (shown in Riedinger et al., 2005) did not reveal an enhanced accumulation of Fe^{2+} in the sediments of the sulfidic zone, but they did indicate slightly elevated sulfur contents.
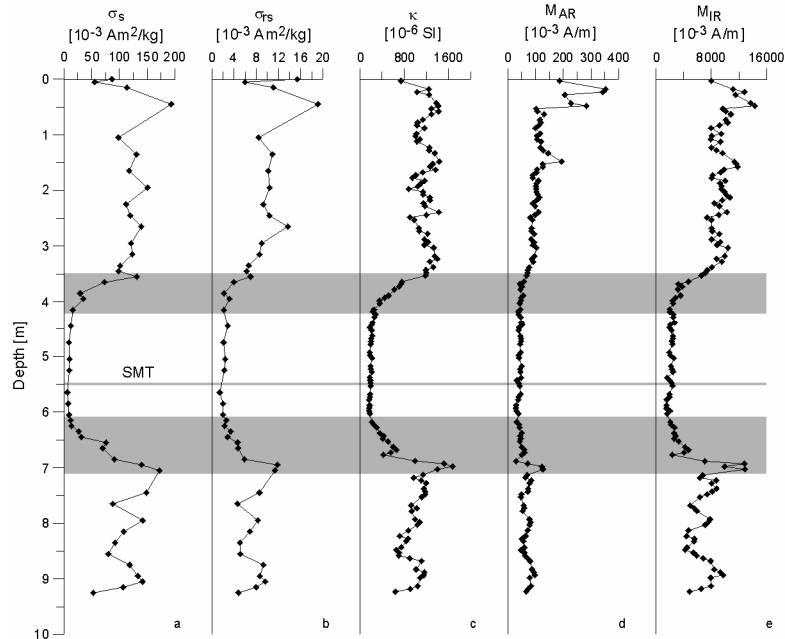
Fig. 3. Depth profiles of rock magnetic parameters that delineate variations in magnetic mineral content. Mass specific (a) saturation magnetization σ_s, and (b) remanent saturation magnetization σ_{rs}, volume specific (c) low field magnetic susceptibility κ (d) anhysteretic remanent magnetization M_{AR}, and (e) isothermal remanent magnetization M_{IR}. Gray shaded areas mark the transitions between the sulfidic zone and the upper and lower sediment series. The horizontal line indicates the approximate position of the sulfate-methane transition (SMT).

4.2 Magnetic Mineral Inventory

4.2.1 Mineralogy and Concentration

Variations in (titano-)magnetite content, delineated by the hysteresis parameters σ_s and σ_{rs} as well as M_{AR} and M_{IR} (all referring to peak fields of 0.3 T), are illustrated in Fig. 3, together with κ. Respective arithmetic means for the upper part, the sulfidic zone and the lower part of the sediment sequence are listed in Table 1. Note that the intervals from 3.5 to 4.2 m between the upper part and the sulfidic zone and from 6.1 to 7.1 m between the sulfidic zone and the lower part, where all magnetic properties exhibit strong gradients, have been excluded from these calculations.

Saturation magnetization σ_s, which is the only strictly grain-size independent measure of magnetic mineral concentration, displays a distinct decrease in the sulfidic zone to $9.4\cdot10^{-3}$ Am^2/kg compared to $118.5\cdot10^{-3}$ Am^2/kg and $110.4\cdot10^{-3}$ Am^V/kg in the upper and lower sediments, respectively (Fig. 3a). This more than 90% decrease is clearly indicative of reductive dissolution of the ferrimagnetic mineral fraction and corresponds to a similar, somewhat less pronounced decline in saturation remanence, σ_{rs} (Fig. 3b). It is also consistent with the susceptibility profile (Fig. 3c). Differences in these concentration related parameters between the sediments above and below the sulfidic zone are minor for σ_s (-7%), but are significant for σ_{rs}, (-29%) and κ (-17%). This likely hints at grain-size effects, namely the presence of higher amounts of fine to very fine grained (titano-)magnetite in the upper part of the core.

Single-domain (SD) and small pseudo-single-domain (PSD) crystals acquire the strongest anhysteretic remanent magnetizations (Banerjee et al., 1981). The decrease in M_{AR} intensity in the sulfidic zone, from on average $121\cdot10^{-3}$ A/m in the upper part, to $42\cdot10^{-3}$ A/m (Fig. 3d), is noticeably less pronounced than for M_{IR}, which quantifies the total ferrimagnetic mineral component (9476 to $2146\cdot10^{-3}$ A/m, Fig. 3e). In view of previous evidence, that fine grained magnetite undergoes diagenetic dissolution more rapidly than coarse grained magnetite due to its larger surface area to volume ratio, this apparent grain-size fining appears to be puzzling. As indicated by the sharp intensity decline in the M_{AR} profile (Fig. 3d), from a mean of $267\cdot10^{-3}$ A/m in the uppermost 0.5 m to $104\cdot10^{-3}$ A/m below, the principal reductive dissolution of the fine grained ferrimagnetic fraction appears to have already occurred in the top most part of the sediment column. It is associated with the modern iron redox boundary, which is located at ~0.1 m, although no characteristic change in color (Lyle, 1983) or conspicuous features in the pore water data (Fig. 2) were observed at around this level. In the suboxic environment, only 39% of the original fine grained ferrimagnetic fraction is left, as inferred from M_{AR}, compared to 77% of the coarser grained portion, as inferred from M_{IR}. In the sulfidic zone, 16% of the M_{AR} and 18% of the M_{IR} intensities remain. The persisting (titano-)magnetite minerals are presumably protected against diagenetic dissolution (e.g., as inclusions in a silicate matrix). Below the sulfidic zone, M_{AR} and M_{IR} increase to 69 and $6751\cdot10^{-3}$ A/m, respectively, corresponding to 26 and 56% of the intensities in the top layer of the core. This implies that diagenetic alteration has also affected the lower section of the core, possibly when the SMT rapidly ascended to its present horizon from a deeper position (Riedinger et al., 2005) and from that time on, while it was in an anoxic methanic environment.

Table 1. Average rock magnetic parameters for the upper part, the sulfidic zone and the lower part of the studied sediment sequence.

Parameter	Upper part	Sulfidic Zone	Lower part
σ_s (10^{-3} Am^2/kg)	118.5	9.4	110.4
σ_{rs} (10^{-3} Am^2/kg)	10.1	2.2	7.2
κ (10^{-6} SI)	1179	200	974
M_{AR} (10^{-3} A/m)	121.4	41.9	69.3
M_{IR} (10^{-3} A/m)	9476	2146	6751
M_{HIR} (10^{-3} A/m)	425	240	340
S Ratio	0.98	0.95	0.98
χ_{nf}/χ	0.03	0.40	0.05
B_c (mT)	8.2	18.3	6.6
B_{cr} (mT)	31.7	62.2	32.4
$B_{1/2}$ M_{AR} (mT)	30.2	57.0	37.1
$B_{1/2}$ M_{IR} (mT)	17.1	49.9	17.2
C1 $B_{1/2}$ M_{IRA} (mT)	39.0	42.2	37.2
C2 $B_{1/2}$ M_{IRA} (mT)	81.9	90.5	69.9
C3 $B_{1/2}$ M_{IRA} (mT)	1000	887	416
C1 % M_{IR}	57.9	11.7	54.0
C2 % M_{IR}	39.8	75.6	40.7
C3 % M_{IR}	2.3	12.7	5.3
σ_{rs}/σ_s	0.09	0.23	0.07
B_{cr}/B_c	3.98	3.45	4.90
M_{AR}/M_{IR}	0.01	0.02	0.01
κ_{AR}/κ	3.3	6.6	2.3

To evaluate variations in other magnetically relevant minerals, the hard isothermal remanent magnetization M_{HIR}, the S-ratio and the χ_{nf}/χ ratio were examined (Fig. 4, Table 1). M_{HIR} (Stoner et al., 1996) quantifies contributions of high coercivity iron oxides (hematite, hemoilmenite) and iron hydroxides (e.g., goethite) to the total remanence. In the upper part of the core, it amounts to on average $425 \cdot 10^{-3}$ A/m (Fig. 4a). Assuming a hematite to (titano-)magnetite saturation remanence proportion of 1:10, implies that hematite makes up approximately one third of the total magnetic mineral assemblage. This admittedly rough estimate nevertheless suggests a much lower hematite content than is generally observed in the South Atlantic, particularly in areas with significant deposition of eolian terrigenous material.

In the sulfidic zone, M_{HIR} drops by 44% to $240 \cdot 10^{-3}$ A/m, which indicates that high coercivity minerals are also diagenetically dissolved in this environment, although they are relatively more stable than the ferrimagnetic oxides, as was recently also shown by Yamazaki et al. (2003), Liu et al. (2004) and Emiroglu et al. (2004). Compared to the

upper part of the core, the 20% lower M_{HIR} in the sediments under the sulfidic zone suggests some minor diagenetic alteration. S-ratios calculated after Bloemendal et al. (1992) are on average 0.98 in the upper and lower sediment series (Fig. 4b) and confirm comparatively minor primary high coercivity mineral concentrations. Because of the drastically diminishing ferrimagnetic fraction in the sulfidic zone, the S-ratio drops to 0.95 and the relative content of high coercivity minerals increases to somewhat more than 50%.
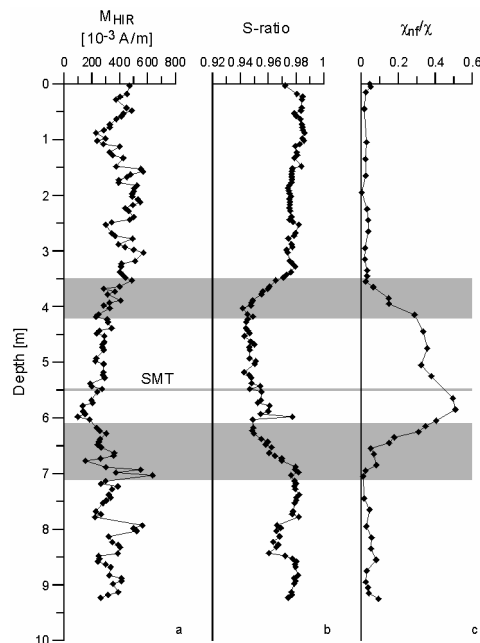
Fig. 4. Depth profiles of rock magnetic parameters that characterize variations in magnetic mineralogy. (a) Hard isothermal remanent magnetization M_{HIR} quantifies contributions of high coercivity iron oxides and hydroxides to the total remanence (Stoner et al., 1996), (b) the S-ratio provides an estimate of the relative proportions of hard and soft magnetic minerals (Bloemendal et al., 1992), (c) the χ_{nf}/χ ratio estimates paramagnetic sediment matrix contributions to the bulk magnetic susceptibility. Gray shaded areas mark the transitions between the sulfidic zone and the upper and lower sediment series. The horizontal line indicates the approximate position of the sulfate-methane transition (SMT).

The χ_{nf}/χ ratio (Fig. 4c), which provides an estimate of the contribution of non-ferrimagnetic sediment matrix constituents to bulk susceptibility, is successfully used to separate distinctly different depositional regimes or to delimit zones of diagenetic alteration (Frederichs et al., 1999). Continually low ratios of 0.03 and 0.05 are observed in the upper and lower parts of the core. In the sulfidic zone, substantially more iron is bound in paramagnetic compounds, the χ_{nf}/χ ratio increases to an average of 0.4 and reaches maxima of up to 0.5. This essentially records the combined effects of ferrimagnetic and

also of high coercivity mineral dissolution by reductive diagenesis and a concurrent precipitation of Fe-bearing paramagnetic minerals. As indicated by slightly enhanced sulfur concentrations in the solid phase (Riedinger et al., 2005), the formation of pyrite should be of particular importance in this respect.
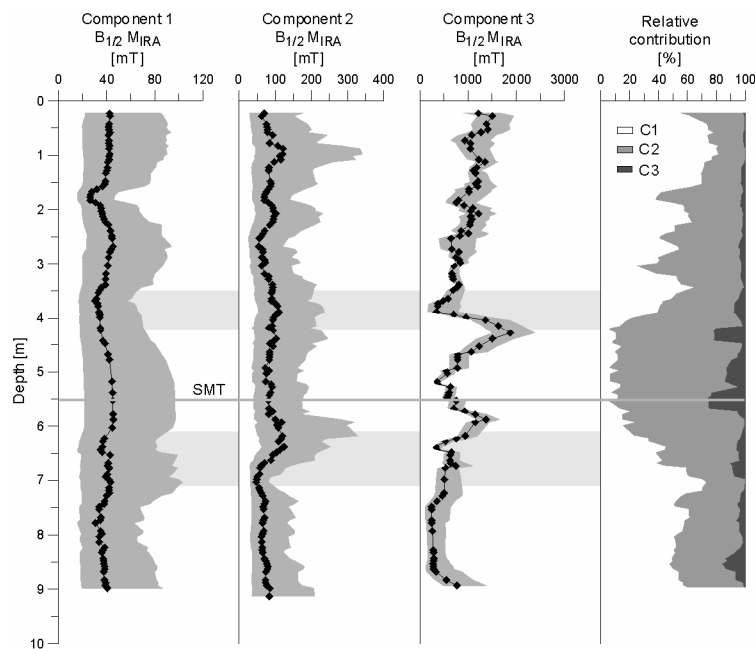
4.2.2 Coercivity and IRM Component Analysis

Depth profiles of coercivity parameters B_c and B_{cr} derived from hysteresis measurements to maximum fields of 0.3 T and medium destructive fields $B_{1/2}$ of M_{AR} and M_{IR} (both acquired in 0.3 T fields) reveal remarkably different patterns compared to the concentration indicative parameters (Fig. 5, Table 1). Coercivities are relatively low and show limited variability within the upper and lower parts of the sediment column. Strikingly higher coercivities in the sulfidic zone result in an approximately twofold increase of B_c, B_{cr} and $B_{1/2} M_{AR}$ and even an almost threefold increase of $B_{1/2} M_{IR}$.
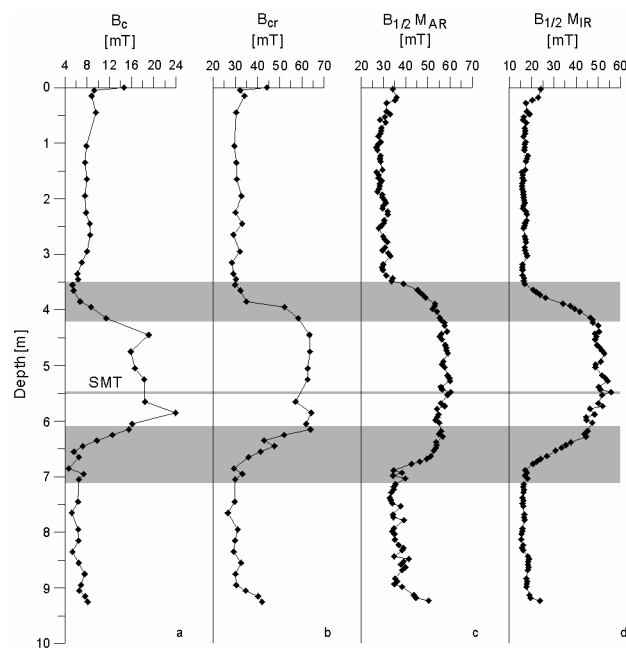
Fig. 5. Depth profiles of rock magnetic parameters that characterize variations in magnetic coercivity. (a) Coercive field B_c, (b) remanent coercive field B_{cr}, (c) median destructive field of the anhysteretic remanent magnetization $B_{1/2} M_{AR}$, and (d) median destructive field of the isothermal remanent magnetization $B_{1/2} M_{IR}$. Gray shaded areas mark the transitions between the sulfidic zone and the upper and lower sediment series. The horizontal line indicates the approximate position of the sulfate-methane transition (SMT).

All of these parameters can be used as sensitive indicators of grain-size provided that the mineralogy is reasonably uniform (Thompson and Oldfield, 1986). In this scenario, multi-domain (MD) grains have substantially lower coercivities than PSD or SD grains. Under the assumption of uniform mineralogy, the observed strong increase in coercivity in the sulfidic zone would imply a change to predominantly finer grained magnetic mineral assemblage, a conclusion that is not in agreement with the above discussed variations in M_{AR} and M_{IR}.

Fig. 6. Results of IRM component analysis. Black diamonds represent the 5-point mean, shading the standard deviation of coercivities obtained for a 3-component solution that discriminates a 'soft' (titano-)magnetite component, a 'hard' (titano-)magnetite/hematite component and a 'highest coercivity' goethite/hematite fraction. Variations in the relative contribution of individual components to the isothermal remanent magnetization are shown in the right-hand panel. Gray shaded areas mark the transitions between the sulfidic zone and the upper and lower sediment series. The horizontal line indicates the approximate position of the sulfate-methane transition (SMT).

To achieve more insight into this problem, an IRM component analysis has been performed to discriminate between magnetization components. The three component solution is illustrated in Fig. 6 and is summarized in Table 1. It results in a 'soft' component (C1), with an average half IRM acquisition field $B_{1/2} M_{IRA}$ of around 40 mT, in all three parts of the sediment column and should exclusively incorporate the (titano-)magnetite fraction. In the upper and lower sediment sections, where these minerals largely dominate the magnetic inventory, $B_{1/2} M_{IRA}$ of C1 plausibly corresponds to the bulk B_{cr} data. Considerably higher coercivities characterize the second component C2

for which average $B_{1/2} M_{IRA}$ of 82.0, 90.5 and 69.9 mT were determined in the upper part, the sulfidic zone and the lower part, respectively. Apparently, there is no straightforward interpretation of this 'hard' component in terms of an individual mineral fraction. Hematite of appropriate grain-size (Kletetschka and Wasilewski, 2002), but also titanomagnetites with higher titanium contents and/or elevated oxidation states could be the carrier of C2 which is therefore tentatively termed a hard (titano-)magnetite/hematite component. The second high coercivity constituent, labeled goethite/hematite component C3, since it should mainly reside in goethite possibly with some hematite contributions, displays a continuous trend of declining $B_{1/2} M_{IRA}$ with depth, averaging 1000, 887 and 416 mT in the upper part, the sulfidic zone and the lower part, respectively.

Relative contributions of the three components to the total isothermal remanent magnetization contrast in the different sediment sections. The soft (titano-)magnetite component C1 dominates in the upper and lower part and comprises 58 and 54%, respectively. In the sulfidic zone, it is reduced to on average only 12%. The opposite trend is found for the hard (titano-)magnetite/hematite component C2, which contributes about 40% in the upper and lower part of the core and 76% in the sulfidic zone. The high coercivity goethite/hematite component C3 is of minor importance, carrying only 2 and 5% of the total remanence in the upper and lower part of the core. It rises to on average 13% in the sulfidic zone, where it is highly variable. Compared to components C1 and C2, which should be reliably defined, several limitations may affect C3. Most important is the restriction to 2.5 T maximum fields, which is far too low to saturate goethite and hence to appropriately evaluate such a mineral fraction with the *Irmunmix* program. It should therefore not be regarded as a quantitative measure, but as an indication that such a high coercivity component is present in the sediments.

The IRM component analysis provides convincing evidence for a marked shift in coercivity associated with a change in predominant magnetic mineralogy between the upper and lower sediment series and the sulfidic zone. Preferential dissolution of the soft (titano-)magnetite component in the sulfidic zone leaves the hard (titano-)magnetite/hematite component as the principal carrier of remanence. Apparently, it also largely controls M_{AR}, M_{IR} and the hysteresis data (measured in maximum fields of 0.3 T).

4.2.3   Grain Size

The hysteresis parameter ratios $_{rs}/_{s}$ (Fig. 7a) and B_{cr}/B_{c} (Fig. 7b) are popular measures to characterize the bulk (titano-)magnetite grain-size distribution (Day et al., 1977; Dunlop, 2002). They indicate relatively coarse grain-sizes spectra above and below the sulfidic zone, where these minerals dominate. More MD-like data in the lower part

probably documents a relatively mild alteration that mainly affected the finer grained ferrimagnetic oxides. In the sulfidic zone, a mean of 0.23 for σ_{rs}/σ_s and 3.5 for B_{cr}/B_c (lowest B_{cr}/B_c are around 2.7) approach the medium PSD range suggesting an apparent grain-size fining.

The M_{AR}/M_{IR} and κ_{AR}/κ ratios (Figs. 7c and 7d), also widely used magnetic grain-size indicators (Maher, 1988; Heider et al., 1996), show slightly elevated concentrations of fine grained (titano-)magnetite in the uppermost layers. As already seen in the M_{AR} data, fine grained (titano-)magnetite disappears at a depth of 0.5 m, being dissolved in the suboxic environment below the iron redox boundary. M_{AR}/M_{IR} ratios and κ_{AR}/κ ratios confirm the coarse grained magnetic mineral inventory recognized in the hysteresis data. The same is true for the relatively finer grain-size spectra in the sulfidic zone, which is indicated by increasing M_{AR}/M_{IR} and κ_{AR}/κ ratios.
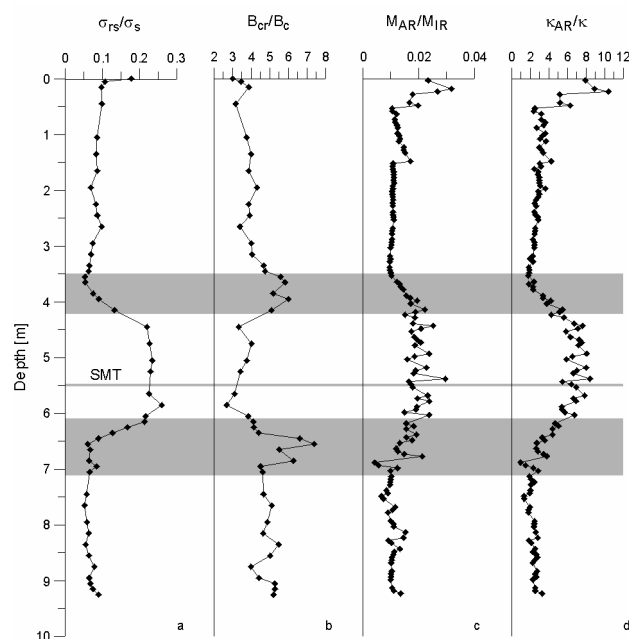

Fig. 7. Depth profiles of rock magnetic parameters that characterize magnetic grain-size variations. Bulk magnetogranulometric ratios of (a) saturation magnetization to saturation remanence σ_{rs}/σ_s, and (b) coercivity of remanence to coercive field B_{cr}/B_c, (c) M_{AR}/M_{IR}, and (d) κ_{AR}/κ ratios, which delineate variations in the fine grained magnetic fractions. Gray shaded areas mark the transitions between the sulfidic zone and the upper and lower sediment series. The horizontal line indicates the approximate position of the sulfate-methane transition (SMT).

The shift to smaller magnetic grain-sizes in an environment of strong diagenetic alteration is an unexpected result. Numerous reports in the literature and our own experience typically indicate the opposite trend. However, considering an initially coarse

grained iron oxide mineral assemblage, dissolution will inevitably result in overall finer grain-sizes. This process has necessarily affected the hard (titano-)magnetite/hematite component, which is by far the dominant magnetic mineral fraction in the sulfidic zone. Increasing coercivities in these sediments should therefore to some extent result from decreasing magnetic grain-sizes.

On the other hand, the possible diagenetic formation of magnetic iron sulfides, like greigite, could also be responsible for a fining of the magnetic grain-sizes (Roberts et al., 1999; Liu et al., 2004). In a recent study Neretin et al. (2004) identified two processes of diffusion limited pyrite formation surrounding the SMT. One involved the precipitation of a pyrite precursors including ferrimagnetic greigite.
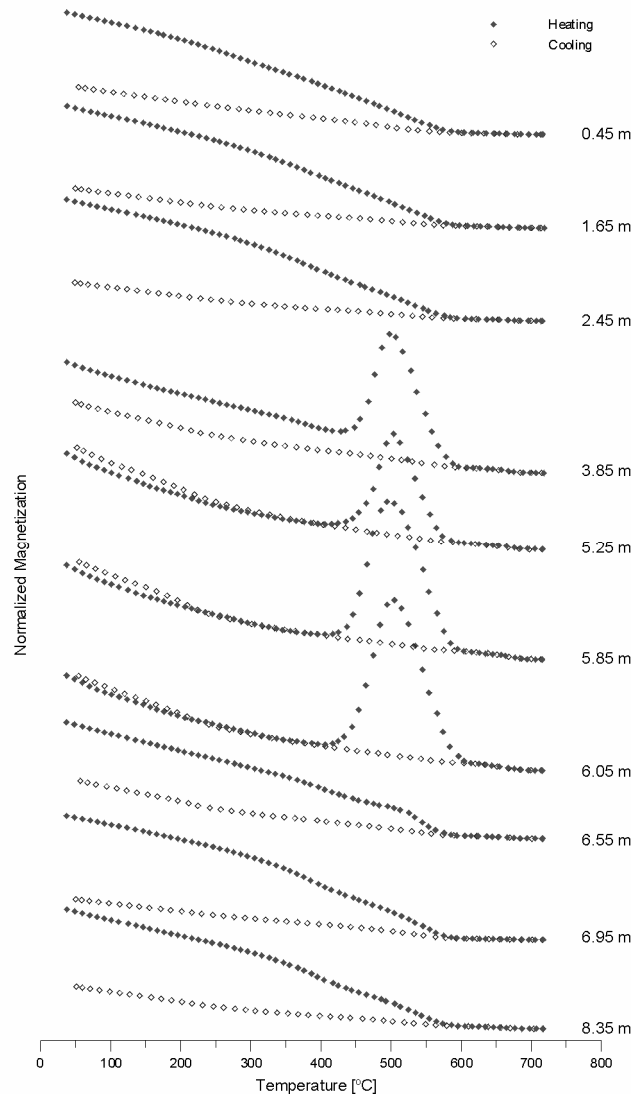
Fig. 8. Thermomagnetic cycles measured on a translation type Curie balance in air. Numbers on the right denote sample depths.

4.2.4   Thermomagnetic Analyses

Significant Curie temperatures in the upper and lower part of the sediment sequence are around 580ºC (Fig. 8), which identifies magnetite as the predominant magnetic phase. Minor inflections between 300 and 500ºC in the heating records hint at titanomagnetite with variable titanium content. The continuous decrease of magnetization upon heating may imply a broad range of titanomagnetite compositions. At 720ºC, the magnetic Fe oxides are largely destroyed in air, which produces much lower magnetizations during cooling.

In samples from the interval between 3.85 and 6.05 m pyrite was identified by its oxidation to magnetite, maghemite and finally to hematite, which causes an increase and subsequent decrease in magnetization (Fig. 8). The sulfide phase always oxidizes above 450ºC, suggesting that mostly euhedral pyrite is present (Passier et al., 2001). Thermomagnetic analyses of sediments from the sulfidic zone do not reveal any definite evidence of magnetic iron sulfide compounds like pyrrhotite or greigite.

4.3   Scanning Electron Microscopy

Figs. 9 and 10 include representative micrographs of magnetic extracts together with X-ray spectra from microanalyses at selected spots. The elemental spectra could not be quantitatively evaluated, but provide valuable information to differentiate iron sulfide phases as well as to assess variations in the titanium content of iron oxides. Throughout the sediment column (titano-)magnetite is present, both as individual crystals (Figs. 9a, 9b) and as intergrowths within silicates (Fig. 9c). Iron sulfides were only detected in the sulfidic zone (Figs. 10a to 10c), but nowhere above and below. Separate aggregates of sulfide minerals with uniform morphology and grain-size (Fig. 10b) striking resemble euhedral pyrite formed in laboratory experiments (Wang and Morse, 1996), which is consistent with conclusions from the thermomagnetic measurements.

Individual (titano-)magnetites are relatively large (commonly > 20   m). Evidence for their low temperature oxidation is ubiquitous; in places, shrinkage cracks fragment the grains. High temperature dissolution patterns are more abundant in the lower sediment layers. Although large individual crystals are still present in the sulfidic zone, (titano-)magnetite is mainly preserved as inclusions in silicate minerals, where the original magmatic structure was not disintegrated by erosion. Nevertheless, in part they are replaced by iron sulfides (Fig. 10a). Apparently, this process mainly involves the larger crystals, whereas the smaller, well sheltered (titano-)magnetite fraction seems unaffected by alteration, which suggests that they might significantly contribute to the magnetic

characteristics of the sulfidic zone. High temperature oxidized individual grains reveal extensive to complete dissolution of the of the low Ti titanomagnetite fraction, leaving the high Ti titanohematite lamellae fully intact (Fig. 10d). Such minerals were quite frequently found in the magnetic extracts from the sulfidic zone.
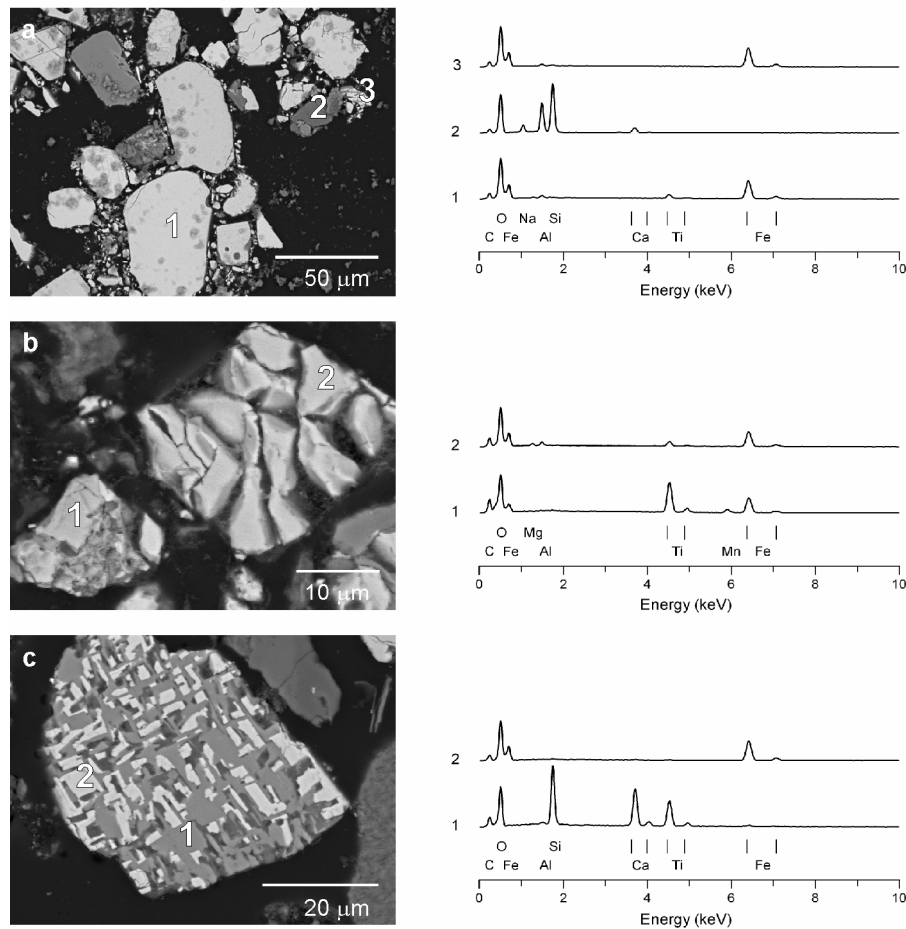
Fig. 9. Micrographs of magnetic extracts. (a) Cluster of small and large magnetic oxides (light gray) from the upper sediment series (2.45 m depth) containing titanomagnetite (1) and magnetite (3) with indications of limited maghemitization. Silicate minerals (2) appear dark gray. (b) Cluster of magnetic oxides from the lower sediment series (8.35 m depth) comprising of titanomagnetite (1 and 2) with variable Ti content and advanced degree of maghemitization. (c) Intergrowth of a silicate (1) with magnetite (2) from the sulfidic zone (5.85 m depth). Element spectra are normalized to the oxygen peak.

5 Discussion and Conclusions

Enhanced influx of organic material and methane rising from deep sources are the two key factors that create a distinct geochemical scenario in the upper sedimentary column on the Argentine continental slope in front of the Rio de la Plata estuary. The

present geochemical zonation has been established as a result of a drastic decrease in sedimentation rate from about 100 to 5 cm/kyr toward the end of the last glacial period (Riedinger et al., 2005). It caused a rapid ascent of the SMT from greater depth to around its current position just a few meters below the sediment surface. At around the SMT, free sulfide in the pore water is generated by AOM.

The intensely reducing environment in the sulfidic zone, extending from depths of 3.9 to 6.6 m in the investigated sequence, has a strong impact on the magnetic mineral inventory. However, significant magnetic mineral modification already occurs in the upper 0.5 m of the sedimentary sequence, as documented by a marked decrease in M_{AR} (Fig. 3d). The position of the first magnetically important diagenetic horizon may also be related to the last glacial/interglacial transition (Riedinger et al., 2005). Approximately 60% of the primary fine grained (titano-)magnetite fraction is dissolved at this level. A simultaneous lesser drop in isothermal remanent magnetization (Fig. 3e) indicates that about three quarters of the bulk ferrimagnetic mineral content persists in the sediments below where M_{AR}/M_{IR} and $_{AR}/$ (Figs. 7c and 7d) delimit a substantial shift to coarser grain-sizes. None of the magnetic parameters hint at formation of bacterial magnetite, which is found elsewhere just above the iron-redox boundary (e.g., Karlin et al., 1987; Tarduno and Wilkison, 1996). As specified by M_{HIR} (Fig. 4a), higher coercivity iron oxides and hydroxides appear to be scarcely affected by alteration at this diagenetic front.

This mode of reductive diagenesis, driven by microbially mediated degradation of organic matter under suboxic conditions, has previously been reported for various marine settings. In continental margin regions, especially where upwelling gives rise to elevated concentrations of organic carbon in the sediments, quite severe diagenetic alterations are typically observed. A main reason for the relatively limited dissolution of the magnetic iron oxides in the study area is their uncommonly coarse grain-size spectrum (Figs. 9a to 9c). This agrees with the nature of coarse sedimentary deposits that reflect the offshore distribution of the Rio de la Plata fluvial load (Frenz et al., 2004). The primary detrital magnetic mineralogy is dominated by (titano-)magnetite, which is most probably derived from the Paraná volcanic province and delivered by the Uruguay and Paraná rivers. Hematite and goethite contents, which are estimated to make up around one third of the total magnetic mineral assemblage, are remarkably depleted compared to most other regions of the South Atlantic (Pye, 1987; Balsam and Otto-Bliesner, 1995; Schmidt et al., 1999).
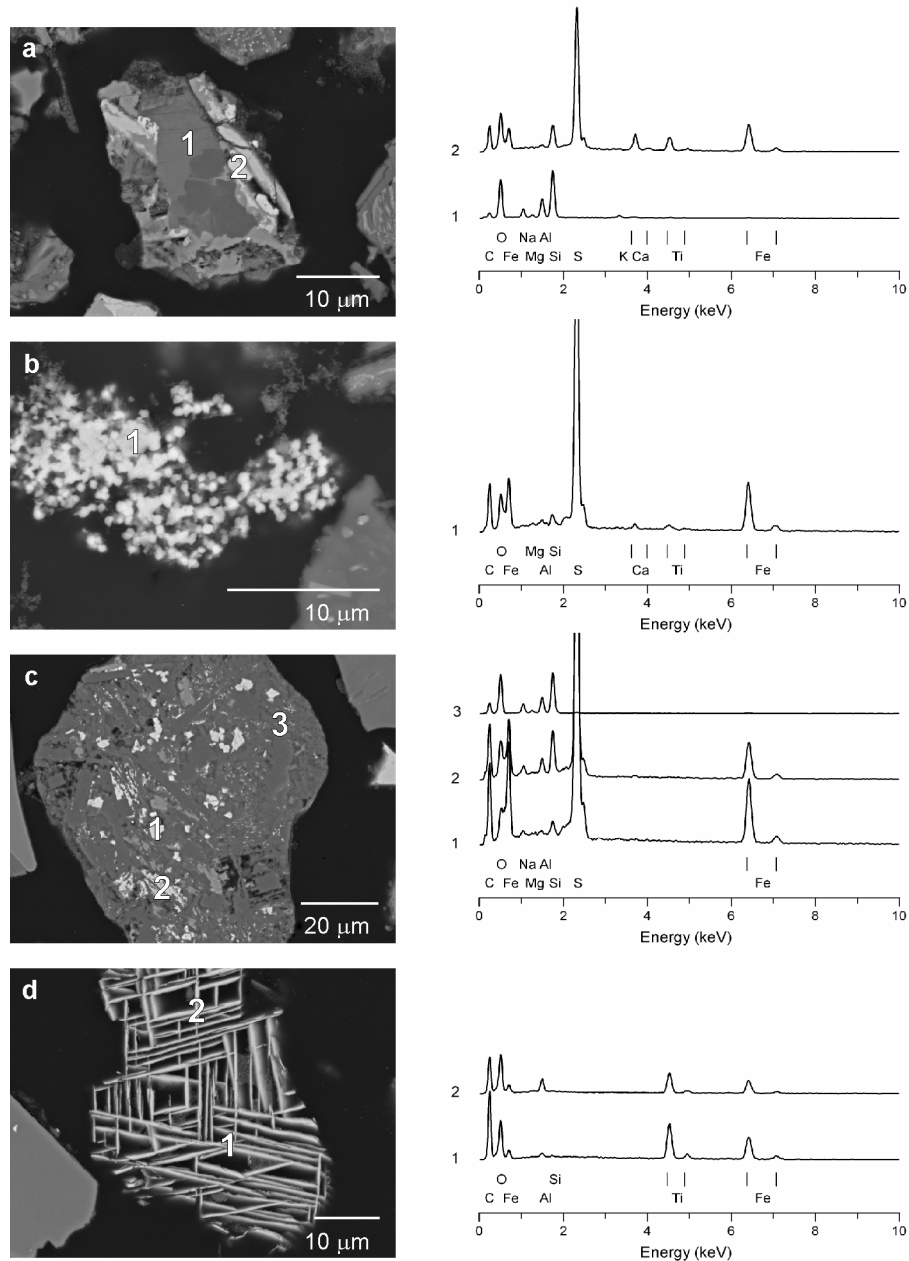
Fig. 10. Micrographs of magnetic extract from the sulfidic zone. (a, 5.25 m depth) Dark gray silicates (1) with iron sulfide overgrowth, identified as pyrite, probably replacing iron oxides. (b, 6.05 m depth) Cluster of euhedral pyrite (1) identified after Wang and Morse (1996). (c, 5.25 m depth) Iron sulfide minerals (white; 1 and 2) apparently replacing (titano)magnetite in a silicate matrix (3) which also contains fine grained iron oxide inclusions (light gray). (d, 6.55 m depth) High Ti titanohematite lamellae (1 and 2) resulting from high temperature oxidation. Note that the originally present magnetite intergrowth has been entirely dissolved. Element spectra are normalized to the oxygen peak.

The sulfidic environment at around the SMT caused dissolution of more than 80% of the primary ferrimagnetic mineral fraction (Fig. 3). Even though large amounts of high coercivity compounds have also been lost, their relative concentration increases to approximately 50% of the total magnetic mineral content in the sulfidic zone. The

comparatively higher resistance of hematite and goethite against diagenetic dissolution implies a lower reactivity towards sulfide than for (titano-)magnetite (Yamazaki et al., 2003; Liu et al., 2004; Emiroglu et al., 2004). According to literature data (Canfield et al., 1992; Haese et al., 2000), the opposite should be expected. The shift in magnetic mineralogy specifically results in considerably higher magnetic stabilities documented in a two- to threefold increase in coercivities (Fig. 5). Further details of this phenomenon were quantified by an IRM component analysis (Fig. 6). A three component solution yields relative contributions to remanent magnetization of approximately 11.7, 75.6 and 12.7% for 'soft' (titano-)magnetite, 'hard' (titano-)magnetite/hematite and 'hardest' hematite/goethite fractions in the sulfidic zone compared to 57.9, 39.8 and 2.3% in the overlying suboxic sediments. The tentative identification of these mineral components is mainly based on their respective average half IRM acquisition fields $B_{1/2}$ M_{IRA} (Table 1). $B_{1/2}$ M_{IRA} of 39.0 and 42.2 mT of 'soft' (titano-)magnetite in the suboxic and sulfidic sediments are best compatible with pure magnetite or low Ti content titanomagnetite (Day et al., 1977). In the sulfidic zone, where their concentrations dramatically decline, they should mainly persist as relatively fine grained inclusions in a silicate matrix (Fig. 9c). The second component has been labeled 'hard' (titano-)magnetite/hematite, because of strikingly higher $B_{1/2}$ M_{IRA} values of 81.9 mT in the suboxic and 90.5 mT in the sulfidic layers, which are most plausibly explained by titanomagnetite with a significant Ti content and/or an advanced degree of maghemitization (Fig. 9b). Hematite of appropriate grain-size is another suitable candidate (Kletetschka and Wasilewski, 2002) and possibly also Ti-rich titanohematite (Fig. 10d). For the third high coercivity component, which is characterized by $B_{1/2}$ M_{IRA} of 1000 and 887 mT in the suboxic and sulfidic sediments, goethite should primarily be responsible, probably with contributions from hematite.

Combined dissolution of iron oxides and enhanced solid phase sulfur concentrations suggest formation of authigenic iron sulfides at around the SMT. Thermomagnetic analyses only positively identified euhedral pyrite by its oxidation temperature above 450°C in air (Fig. 8; Passier et al., 2001). On the other hand, high coercivities (Fig. 5) and an increasing σ_{rs}/σ_s ratio (Fig. 7a) could hint at the presence of the ferrimagnetic iron sulfide mineral greigite (Fe_3S_4; Roberts, 1995), which has been repeatedly found in marine sediments. The reductive diagenetic sequence of iron oxide dissolution, metastable iron monosulfide and lastly stable pyrite formation is in principle well understood (Canfield and Berner, 1987). The intermediate phase greigite is ferrimagnetic and carries a stable intense magnetic remanence at room temperature (Berner, 1967; Goldhaber and Kaplan, 1974; Roberts and Turner, 1993; Wang and Morse, 1996; Wilkin and Barnes, 1996). Greigite might be preserved by arresting pyritization reactions, for

example when pyrite forms as overgrowths on precursor minerals (Wang and Morse, 1996) or dissolved iron is produced at a faster rate than HS^- (Kao et al., 2004).

Scanning electron microscope observations indicate two types of iron sulfide: (1) pyrite replacing iron oxides as overgrowths on silicates (Fig. 10a) or as inclusions in a silicate matrix (Fig. 10c), and (2) agglomerates of pyrite crystals which display uniform shape and size (Fig. 10b). Wilkin and Barnes (1997) and Canfield and Berner (1987) concluded that the latter feature is the result of a single framboidal greigite nucleation event in pore waters containing low concentration of iron and sulfide. Iron limitation subsequently leads to the formation of pyrite. The absence of dithionite soluble mineral phases, mainly iron oxides, hint at iron-limited pyritization processes (Raiswell and Canfield, 1996). Sequential extraction indeed confirmed low concentration of reactive iron phases in the sulfidic zone of Argentine continental slope sediments (Riedinger et al., 2005).

Another interesting issue in the context of iron limitation is maghemitization, which proceeds through preferential diffusion of Fe^{2+} out of (titano-)magnetite as Fe^{2+} is more easily detached from the mineral structure than Fe^{3+} (Cornell and Schwertmann, 1996). SEM analyses provided widespread evidence for an advanced maghemitization indicated by surficial cracking within and below (Fig. 9b) the sulfidic zone, whereas in the upper sediment series only minor evidence of low temperature oxidation was found. These findings suggest that progressing maghemitization could be an important process in sulfidic environments. It will modify the magnetic characteristics of the residual (titano-)magnetite fraction by, as was observed, a decrease in grain-size and increased coercivities. Moreover, the preferential diffusion of Fe^{2+} out of (titano-)magnetite may give a hint to explaining the superior stability of hematite and titanohematite (Fig. 10d) under sulfidic conditions.

In the sulfidic sediments, grain-size variations (Fig. 7) indicate the opposite trend to that expected for iron oxide dissolution. The already coarse grained primary ferrimagnetic mineral assemblage loses almost all of its finer grained fraction at the first magnetically important diagenetic front under suboxic conditions. The subsequent strong diagenetic dissolution that affects all magnetic iron oxide minerals in the sulfidic environment will eventually cause a fining of the grain-size spectrum. Major factors contributing to this effect should be the small (titano-)magnetite grains preserved as inclusions in silicates and, possibly of prime importance, reduced effective magnetic grain-sizes, due to comprehensive fragmentation in the course of maghemitization (e.g. Cui et al., 1994).

The sediment series above and below the sulfidic zone reveal similar, though not identical magnetic characteristics which indicate that some alteration has also affected the

lower part of the core during rapid passage of the SMT and prolonged exposure to a methanic environment. Under these conditions precipitation of authigenic minerals, such as iron sulfides, iron and manganese carbonates and phosphates is likely (Berner, 1981). Thermomagnetic analyses (Fig. 8) did not identify a magnetic sulfide phase, specifically not at around 7 m, where a peculiar maximum is observed in the concentration indicative parameters (Figs. 3 and 4c). Other possible iron and manganese bearing authigenic mineralizations may form in the non-sulfidic sediments below the SMT (Berner, 1981; Sagnotti et al., 2005), such as siderite, rhodochrosite and vivianite, which are paramagnetic at room temperature, and can be identified with low temperature magnetic analyses. More work is clearly needed to better understand the magnetic mineral alteration in the lower part of the sediment column.

Acknowledgements

Chapter 2.4 Low-temperature partial magnetic self-reversal in marine sediments

Abstract

Various low-temperature experiments were performed on magnetic mineral extracts of marine sediments from the Argentine continental slope near the Rio de la Plata estuary. In these sediments the sulphate-methane transition zone is situated at depths between 4-8 meters. At around this transition, the magnetic mineralogy of the sediments is severely altered by reductive diagenesis. The magnetic mineral assemblage of the extracts, throughout the core, comprises of (titano-)magnetite of varying compositions, titanohematite and ilmenite. In the sulphate-methane transition zone (titano-)magnetite only occurs as inclusions in siliceous matrix and as intergrowths with lamellar titanohematite and ilmenite, originating from high temperature deuteric oxidation within the volcanic host rocks. These relic structures were visualized by scanning electron microscopy and analysed by energy dispersive spectroscopy. While warming of a field-cooled low-temperature saturation remanence (FC-SIRM) only indicates the Verwey transition of magnetite, cooling of a room-temperature saturation remanence (RT-SIRM) shows a marked drop below ~210K, corresponding to the Curie temperature of titanohematite with an approximate composition of $Fe_{1.15}Ti_{0.85}O_3$ (~TH85). The mechanism responsible for this loss of remanence at the moment of ordering is sought in partial magnetic self-reversal caused by magnetostatic interaction of both Fe-Ti-oxides. When titanohematite becomes ferrimagnetic upon cooling, its spontaneous magnetic moments order anti-parallel to the remanence of the RT-SIRM carrying (titano-)magnetite. Low-temperature cycling of RT-SIRM appears to be a valuable low-temperature method for the rock magnetic characterization of certain sedimentary iron-titanium oxides, in particular relic intergrowths of titanomagnetite and titanohematite.

1 Introduction

Sediments from the Argentine continental slope off the Rio de la Plata estuary have recently been analysed in detail for their geochemical and rock magnetic characteristics by Riedinger *et al.* (2005) and Garming *et al.* (2005), respectively. The principal source of their detrital magnetic mineral fraction is the drainage area of the Rio de la Plata tributaries in the Mesozoic flood basalts of the Paraná Basin (Fig. 1). Carriers of natural remanent magnetisation of these basalts are magnetite and low Ti bearing, slightly maghematised, titanomagnetite (Kosterov *et al.*, 1998; Tamrat and Ernesto, 1999).
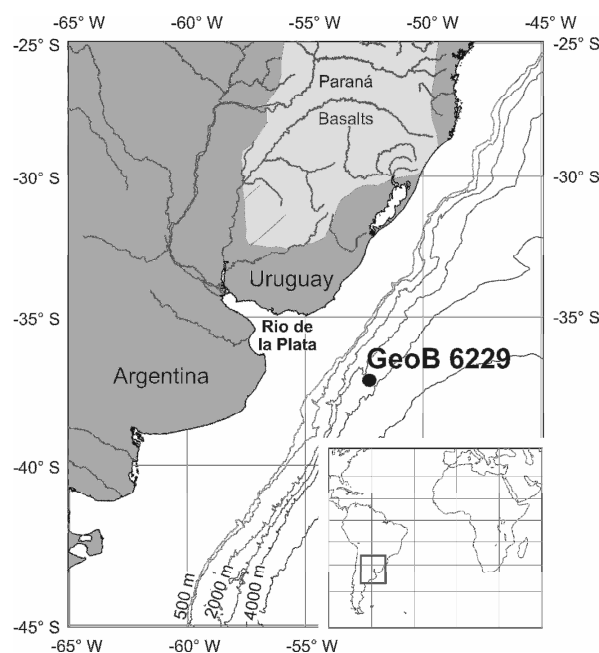
Fig. 1. Location of core GeoB 6229 at the South American continental margin off the Rio de la Plata estuary. Grey shading schematically outlines titanium bearing Mesozoic flood basalts of the Paraná Basin (Peate *et al.*, 1992). Isobaths at 1000 m intervals, including the 500 m isobath, are according to GEBCO.

At gravity core location GeoB 6229 (37°12.4'S / 52°39.0'W water depth 3446 m, Schulz et al., 2001) suboxic conditions are established close to the sediment surface and anaerobic oxidation of methane (AOM) is observed in a few meters sediment depth (Riedinger *et al.*, 2005, Fig. 2). In this distinct redox zonation the magnetic iron oxide mineral inventory undergoes a two-stage diagenetic alteration. At the iron redox boundary, situated in the first meter, about one quarter of the bulk ferrimagnetic mineral content has been dissolved resulting in a significant coarsening in magnetic grain-size and diminishing of bulk coercivities (Garming *et al.*, 2005). Reductive diagenesis in the suboxic zone is a

common and frequently studied phenomenon in organic-rich marine sediments (e.g., Karlin and Levi, 1983; Canfield and Berner, 1987; Karlin, 1990a, 1990b; Funk *et al.*, 2004a, 2004b). In contrast the diagenetic processes in the intensely reducing environment of the sulphate methane transition (SMT) zone surrounding the AOM have been scarcely investigated so far.
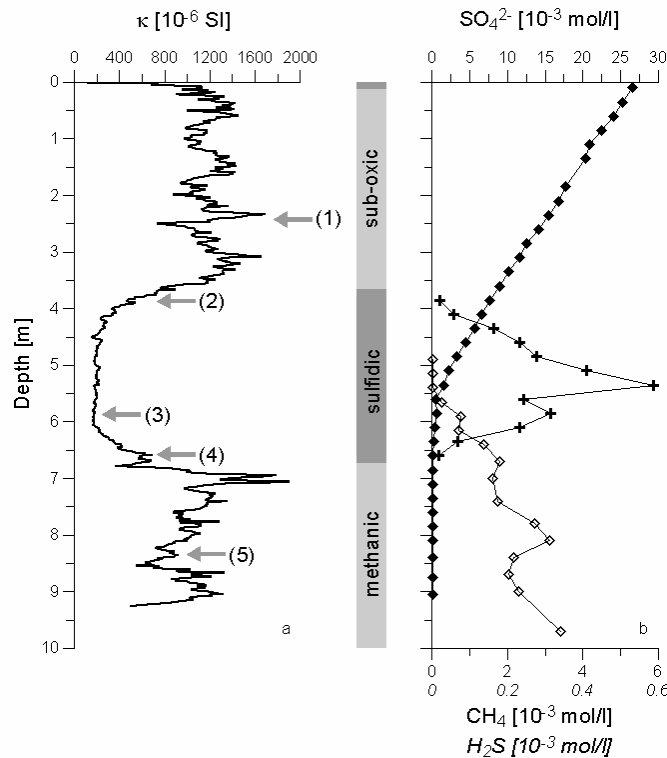
Fig. 2. Core GeoB 6229-6 depth profiles of (a) low field magnetic susceptibility κ. (grey arrows indicate the sample positions for the low-temperature studies), and (b) pore water concentrations of sulphate (solid diamonds), methane (open diamonds) and sulphide (crosses) as measured directly after core recovery. Redrawn after Riedinger *et al.* (2005) and Garming *et al.* (2005).

In the present example, only a small fraction below 10 %, of the primary (titano-)magnetite escaped dissolution being protected either as inclusions in a siliceous matrix or as relic intergrowths with high titanium bearing and well-preserved titanohematite lamellae (Garming *et al.*, 2005). A greater stability of Ti bearing oxides relative to pure Fe oxides has been frequently observed (e.g., Karlin, 1990b; Emiroglu *et al.*, 2004). It can be plausibly explained by the fact that every Ti^{4+} substitution in Fe oxides lowers twofold the number of Fe^{3+} cations acting as electron acceptors under anaerobic conditions. In case of substantial Ti^{4+} substitution, the remaining iron is almost entirely in

the reduced ferrous (Fe^{2+}) state, rendering the mineral less reactive and vulnerable to reductive dissolution.

To demonstrate the compositional changes of the magnetic mineral fraction during progressive sub- and anoxic diagenesis, various low-temperature cycling experiments were performed on magnetic mineral extracts. Their results are discussed here together with the findings of scanning electron microscopic (SEM) analyses and energy dispersive spectroscopy (EDS).

2   Samples and measurements

The magnetic extraction technique of Petersen *et al.* (1986) was applied to obtain magnetic separates for five samples located at key positions within the vertical redox zonation of gravity core GeoB 6229 (Fig. 2): (1) The suboxic zone below the iron redox boundary (2.45 m depth), (2) the transitional interval from suboxic to sulphidic conditions of the SMT zone (3.85 m depth), (3) the sulphidic SMT zone (5.85 m depth), (4) the transitional interval between the SMT zone and methanic zone (6.55 m depth) and (5) the methanic zone (8.35 m depth).
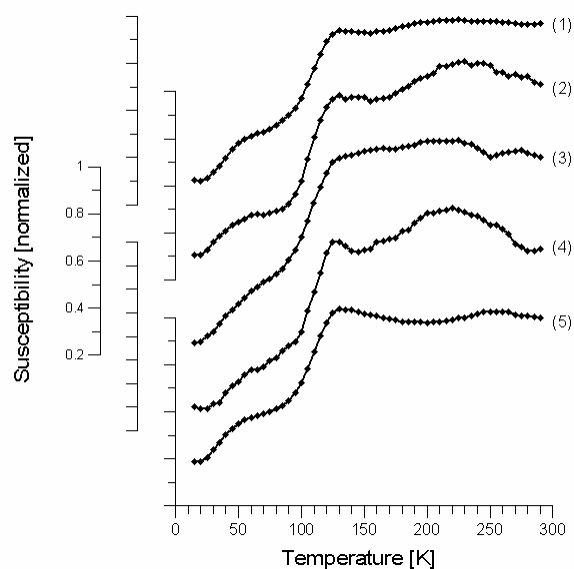
Fig. 3. Normalized and smoothed (5 point average) magnetic susceptibilities measured between 5 and 300 K applying a 110 Hz field of 0.4 mT amplitude.

For low-temperature measurements with a *Quantum Design* Magnetic Property Measurement System (MPMS XL-7), accurately weighed amounts of these extracts were

fixed with vacuum grease in small gelatine capsules. Susceptibility was determined from 5 to 300 K in 5 K steps applying a 110 Hz field of 0.4 mT amplitude. Saturation isothermal remanent magnetisation (SIRM) experiments comprised thermal demagnetisation to room temperature of a 5 T LT-SIRM acquired at 5 K after zero field cooling (ZFC) as well as after field cooling (FC), and cycling of a 5 T room temperature (300 K) SIRM down to 5 K and back in zero field. For sample (4) hysteresis loops were determined with peak fields of 2 T at 18 selected temperatures between 275 and 160 K.

SEM observations of polished thin sections were made with a *Phillips* XL20 *SFEG*, equipped with an EDS detector. Element compositions were determined from the EDS spectra using the '*Remote SEM Quant Phiroz*' program version 3.4.

3   Results

3.1   Low-Temperature Susceptibilities

The smoothed (5 point average) in-phase susceptibility data (Fig. 3) exhibits generally similar characteristics for all five samples. Increasing gradients above ~ 30 K and inflections in slope at around 60 K likely hint at the presence of ilmenite (Nagata and Akimoto, 1956). A steep rise of susceptibilities above 90 K and a maximum at about 130 K reflect reduced coercivities towards and at the Verwey transition T_V and the isotropic point T_I of magnetite (Dunlop and Özdemir, 1997). A third broad maximum around 220 to 230 K is most clearly developed for samples (2) to (4) from the sulphidic SMT zone and its transitional margins to the suboxic and methanic zones. In the suboxic sediment (1) this feature is faint; in the methanic zone it seems to be shifted to higher temperatures (~ 255 K). Analogous observations at 210 K, for the central Alaskan Old Crow tephra, have also been attributed to the transition of a titanohematite phase from the ferrimagnetic to the paramagnetic state (Lagroix *et al.*, 2004).

3.2   Low-Temperature SIRM Experiments

Thermal demagnetisation curves of FC- and ZFC-SIRM are shown in Fig. 4. Samples (2) to (4) from the SMT zone acquired 21 to 26 % more remanence by FC than by ZFC, while the difference is noticeably smaller for sample (1) from the suboxic (14 %) and sample (5) from the methanic (8 %) zones, possibly indicating coarser grained magnetic particles. All samples lose ~ 90 % of their initial 5 K remanence upon warming to 300 K; the remanence loss is largest between 5 and 20 K. The Verwey transition ($T_V \approx 120$ K) is broadened, indicating partially oxidized and/or Ti-rich magnetite (Ozdemir *et al.*, 1993).

Unlike the κ (T) curves, the FC- and ZFC-SIRM warming curves carry no particular features at around 60 K or in the 220 to 255 K interval, not even in their first derivatives (not shown).
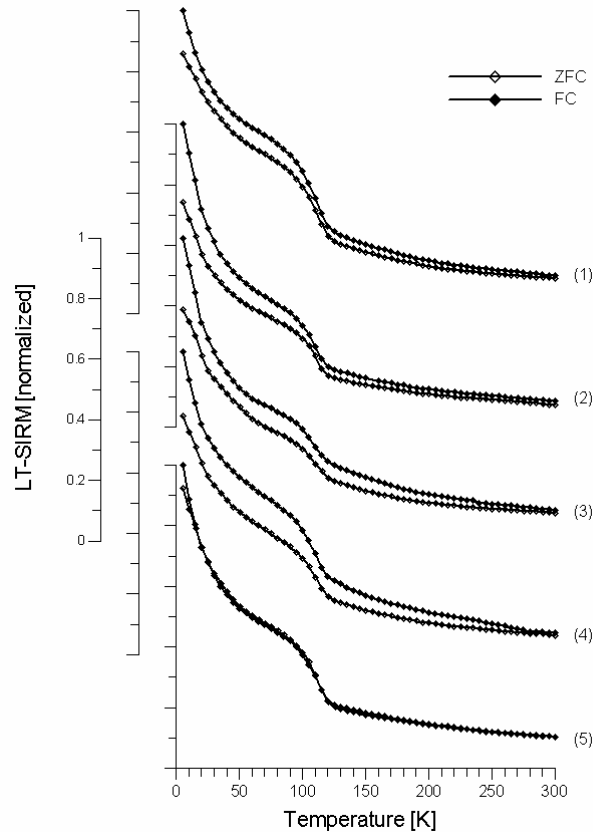
Fig. 4. Thermal demagnetisation between 5 and 300 K of normalized 5 T SIRM acquired at 5 K after zero field cooling (open symbols) and 5 T field cooling (solid symbols).

Although zero field cooling curves (Fig. 5) also reveal marked slope changes around the Verwey point for all samples, a more prominent remanence loss occurs at higher temperatures. It is most clearly developed in the samples (2) and (4) of the SMT transitional zones, where abrupt breaks in slopes are observed at 210 and 215 K, respectively. Suboxic sample (1) shows a similar kink, whereas the remanence loss of the SMT zone sample (3) extends over a wider temperature range. For methanic zone sample (5) the decline of the RT-SIRM already starts at about 260 K; a faint undulation in gradient can be seen at around 210 K. Overall, these results are fully consistent with the susceptibility data, indicating the presence of a titanohematite phase, with a Cure temperature of about 210 K. At 5 K between 40 to 60 % of the initial RT-SIRM remains,

and is reversible up to ~ 50 K and showing a very limited recovery passing through T_V and in case of sample (4) slightly increases above 235 K. In the other samples the latter effect is restricted to very minor slope changes, (1) to (3), or missing (5).
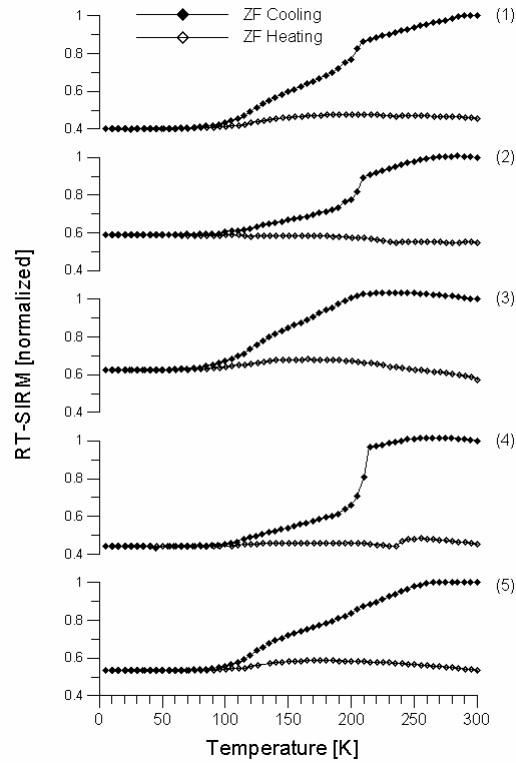

Fig. 5. Zero field cooling (300 to 5 K, solid symbols) and warming (5 to 300 K, open symbols) of normalized 5 T room temperature (300 K) SIRM.

3.3   Low-Temperature Hysteresis Properties

For transition zone sample (4) the temperature dependence of hysteresis properties has been determined between 160 and 275 K at peak fields of 2 T. Saturation magnetisation (σ_s), saturation remanent magnetisation (σ_{rs}), coercive field (B_c) and domain state index (σ_{rs}/σ_s) were quantified after subtracting para- and diamagnetic components. Saturation magnetisation (Fig. 6a) increases linearly by rates of 0.008 and 0.007 (Am^2/kg per Kelvin) when cooling from 275 to 245 K and from 230 to 160 K, respectively. The shift of 8 % between 245 and 230 K suggests that a new magnetic phase is ordering in correspondence to the previous findings (Figs. 3 to 5). A continuous increase with cooling is also observed for saturation remanence (Fig. 6b). The σ_{rs}/σ_s ratio (Fig. 6c) indicates grain-sizes at the multi-domain to pseudo-single-domain boundary,

slightly fining towards deeper temperatures. Like the coercive field B_c (Fig. 6d), it reaches a minimum at 230 K. B_c changes at a higher rate (~ 0.03 mT per Kelvin) below 210 K above 245 K (~ 0.01 mT per Kelvin).
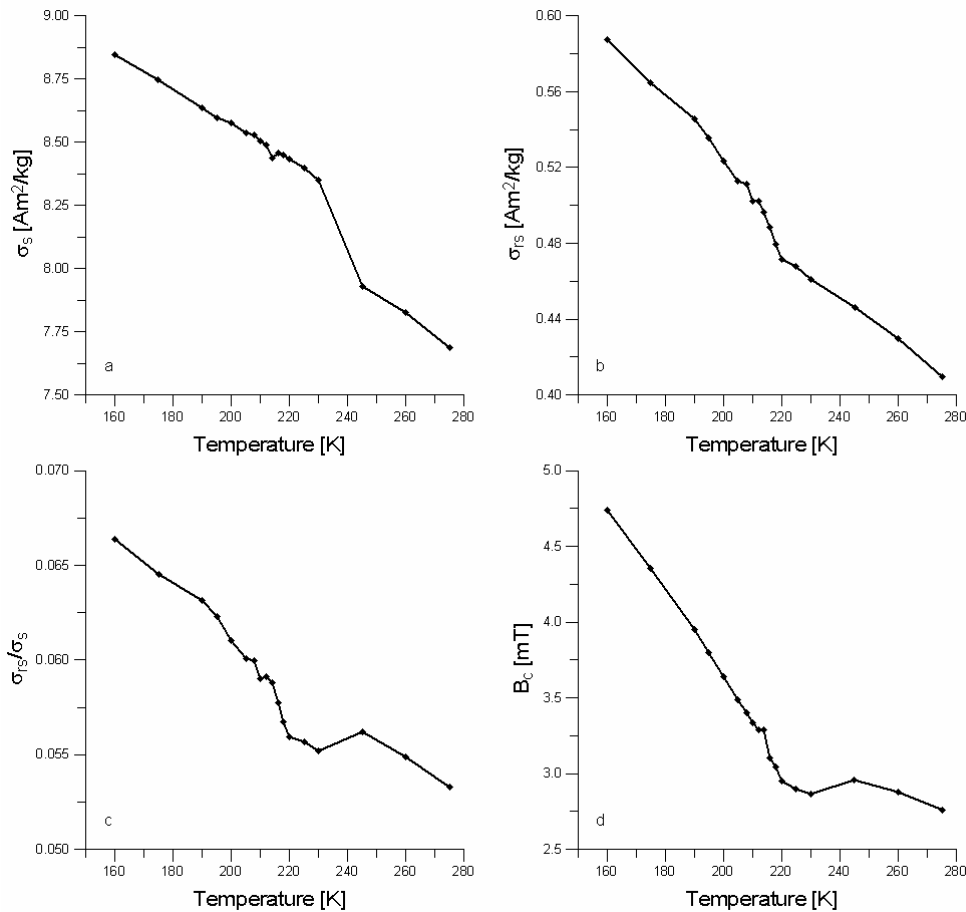
Fig. 6. Results of hysteresis measurements for sample (4). Low-temperature dependence of (a) specific saturation magnetisation, σ_s, (b) specific saturation remanent magnetisation, σ_{rs}, (c) magnetic grain-size ratio, σ_{rs}/σ_s, and (d) coercive field, B_c.

3.4   Energy dispersive spectroscopy (EDS)

Electron optical examination and EDS of polished sections revealed the presence of a variety of iron-titanium-oxide minerals both from the titanomagnetite and the titanohematite solid solution series. According to the EDS analysis, the titanohematite lamellae (Figs. 7a and b), have an approximate composition of $0.85\ FeTiO_3 \cdot 0.15\ Fe_2O_3$ (y = 0.85, TH85), but higher Ti contents of up to almost pure ilmenite were also

determined. Franke *et al.* (subm.) verified the presence of the titanomagnetite and titanohematite, using an electron backscatter diffraction (EBSD) technique.

Composition estimates for their relic titanomagnetite intergrowths (Fig. 7b), suggest implausibly high Ti contents of 0.40 $Fe_2TiO_4 \cdot$ 0.60 Fe_3O_4 (x = 0.4, TM40). Most likely the analyses were biased by the adjacent and underlying titanohematite lamellae. Almost pure magnetite, positively documented in the low-temperature susceptibility and SIRM records (Figs. 3 to 5), could not be detected elsewhere in the polished sections, supporting this assumption.
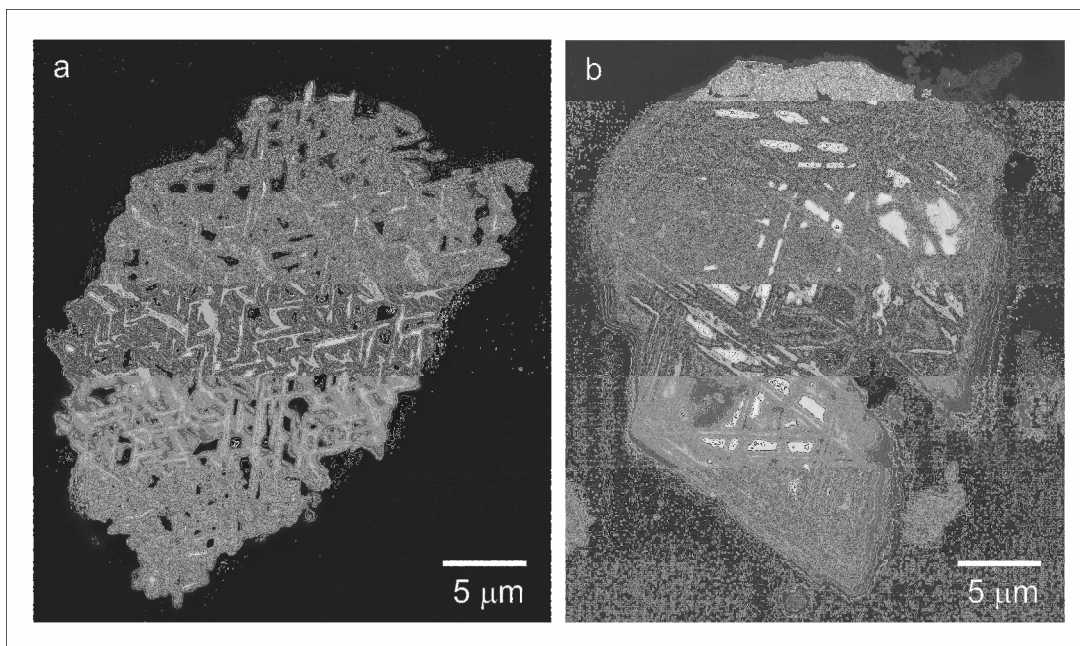
Fig. 7. SEM micrograph showing (a) titanohematite lamellae and (b) intergrown titanohematite lamellae (TH) and (titano-)magnetite (TM).

4   Discussion and conclusions

This study has shown that the magnetic mineral extracts of the continental slope sediments off the Rio de la Plata estuary consist of (titano-)magnetites of various compositions, titanohematite and ilmenite. Garming *et al.* (2005) identified the secondary mineral pyrite in the sulphidic zone surrounding the SMT.

The only plausible magnetic carrier at room temperature is (titano-)magnetite, which is in the sulphidic zone, is either present as inclusions in a siliceous matrix or intergrown with titanohematite lamellae (Fig. 7b). The data indicates compositions from almost pure to up to 40 % Ti-substituted magnetite. Indications for partial low-temperature oxidation of the

(titano-)magnetites are present in form of a broad and down-shifted Verwey transitions (Fig. 4, Dunlop and Özdemir, 1997) and shrinking cracks (Fig. 7b, Garming *et al.*, 2005).

The titanohematite lamellae have approximate compositions of TH85 and higher and therefore do not contribute to room temperature remanence; they only become ferrimagnetic at their Curie temperatures of 210 K and lower (Nagata and Akimoto, 1956; Dunlop and Özdemir, 1997). Low-temperature hysteresis parameters (Fig. 6a and b) document a gradual transition from a paramagnetic to a superparamagnetic and finally to a stable ferrimagnetic state between 190 and 245 K. Grain-size and compositional effects (Fig. 6c) affect the width of this interval. The coercive field minimum at 230 K confirms, in agreement with susceptibility and SIRM data, that the TH phase is predominantly superparamagnetic at this temperature.

Cycling of a RT-SIRM showed that the magnetic moments of the titanohematites order in anti-parallel direction to the RT-SIRM of the intergrown (titano-)magnetite (Fig. 5) on cooling through their Curie and blocking temperature, resulting in an apparent partial SIRM self-reversal. Titanohematites with compositions $y \geq 0.5$ are ferrimagnetic and do show self-reversing properties (Stacey and Banerjee, 1974; Dunlop and Özdemir, 1997, and references cited therein). Negative exchange coupling to an intergrown second titanohematite phase of lower Ti content ($y < 0.5$) has often been identified as underlying mechanism. There is no supporting evidence, however, that such a process could be responsible for the drop in RT-SIRM as observed here at around 210 K and higher temperatures (Fig. 5). The host rocks of the detrital sedimentary magnetic mineral assemblage are basalts, that different from felsic volcanics, typically do not contain two phases of intergrown titanohematites. No low Ti titanohematite ($y < 0.5$) was actually detected. Instead, high Ti titanohematite ($y \geq 0.7$), a common product of high temperature titanomagnetite deuteric oxidation, is found intergrown with titanomagnetite (Fig. 7b). Between such physically decoupled magnetic phases magnetostatic interaction seems the only conceivable mechanism for self-reversal (Dunlop and Özdemir, 1997). Compared to exchange coupling, magnetostatic interaction is weak. This explains the absence of any anomaly in the critical temperature interval of the LT-SIRM thermal demagnetisation to room temperature (Fig. 4).

The superiour stability of Ti-rich titanohematites to reductive diagenesis (e.g., Karlin, 1990b; Emiroglu *et al.*, 2004) and the relative easy technique of RT-SIRM cycling, can be used as proxy indicator of strongly reducing sedimentary environments by the presence of the shown partial RT-SIRM self-reversal, providing that there are TM/TH intergrowths. The partial self-reversal documented here is probably absent in the parent rocks, the Mesozoic flood basalts of the Paraná Basin. The large abundance of titanomagnetite in the unaltered rock would most likely mask the here observed effect.

Acknowledgements

SEM and EDS analyses were performed at the electron microscopy & structural analysis (EMSA) center, Utrecht University, the Netherlands. The Deutsche Forschungsgemeinschaft (DFG) and the Netherlands Organization of Scientific Research (NWO) supported this study as part of the European Graduate College '*Proxies in Earth History*'. This is DFG Research Center Ocean Margins Publication no: RCOM###.

Chapter 2.5 Identification of magnetic Fe-Ti-oxides by electron back-scatter diffraction (EBSD) in scanning electron microscopy

Abstract

In paleomagnetic and environmental magnetic studies the magneto-mineralogical identification is usually based on a set of rock magnetic parameters, complemented by crystallographic and chemical information retrieved from X-ray diffraction (XRD), (electron) microscopy, or energy dispersive spectroscopy (EDS) of selected samples. While very useful, each of these accessory techniques has its limitations when applied to natural sample material. Identification of the magnetic minerals might be complicated by the limit of detection. Difficulties may also arise for particles of very fine grain-size. For example in marine sediments, concentrations of magnetic particles are typically down to the ppm range and they occur down to the nm range. Therefore, meaningful application of such techniques depends on sample quality. Electron backscatter diffraction (EBSD) of individual grains in scanning electron microscopy (SEM) enables mineralogical identification of individual grains down to ~0.2 micrometer and is particularly powerful when combined with EDS. EBSD is a relatively commonly used technique in structural geology and petrology. In this study we show the merits of EBSD for rock magnetic investigations by analyzing titanomagnetites and hemoilmenites of various compositions and submicron lamella of titanomagnetitehemoilmenite intergrowths. In natural particles, EDS often has a semi-quantitative character and compositionally similar intergrowths may be difficult to distinguish. With the mineralogical information provided by EBSD unambiguous identification of spinel-type and rhombohedral oxides is obtained. Optimal EBSD patterns are gathered from smooth, polished surfaces but here we show that interpretable EBSD patterns can be obtained as well from loose, so called 'non-embedded' particles from marine sediments.

Chapter 3

Diagenetic imprints on magnetic mineral assemblages in marine sediments: A synthesis

1 Synthesis

The rock magnetic signal of sediments greatly depends on the nature of the magnetic terrigeneous fraction added to the sedimentary record as well as the preservation and alteration of these minerals by diagenetic processes and the formation of authigenic magnetic minerals phases. Being able to distinguish between the primary and secondary magnetic mineral signals in marine sediments is of key importance, when studying past physical and climatic variations. The timing and nature of the diagenetic signature can hold important clues to past conditions.

Combining geochemical and geophysical techniques proved to be a valuable tool to investigate the magnetic mineral assemblage of different sedimentary settings, and in some cases to study past conditions. In the following sections the main conclusions of this study are summarized by working area.

1.1 The Mediterranean Sea

In **chapter 2.1** mineral magnetic methods in combination with sequential iron phase extraction brought us closer to understanding the diagenetic processes occurring in re-oxidation of the sapropelic sediments of the eastern Mediterranean and how these alterations influence the magnetic signal of these sediments.

Previous research has revealed that upon cessation of sapropel deposition the anoxic organic rich sapropelic sediments are slowly re-oxidised from the top down. Reduced phases are replaced by iron oxides (e.g. van Santvoort *et al.*, 1996; Passier and Dekkers, 2002), some of these are able to carry a (stable) remanent magnetisation. Measuring magnetic properties before and after the different steps of the applied sequential extraction method, allowed a better view on the mineral phases carrying this signal. It revealed that the influence of biologically mediated magnetic minerals in these sediments is substantial. In the lower part of the active oxidation front magnetosomes contribute significantly to the observed magnetic signal, whereas further down in the oxidised zone coatings composed of ferro-silicates and/or 'amorphous' hematite/goethite are among the carriers of the magnetic signal. The 'primary' detrital magnetic signal is also retained in these sediments, but in the oxidised part of the sapropel distinction by conventional means is laborious and complicated.

1.2   The South Atlantic

Chapters 2.2 and **2.3** brought us closer to a more complete understanding of the diagenetic process involving magnetic minerals at around the sulphate methane transition (SMT) as found in a few meters sediment depth near the mouth Rio de la Plata in the south-western part of the South Atlantic.

In **chapter 2.2** the non-steady state pore-water conditions are discussed in relation with the typical feature of a minimum in susceptibility encountered in a few meters depth. Numerical modelling of the geochemical data indicated that a sharp drop in sedimentation rate is needed to fix the SMT for a prolonged period of time in order to generate strong enough sulphidic conditions that cause dissolution of the magnetic mineral fraction, resulting in the observed minimum in susceptibility.

The alteration of the magnetic mineral assemblage, as described in **chapter 2.3**, of the sediments starts with the early diagenetic processes of oxygen and nitrate consumption and iron reduction (Froelich *et al.*, 1979), in approximately the upper meter of the sedimentary sequence. In the investigated sediments about 40 % of the fine grained magnetic fraction remains after this initial stage of early diagenesis. Only 10% of the magnetic minerals survive the strong diagenesis related to the AOM, either as inclusion in siliceous matrixes or as intergrowths with titanohematite lamellae. The latter are more resistant to reductive diagenetic dissolution where increasing titanium substitution effectively takes out the reactive iron (Fe^{3+}) from mineral matrix.

The low-temperature magnetic characteristics of the titanomagnetite inclusions and the titanohematite lamellae are discussed in **chapter 2.4**. The inclusions and lamellae most likely originate from the flood basalts of the Paraná Basin, in which high temperature (deuteric) oxidation can cause such features. At room temperature the titanomagnetite inclusions carry the remanent magnetisation, but below ~210K the titanohematites, with compositions ranging from TH85 to ilmenite, become ferrimagnetic. Cooling of a room temperature (RT) SIRM in zero field revealed that the magnetic moment of the titanohematites align anti-parallel to the magnetic moment of the titanomagnetites, giving rise to a partial self-reversal. The only conceivable mechanism between such physically decoupled phases is sought in magnetostatic interaction. This weak interaction would also explain the absence of an anomaly at around ~210K of the low temperature (LT) SIRM demagnetisation to room temperature. The observed decrease in remanent magnetisation in the RT-SIRM cycling may also be used as a proxy in the identification of high Ti bearing titanohematites in marine sediments.

To verify the findings of the microanalyses the technique of electron backscatter diffraction (EBSD) was applied to the magnetic extracts of various sediments including

sediments of the continental slope near the Rio de la Plata estuary. The results are summarised in **chapter 2.5**. EBSD is not a frequently applied technique in mineral magnetic investigations, but has proved itself to be a powerful tool in distinguishing between the compositionally identical minerals titanomagnetite and titanohematite.

1.3 Future work and recommendations

1.3.1 Paleomagnetic field

Although this study has provided insights into what extent the sulphate methane transition, as observed on the continental slope sediments off the Rio de la Plata estuary, has affected the recording of the paleomagnetic field, there are still open questions. The magnetic fraction able to carry the signal according to the criteria postulated by Tauxe (1993), is dissolved in the upper meter, where after the strong reducing environment only leaves magnetite as inclusions in a siliceous matrix or as intergrowth with titanohematite. The siliceous particles are relatively large, > 20μm (Garming *et al.*, 2005), and their orientating potential to the prevailing magnetic field in sediments is questionable. However in the absence of authigenic ferrimagnetic minerals, these minerals might be used to obtain an indication of the paleomagnetic field direction.

Sediments, in which authigenic ferrimagnetic minerals, like greigite, carry the mineral magnetic signal, resulting from anaerobic oxidation of methane (AOM) have been found. However the interpretation of the relative paleointensity will meet with additional different problems. Modelling of the non-steady state conditions in continental slope sediments off the Rio de la Plata estuary has revealed that approximately 10.000 years were needed to create the minimum in susceptibility as observed in the studied sediments (Riedinger *et al.*, 2005). A significant different magnetic field intensity and direction may be recorded, providing that the non-steady state geochemical conditions prevail for approximately 10.000 years and that a magnetic field reversal takes approximately 5-6 thousand years (Kristjansson, 1985).

1.3.2 Magnetic mineral extraction

In this study the technique of Petersen *et al.*, (1986) and von Dobeneck *et al.*, (1987) has been applied to extract ferrimagnetic minerals (at room temperature) from sediment slurries. Another technique, which may be used in mineral separation, is flotation. This gravity separation process is a physicochemical method based on the different hydrophobicities of particles to be separated (Matis *et al.*, 1993). Flotation is independent

of magnetic particle properties, there during conditioning, hydrophobicity can be induced and consequently different minerals can be separated.

Conditioning of the solution/particles maybe attained by adding a flotation aid, i.e., oleate (Drzymala, 1995), and starch (Ravishankar *et al.*, 1995; Weissenborn *et al.*, 1995), or simply by adjusting the pH (Lekki and Drzymala, 1990).

Attempts have been made during this study, on mixtures of pure minerals and the marine sediments investigated. The results however were not satisfying and therefore the application of this technique during this study was not pursued further. Improvements made to the experimental set-up can certainly show the effectiveness of this technique.

A possible application for this technique is in the identification of 'magnetic' carbonates and phosphates (i.e., siderite, rhodochrosite and vivianite). Previous studies have revealed that the low-temperature detection limit of these minerals does not lie in their own concentration, but rather in the presence of other strongly magnetic minerals, with similar transition temperatures, like pyrrhotite (Dekkers *et al.*, 1989; Frederichs *et al.*, 2003).

References

Adler, M., Hensen, C. and Schulz, H.D., 2000. *CoTreM-Column Transport and Reaction Model, User Guide, Version 2.3*. http://www.geochemie.uni-bremen.de/cotrem.html.

Adler, M., Hensen, C., Wenzhöfer, F., Pfeifer, K. and Schulz, H.D., 2001. Modeling of subsurface calcite dissolution by oxic respiration in supralysoclinal deep-sea sediments. *Mar. Geol.*, 177, 167-189.

Aller, R.C. and Burke, P.D., 1988. Complete oxidation of solid phase sulfides by manganese and bacteria in anoxic marine sediments. *Geochim. Cosmochim. Acta*, 52, 751-765.

Aloisi, G., Wallmann, K., Drews, M. and Bohrmann, G., 2004. Evidence for the submarine weathering of silicate minerals in Black Sea sediments: Possible implications for the marine Li and B cycles. *Geochem. Geophys. Geosyst.*, 5, 1-22.

Antoine, D., Andre, J.-M. and Morel, A., 1996. Oceanic primary production:2. Estimation at global scale form satellite (coastal zone color scanner) chlorophyll. *Glob. Biogeochem. Cycles*, 10, 57-69.

Archer, D., 1996. A data-driven model of the global calcite lysocline. *Glob. Biogeochem. Cycles*, 10, 511-526.

Balsam, W.L. and Otto-Bliesner, B.L., 1995. Modern and last glacial maximum eolian sedimentation patterns in the Atlantic Ocean interpreted from sediment iron oxide content. *Paleoceanography*, 2, 531-542.

Banerjee, S.K., King, J. and Marvin, J., 1981. A rapid method of magnetic granulometry with applications to environmental studies. *Geophys. Res. Lett.*, 8, 333-336.

Barnes, R.O. and Goldberg, E.D., 1976. Methane production and consumption in anoxic marine sediments. *Geology*, 4, 297-300.

Behrenfeld, M.J. and Falkowski, P.G., 1997. Photosynthetic rates derived from satellite-based chlorophyll concentration. *Limnol. Oceanogr.*, 42, 1-20.

Bernard, B.B., 1979. Methane in marine sediments. *Deep-Sea Res.*, 26A, 429-443.

Berner, R.A., 1967. Thermodynamic stability of sedimentary iron sulfides. *Am. J. Sci.*, 265, 773-785.

Berner, R.A., 1970. Sedimentary pyrite formation. *Am. J. Sci.*, 268, 1-23.

Berner, R.A., 1981. A new geochemical classification of sedimentary environments, *J. Sediment. Petrol.*, 51, 359-365.

Berner, R.A., 1982. Burial of organic carbon and pyrite sulphur in the modern ocean: Its geochemical and environmental significance. *Am. J. Sci.*, 282, 451-473.

Berner, R.A., 1984. Sedimentary pyrite formation: An update, *Geochim. Cosmochim. Acta*, 48, 605-615.

Béthoux, J.P. and Pierre, C., 1999. Mediterranean functioning and sapropel formation: respective influences of climate and hydrological changes in the Atlantic and Mediterranean. *Mar. Geol.*, 153, 29-39.

References

Biscaye, P.E. and Dasch, E.J., 1971. The rubidium, strontium, strontrium-isotope system in deep-sea sediments: Argentine Basin. *J. Geophys. Res.*, 76, 5087-5096.

Blair, N.E. and Aller, R.C., 1995. Anaerobic methane oxidation on the Amazon shelf. *Geochim. Cosmochim. Acta*, 59, 3707-3715.

Bleil U., 2000. Sedimentary magnetism. In: *Marine Geochemistry*, Schulz H.D. and Zabel M. (Eds.), Springer-Verlag, Berlin Heidelberg New York Tokyo, pp. 73-83.

Bleil, U., et al., 1994. *Report and preliminary results of Meteor Cruise 29/2*. Berichte, Fachbereich Geowissenschaften, Universität Bremen, 59, 153 pp.

Bleil, U., et al., 2001. *Report and preliminary results of Meteor Cruise M46/3*. Berichte, Fachbereich Geowissenschaften, Universität Bremen, 172, 161 pp.

Bloemendal, J., King, J.W., Hall, F.R. and Doh, S.-J., 1992. Rock magnetism of Late Neogene to Pleistocene deep-sea sediments: relationship to sediment source, diagenetic processes and sediment lithology. *J. Geophys. Res.*, 97, 4361-4375.

Boetius, A., Ravenschlag, K., Schubert, C.J., Rickert, D., Widdel, F., Gieseke, A., Amann, R., Jørgensen, B.B., Witte, U. and Pfannkuche, O., 2000. A marine microbial consortium apparently mediating anaerobic oxidation of methane. *Nature*, 407, 623-626.

Borowski, W.S., Paull, C.K. and Ussler, W., 1996. Marine pore-water sulfate profiles indicate in situ methane flux from underlying gas hydrate. *Geology*, 24, 655-658.

Boudreau, B.P., 1997. *Diagenetic models and their implementation: Modelling transport and reactions in aquatic sediments*. Springer-Verlag, Berlin Heidelberg New York Tokyo, 414 pp.

Bradley, W.H., 1938. Mediterranean sediments and Pleistocene sea levels, *Science*, 88, 376-379.

Butler, I.B. and Rickard, D., 2000. Framboidal pyrite formation via the oxidation of iron (II) monosulfides by hydrogen sulphide. *Geochim. Cosmochim. Acta*, 6, 2665-2672.

Calvert, S.E., 1983. Geochemistry of Pleistocene sapropels and associated sediments from the Eastern Mediterranean, *Oceanol. Acta*, 6, 255-267.

Canfield, D.E., 1989. Reactive iron in marine sediments. *Geochim. Cosmochim. Acta*, 53, 619-632.

Canfield, D.E. and Berner, R.A., 1987. Dissolution and pyritization of magnetite in anoxic marine sediments, *Geochim. Cosmochim. Acta*, 51, 645-659.

Canfield, D.E., Raiswell, R. and Bottrell, S., 1992. The reactivity of sedimentary iron minerals toward sulfide. *Am. J. Sci.*, 292, 659-683.

Carlson, L. and Schwertmann, U., 1981. Natural ferrihydrites in surface deposits from Finland and their association with silica. *Geochim. Cosmochim. Acta*, 45, 421-429.

Channell, J.E.T. and Hawthorne, T., 1990. Progressive dissolution of titanomagnetites at ODP site 653 (Tyrrhenian Sea). *Earth Planet. Sci. Lett.*, 96, 469-480.

Channell, J.E.T. and McCabe, C., 1994. Comparison of magnetic hysteresis parameters of unremagnetized and remagnetized limestones. *J. Geophys. Res.,* 99, 4613-4623.

Channell, J.E.T. and Stoner, J.S., 2002. Plio-Pleistocene magnetic polarity stratigraphies and diagenetic magnetite dissolution at ODP Leg 177 Sites (1089, 1091, 1093 and 1094). *Mar. Micropaleontol.*, 45, 269-290.

Chester, R. and Hughes, M.J., 1967. A chemical technique for the separation of ferro-manganese minerals, carbonate minerals and adsorbed trace elements from pelagic sediment. *Chem. Geol.*, 2, 249-262.

Cita, M.B., Vergnaud-Grazzini, C., Robbert, C., Chamley, H., Ciaranfi, N. and d'Onofrio, S., 1977. Paleoclimatic record of a long deep sea core from the eastern Mediterranean. *Quatern. Res.*, 8, 205-235.

Clark, D.A., 1984. Hysteresis properties of sized dispersed monoclinic pyrrhotite grains, *Geophys. Res. Lett.*, 11, 173-176.

Coleman. M.L. and Raiswell, R., 1995. Source of carbonate and origin of zonation in pyritiferous carbonate concretions: Evaluation of a dynamic model. *Am. J. Sci.*, 295, 282-308.

Colley, S., Thomson, J., Wilson, T.R.S. and Higgs, N.C., 1984. Post-depositional migration of elements during diagenesis in brown clay and turbidite sequences in the North East Atlantic, *Geochim. Cosmochim. Acta*, 48, 1223-1235.

Cornell, R.M. and Schwertmann, U., 1996. *The iron oxides - Structure, Properties, Reactions, Occurrences and Uses*, VCH, Weinheim, 573 pp.

Cui, Y., Verosub, K.L. and Roberts, A.P., 1994. The effect of low-temperature oxidation on large multi-domain magnetite. *Geophys. Res. Lett.*, 21, 757-760.

Day, R., Fuller, M.D. and Schmidt, V.A., 1977. Hysteresis properties of titanomagnetites: grain-size and compositional dependence. *Phys. Earth Planet. Inter.*, 13, 260-267.

Dekkers, M.J., 1988. Magnetic properties of natural pyrrhotite Part I: Behaviour of initial susceptibility and saturation-magnetization-related rock-magnetic parameters in a grain-size dependent framework, *Phys. Earth Planet. Inter.*, 52, 376-393.

Dekkers, M.J., 1989. Magnetic properties of natural pyrrhotite. II. High- and low-temperature behavior of J_{rs} and TRM as a function of grain size, *Phys. Earth Planet. Inter.*, 57, 266-283.

Dekkers, M.J., 1997. Environmental magnetism: an introduction, *Geologie en Mijnbouw*, 76, 163-182.

Dekkers, M.J., Mattéi, J.-L., Fillion, G. and Rochette, P., 1989. Grain-size dependence of the magnetic behaviour of pyrrhotite during its low-temperature transition at 34 K, *Geophys. Res. Lett.*, 16, 855-858.

Dekkers, M.J., Langereis, C.G., Vriend, S.P., van Santvoort, P.J.M. and de Lange, G.J., 1994. Fuzzy c-means cluster analysis of early diagenetic effects on natural remanent magnetization acquisition in a 1.1 Myr piston core from the Central Mediterranean. *Phys. Earth Planet. Inter.*, 85, 155-171.

de Lange, G.J., 1983. Geochemical evidence of a massive slide in the southern Norwegian Sea. *Nature*, 305, 420-422.

de Rijk, S., Hayes, A., and Rohling, E.J., 1999. Eastern Mediterranean sapropel S1 interruption: an expression of the onset of climate deterioration around 7 ka BP. *Mar. Geol.*, 153, 337-343.

Ding, Z.L., Sun, J.M., Liu, T.S., Zhu, R.X., Yang, S.L. and Guo, B., 1998. Wind-blown origin of the Pliocene red clay formation in the central Loess Plateau, China, *Earth Planet. Sci. Lett.*, 161, 135-143.

References

Drzymala, J., 1995. Interaction of coarse particles during oleate flotation in a mono-bubble hallimond tube, *Min. Engin.*, 8, 1023-1034.

Dunlop, D.J., 2002. Theory and application of the Day plot (M_{rs}/M_s versus H_{cr}/H_c) 1. Theoretical curves and tests using titanomagnetite data. *J. Geophys. Res.*, 107, 10.1029/2001JB000486.

Dunlop, D.J. and Özdemir, Ö. 1997. *Rock Magnetism: Fundamentals and Frontiers*. Cambridge University Press, Cambridge, 573 pp.

Emiroglu, S., Rey, D. and Petersen, N., 2004. Magnetic properties of sediment in the Ría de Arousa (Spain): dissolution of iron oxides and formation of iron sulphides, *Phys. Chem. Earth*, 29, 947-959.

Evans, M.E. and Heller, F., 2003. *Environmental magnetism: Principles and applications of enviromagnetics*. Elsevier Science, London, 299 pp.

Ewing, M., Ludwig, W.J. and Ewing, J.I., 1964. Sediment distribution in the oceans: the Argentine Basin. *J. Geophys. Res.*, 69, 2003-2032.

Ewing, M., Eittreim, S.L., Ewing, J.I. and Le Pichon, X., 1971. Sediment transport and distribution in the Argentine Basin. 3. Nepheloid layer and processes of sedimentation. *Phys. Chem. Earth*, 8, 49-77.

Ewing, M. and Leonardi, A.G., 1971. Sediment transport and distribution in the Argentine Basin. 5. Sedimentary structure of the Argentine margin, basin and related provinces. *Phys. Chem. Earth*, 8, 125-251.

Ferdelman, T.G., Fossing, H., Neumann, K. and Schulz, H.D., 1999. Sulfate reduction in surface sediments of the southeast Atlantic continental margin between $15^o38'S$ and $27^o57'S$ (Angola and Namibia). *Limnol. Oceanogr.*, 44, 650-661.

Flood, R.D., et al., 1995. *Proc. ODP Init. Repts.*, 155, Ocean Drilling Program.

France, D.E. and Oldfield, F., 2000. Identifying goethite and hematite from rock magnetic measurements of soils and sediments, *J. Geophys. Res.*, 105, 2781-2795.

Franke, C., Pennock, G.M., Drury, M.R., Engelmann, R., Lattard, D., Garming, J.F.L., von Dobeneck, T. and Dekkers, M.J., subm. Identification of magnetic Fe-Ti-oxides by electron backscatter diffraction (EBSD) in scanning electron microscopy, S*ubm. to J. Geophys. Res.*

Frederichs, T., Bleil, U., Däumler, K., von Dobeneck, T. and Schmidt, A.M., 1999. The magnetic view on the marine paleoenvironment: parameters, techniques and potentials of rock magnetic studies as a key to paleoclimatic and paleoceanographic changes. In: *Use of proxies in paleoceanography: Examples from the South Atlantic,* Fischer, G., Wefer, G. (Eds.), Springer-Verlag, Berlin Heidelberg New York Tokyo, pp. 575-599.

Frederichs, T., von Dobeneck, T., Bleil, U. and Dekkers, M.J., 2003. Towards the identification of siderite, rhodochrosite, and vivianite in sediments by their low-temperature magnetic properties, *Phys. Chem. Earth*, 28, 669-679.

Frenz, M., Höppner, R., Stuut, J.-B.W., Wagner, T. and Henrich, R., 2004. Surface sediment bulk geochemistry and grain-size composition related to the oceanic circulation along the South American continental margin in the Southwest Atlantic, In: *The South Atlantic in the Late Quaternary: Reconstruction of Material Budgets and Current Systems*, Wefer, G., Mulitza, S. and Ratmeyer, V. (Eds.), Springer-Verlag, Berlin Heidelberg New York Tokyo, pp. 347-373.

Froelich, P.N., Klinkhammer, G.P., Bender, M.L., Luedtke, N.A., Heath, G.R., Cullen, D., Dauphin, P., Hammond, D., Hartman, B. and Maynard, V., 1979. Early oxidation of organic matter in pelagic sediments of the eastern equatorial Atlantic: suboxic diagenesis, *Geochim. Cosmochim. Acta*, 43, 1075-1090.

Funk, J.A., von Dobeneck, T. and Reitz, A., 2004a. Integrated Rock Magnetic and Geochemical Quantification of Redoxomorphic Iron Mineral Diagenesis in Late Quaternary Sediments from the Equatorial Atlantic, In: *The South Atlantic in the Late Quaternary: Reconstruction of Material Budget and Current Systems*, Wefer, G., Mulitza, S. and Ratmeyer, V. (Eds.), Springer-Verlag, Berlin Heidelberg New York Tokyo, pp. 237-260.

Funk, J.A., von Dobeneck, T., Wagner, T. and Kasten, S., 2004b. Late Quaternary sedimentation and early diagenesis in the Equatorial Atlantic Ocean: patterns, trends and processes deduces from rock magnetic and geochemical records, In: *The South Atlantic in the Late Quaternary: Reconstruction of Material Budgets and Current Systems*, Wefer, G., Mulitza, S. and Ratmeyer, V. (Eds.), Springer-Verlag, Berlin Heidelberg New York Tokyo, pp. 461-497.

Furukawa, Y. and Barnes, H.L., 1995. Reactions forming pyrite from precipitated amorphous ferrous sulphide. In: *The South Atlantic in the Late Quaternary: Reconstruction of Material Budgets and Current Systems*, Wefer, G., Mulitza, S. and Ratmeyer, V. (Eds.), Springer-Verlag, Berlin Heidelberg New York Tokyo, pp. 194-205.

Garming, J.F.L., Bleil, U. and Riedinger, N., 2005. Alteration of Magnetic Mineralogy at the Sulfate Methane Transition: Analysis of Sediments from the Argentine Continental Slope, *Phys. Earth Planet. Inter.*, 151, 290-308.

Goldhaber, M.B. and Kaplan, I.R., 1974. The sulfur cycle, In: *The Sea*, Goldberg, E.D. (Ed), John Wiley and Sons, New York, pp. 569-655.

Gornitz, V. and Fung, I., 1994. Potential distribution of methane hydrates in the world's oceans. *Glob. Biogeochem. Cycles*, 8, 335-347.

Groot, J.J., Groot, C.R., Ewing, M., Burckle, L. and Conolly, J.R., 1967. Spores, pollen, diatoms and provenance of the Argentine Basin sediments. *Progr. Oceanogr.*, 4, 179-217.

Haese, R.R., 1997. *Beschreibung und Quantifizierung frühdiagenetischer Reaktionen des Eisens in Sedimenten des Südatlantiks*. Berichte, Fachbereich Geowissenschaften, Universität Bremen, 99, 118 pp.

Haese, R.R., Petermann, H., Dittert, L. and Schulz, H.D., 1998. The early diagenesis of iron in pelagic sediments: A multidisciplinary approach. *Earth, Planet. Sci. Lett.*, 157, 233-248.

Haese, R.R., Schramm, J., Rutgers van der Loeff, M.M. and Schulz, H.D., 2000. A comparative study of iron and manganese diagenesis in continental slope and deep sea basin sediments, off Uruguay (SW Atlantic). *Int. J. Earth Sci.*, 88, 619-629.

References

Haese, R.R., Wallmann, K., Dahmke, A., Kretzmann, U., Müller, P.J. and Schulz, H.D., 1997. Iron species determination to investigate early diagenetic reactivity in marine sediments. *Geochim. Cosmochim. Acta*, 61, 63-72.

Harris, L.C. and Whiting, B.M., 2000. Sequence-stratigraphic significance of Miocene to Pliocene glauconite-rich layers, on- and offshore of the US Mid-Atlantic margin. *Sed. Geol.*, 134, 129-147.

Heider, F., Zitzelsberger, A. and Fabian, F., 1996. Magnetic susceptibility and remanent coercive force in grown magnetite crystals from 0.1 µm to 6 mm. *Phys. Earth Planet. Inter.*, 93, 239-256.

Hensen, C., Zabel, M. and Schulz, H.D., 2000. A comparison of benthic nutrient fluxes from deep-sea sediments off Namibia and Argentina. *Deep-Sea Res. II*, 47, 2029-2050.

Hensen, C., Zabel., M., Pfeifer, K., Schwenk, T., Kasten, S., Riedinger, N., Schulz, H.D. and Boetius, A., 2003. Control of sulfate pore-water profiles by sedimentary events and the significance of anaerobic oxidation of methane for the burial of sulfur in marine sediments. *Geochim. Cosmochim. Acta*, 67, 2631-2647.

Heslop, D., Dekkers, M.J., Kruiver, P.P. and van Oorschot, I.H.M., 2002. Automated fitting of isothermal remanent magnetisation acquisition curves using an expectation-maximisation algorithm. *Geophys. J. Int.*, 148, 58-64.

Hilgen, F.J., 1991. Astronomical calibration of Gauss to Matuyama sapropels in the Mediterranean and implication for the Geomagnetic Polarity Time Scale. *Earth Planet. Sci. Lett.*, 104, 226-244.

Hunt, C.P., Moskowitz, B.M. and Banerjee, S.K., 1995. Magnetic properties of rocks and minerals, In: *A Handbook of Physical Constants*, Ahrens, T.J. (Ed.), Washington, DC, American Geophysical Union, pp. 189-204.

Iriondo, M., 1984. The Quaternary of northeastern Argentina. In: *Quaternary of South America and Antarctic Peninsula 2*, J. Rabassa (ed.), Rotterdam, A.A. Balkema, pp. 51-78.

Iversen, N. and Jørgensen, B.B., 1993. Diffusion coefficients of sulphate and methane in marine sediments: Influence of porosity. *Geochim. Cosmochim. Acta*, 57, 571-578.

Jiang, W.-T., Horng, C.-S., Roberts, A.P. and Peacor, D.R., 2001. Contradictory magnetic polarities in sediments and variable timing of neoformation of authigenic greigite. *Earth Planet. Sci. Lett.*, 193, 1-12.

Jørgensen, B.B., 1982. Mineralization of organic matter in the sea bed – the role of sulphate reduction. *Nature*, 296, 643-645.

Jørgensen, B.B., Böttcher, M.E., Lüschen, H., Neretin, L.N. and Volkov, I.I., 2004. Anaerobic methane oxidation and a deep H_2S sink generate isotopically heavy sulfides in Black Sea sediments. *Geochim. Cosmochim. Acta*, 68, 2095-2118.

Kao, S.-J., Horng, C.-S., Roberts, A.P. and Liu, K.K., 2004. Carbon-sulphur-iron relationships in sedimentary rocks from southwestern Taiwan: influence of geochemical environment on greigite and pyrrhotite formation. *Chem. Geol.*, 203, 153-168.

Karlin, R., 1990a. Magnetite diagenesis in marine sediments from the Oregon continental margin. *J. Geophys. Res.*, 95, 4405-4419.

Karlin, R., 1990b. Magnetic mineral diagenesis in suboxic sediments at Bettis site W-N, NE Pacific Ocean, *J. Geophys. Res.*, 95, 4421-4436.

Karlin, R. and Levi, S., 1983. Diagenesis of magnetic minerals in recent haemipelagic sediments. *Nature,* 303, 327-330.

Karlin, R. and Levi, S., 1985. Geochemical and sedimentological control of the magnetic properties of hemipelagic sediments. *J. Geophys. Res.*, 90, 10373-10392.

Karlin, R., Lyle, M. and Heath, G.R., 1987. Authigenic magnetite formation in suboxic marine sediments, *Nature*, 326, 490–493.

Kasten, S., Freudenthal, T., Gingele, F.X. and Schulz, H.D., 1998. Simultaneous formation of iron-rich layers at different redox boundaries in sediments of the Amazon deep-sea fan. *Geochim. Cosmochim. Acta*, 62, 2253-2264.

Kasten, S., Zabel, M., Heuer, V. and Hensen, C., 2003. Processes and signals of nonsteady-state diagenesis in deep-sea sediments and their pore waters. In: *The South Atlantic in the Late Quaternary: Reconstruction of Material Budgets and Current Systems*, Wefer, G., Mulitza, S. and Ratmeyer, V. (Eds.), Springer-Verlag, Berlin Heidelberg New York Tokyo, pp. 431-459.

Kidd, R.B., Cita, M.B. and Ryan, W.B.F., 1978. Stratigraphy of Eastern Mediterranean sapropel sequences recovered during Leg 42A and their paleoenvironmental significance. *Init. Rep. Deep-Sea Drill. Proj.*, 42, 421-443.

Klaus, A. and Lettbetter, M.T., 1988. Deep-sea sedimentary processes in the Argentine Basin revealed by high-resolution seismic records (3.5 kHz echograms). *Deep-Sea Res.*, 35, 899-917.

Kletetschka, G. and Wasilewski, P.J., 2002. Grain size limit for SD hematite. *Phys. Earth Planet. Inter.*, 129, 173-179.

Konhauser, K.O., 1998. Diversity of bacterial iron mineralization. *Earth Sci. Rev.*, 43, 91-121.

Kosterov, A.A., Perrin, M., Glen, J.M. and Coe, R.S., 1998. Paleointensity of the Earth's magnetic field in Early Cretaceous time: the Parana Basalt, Brazil, *J. Geophys. Res.*, 103, 9739-53.

Kristjansson, L., 1985. Some statistical properties of paleomagnetic directions in Icelandic lava flows, *Geophys. J. R. Astr. Soc.*, 80, 57-71.

Kruiver, P.P., Dekkers, M.J. and Heslop D., 2001. Quantification of magnetic coercivity components by the analysis of acquisition curves of isothermal remanent magnetisation. *Earth Planet. Sci. Lett.*, 189, 269-276.

Kruiver, P.P. and Passier, H.F., 2001. Coercivity analysis of magnetic phases in sapropel S1 related to variations in redox conditions, including an investigation of the S ratio. *Geochem. Geophys. Geosys.*, 2, Paper number 2001GC000181.

Lagroix, F., Banerjee, S.K. and Jackson, M.J., 2004. Magnetic properties of the Old Crow tephra: Identification of a complex iron titanium oxide mineralogy, *J. Geophys. Res.*, 109, doi:10.1029/2003JB002678.

Larrasoaña, J.C., Roberts, A.P., Stoner, J.S., Richter, C. and Wehausen, R., 2003. A new proxy for bottom-water ventilation in the eastern Mediterranean based on diagenetically controlled magnetic properties of sapropel-bearing sediments. *Palaeogeogr., Palaeoclim., Palaeoecol.*, 221-242.

Ledbetter, M.T. and Klaus, A., 1987. Influence of bottom currents on sediment texture and sea-floor morphology in the Argentine Basin. In: *Geology and Geochemistry of Abyssal Plains*. Francis, T.J.G., Weaver, P.P.E. (Eds.). Geol. Soc. London, Spec. Pub., 31, London, pp. 21-31.

Lekki, J. and Drzymala, J., 1990. Flotometric analysis of the collectorless flotation of sulphide materials, *Coll. Surfaces*, 44, 179-190.

Liu, J., Zhu, R., Roberts, A.P., Li, S. and Chang, J.-H., 2004. High-resolution analysis of early diagenetic effects on magnetic minerals in post-middle-Holocene continental shelf sediments from the Korea Strait, *J. Geophys. Res.*, 109, 1-15.

Lovley, D.R., 1991. Dissimilatory Fe(III) and Mn(IV) reduction. *Microbiol. Rev.*, 55, 259-287.

Lyle, M., 1983. The brown-green color transition in marine sediments: a marker of the Fe(III)-Fe(II) redox boundary, *Limn. Oceanogr.*, 28, 1026-1033.

Maher, B.A., 1988. Magnetic properties of some synthetic submicron magnetites. *Geophys. J.*, 94, 83-96.

Maher, B.A. and Thompson, R., 1999. *Quaternary Climates, Environments and Magnetism*, Cambridge University Press, Cambridge, 402 pp.

Manley, P.M. and Flood, R.D., 1993. Paleoflow history determined from mudwave migration: Argentine Basin, Atlantic. *Geochim. Cosmochim. Acta*, 60, 243-263.

Mann, S., Sparks, N.H.C., Frankel, R.B., Bazylinski, D.A. and Jannasch, H.W., 1990. Biomineralization of ferrimagnetic greigite (Fe_3S_4) and iron pyrite (FeS_2) in a magnetotactic bacterium, *Nature*, 343, 258-261.

Matis, K.A., Gallios, G.P. and Kydros, K.A., 1993. Separation of fines by flotation techniques, *Sep. Technol.*, 3, 76-90.

Memery, L., Arhan, M., Alvarez-Salgado, X.A., Messias, M.-J., Mercier, H., Castro, C.G. and Rios, A.F., 2000. The water masses along the western boundary of the south and equatorial Atlantic. *Progr. Oceanogr.*, 47, 69-98.

Morin, F.J., 1950. Magnetic Susceptibility of αFe_2O_3 and αFe_2O_3 with added titanium, 819-820.

Morse, J.W., 2002. Sedimentary geochemistry of the carbonate and sulphide systems and their potential influence on toxic metal bioavailability. In: *Chemistry of marine water and sediments*, Gianguzza, A., Pelizetti, E. and Sammartano, S. (Eds), Springer-Verlag, Berlin Heidelberg New York Tokyo, pp. 165-189.

Morse, J.W. and Cornwell, J.C., 1987. Analysis and distribution of iron sulphide minerals in recent anoxic marine sediments. *Mar. Chem.*, 22, 55-69.

Mullender, T.A.T., van Velzen, A.J. and Dekkers, M.J., 1993. Continuous drift correction and separate identification of ferrimagnetic and paramagnetic contributions in thermomagnetic runs. *Geophys. J. Int.*, 114, 663-672.

Nagata, T. and Akimoto, S., 1956. Magnetic properties of ferromagnetic ilmenites, *Geofis. Pura Appl.*, 34, 36-50.

Neretin, L.N., Böttcher, M.E., Jørgensen, B.B., Volkov, I.I., Lüschen, H. and Hilgenfeldt, K., 2004. Pyritization processes and greigite formation in the advancing sulfidization front in the Upper Pleistocene sediments of the Black Sea. *Geochim. Cosmochim. Acta*, 68, 2081-2093.

Niewöhner, C., Hensen, C., Kasten, S., Zabel, M. and Schulz, H.D., 1998. Deep sulphate reduction completely mediated by anaerobic methane oxidation in sediments of the upwelling area off Namibia. *Geochim. Cosmochim. Acta*, 62, 455-464.

Nolet, G.J. and Corliss, B.H., 1990. Benthic foraminiferal evidence for reduced deep-water circulation during sapropel deposition in the eastern Mediterranean. *Mar. Geol.*, 94, 109-130.

Odin, G.S. and Matter, A., 1981. De glauconiarum origine. *Sedimentology*, 28, 611-641.

Olausson, E., 1961. Studies of deep-sea cores, *Rep. Swed. Deep-Sea Exped. 1947-1948*, 8, 336-391.

Ozdemir, O., Dunlop, D.J. and Moskowitz, B.M., 1993. The effect of oxidation on the verwey transition in magnetite, *Geophys. Res. Lett.*, 20, 1671-1674.

Passier, H.F., 1998. *Sulphur geochemistry and sapropel formation, Syngenetic and diagenetic signals in eastern Mediterranean sediments*. PhD. Thesis, Utrecht University, Geologica Ultraiectina, No 158, 165 pp.

Passier, H.F., Dekkers, M.J. and de Lange, G.J., 1998. Sediment chemistry and magnetic properties in an anomalously reducing core from the eastern Mediterranean Sea. *Chem. Geol.*, 152, 287-306.

Passier, H.F., Bosch, H.J., Nijenhuis, I.A., Lourens, L.J., Böttcher, M.E., Leenders, A., Sinninghe Damste, J.S., de Lange, G.J. and de Leeuw J.W., 1999. Sulphidic Mediterranean surface waters during Pliocene sapropel formation. *Nature*, 397, 146-149.

Passier, H.F., de Lange, G.J. and Dekkers, M.J., 2001. Magnetic properties and geochemistry of the active oxidation front and the youngest sapropel in the eastern Mediterranean Sea. *Geophys. J. Int.*, 145, 604-614.

Passier, H.F. and Dekkers, M.J., 2002. Iron oxide formation in the active oxidation front above sapropel S1 in the eastern Mediterranean Sea as derived from low-temperature magnetism. *Geophys. J. Int.*, 150, 230-240.

Peate, D.W., Hawkesworth, C.J. and Mantovani, M.S.M., 1992. Chemical stratigraphy of the Paraná lavas (South America): Classification of magma and their spatial distribution, *Bull. Volcan.*, 55, 119-139.

Peck, J.A., King, J.W., Colman, S.M. and Kravchinsky, V.A., 1994. A rock-magnetic record from Lake Baikal, Siberia: evidence for Late Quaternary climate change, *Earth Planet. Sci. Lett.*, 122, 221-238.

Petersen, N., von Dobeneck, T. and Vali, H., 1986. Fossil bacterial magnetite in deep-sea sediments from the South Atlantic Ocean. *Nature*, 320, 611-615.

Peterson, R.G. and Stramma, L., 1991. Upper-level circulation in the South Atlantic Ocean. *Progr. Oceanogr.*, 26, 1-73.

Piccolo, M.C. and Perillo, G.M.E., 1999. The Argentina estuaries: A review. In: *Estuaries of South America*, Perillo, G.M.E., Piccolo, M.C. and Pino-Quivira, M. (Eds), Springer-Verlag, Berlin, Heidelberg New York Tokyo, pp. 101-132.

Postma, D. and Appelo, C.A.J., 2000. Reduction of Mn-oxides by ferrous iron in a flow system: Column experiment and reactive transport modelling. *Geochim. Cosmochim. Acta*, 64, 1237-1247.

Pruysers, P.A., de Lange, G.J., Middelburg, J.J. and Hydes, D.J., 1993. The diagenetic formation of metal-rich layers in sapropel-containing sediments in the eastern Mediterranean. *Geochim. Cosmochim. Acta*, 57, 527-536.

Pye, K., 1987. *Aeolian Dust and Dust Deposits*, Academic Press, London, 334 pp.

Pyzik, A.J. and Sommer, S.E., 1981. Sedimentary iron monosulfides: Kinetics and mechanism of formation. *Geochim. Cosmochim. Acta*, 45, 678-698.

Raiswell, R. and Canfield, D.E., 1996. Rates of reaction between silicate iron and dissolved sulfide in Peru Margin sediments. *Geochim. Cosmochim. Acta*, 60, 2777-2787.

Ravishankar, S.A., Pradip and Khosla, N.K., 1995. Selective flocculation of iron oxide from its synthetic mixtures with clays: a comparison of polyacrylic acid and starch polymers, *Int. J. Miner. Process.*, 43, 235-247.

Redfield, A.C., Ketchum, B.H. and Richards, F.A., 1963. The influence of organisms on the composition of sea-water, In: *The Sea*, Hill, M.N. (Ed), pp. 26-77.

Reitz, A., Hensen, C., Kasten, S., Funk, J.A. and de Lange, G.J., 2004. A combined geochemical and rock-magnetic investigation of a redox horizon at the last glacial/interglacial transition. *Phys. Chem. Earth*, 29, 921-931.

Richardson, M.J., Weatherly, G.L. and Gardner, W.D., 1993. Benthic storms in the Argentine Basin. *Deep-Sea Res. II*, 40, 975-987.

Rickard, D., 1997. Kinetics of pyrite formation by the H_2S oxidation of iron(II) monosulfides in aqueous solutions between 25 and 125ºC: The rate equation. *Geochim. Cosmochim. Acta*, 61, 115-134.

Rickard, D., Schoonen, M.A.A. and Luther, G.W., 1995. Chemistry of iron in sedimentary environments. In: *Geochemical transformation of sedimentary sulfur*, Vairavamurthy, M.A. and Schoonen, M.A.A. (Eds), ACS Symposium Series 612, American Chemical Society, Washington, DC, pp. 168-193.

Riedinger, N., Pfeifer, K., Kasten, S., Garming, J.F.L., Vogt, C. and Hensen, C., 2005. Diagenetic alteration of magnetic signals by anaerobic oxidation of methane related to a change in sedimentation rate. *Geochim. Cosmochim. Acta.*, 69, 4117-4126.

Roberts, A.P., 1995. Magnetic properties of sedimentary greigite (Fe_3S_4), *Earth Planet. Sci. Lett.*, 134, 227-236.

Roberts, A.P. and Turner, G.M., 1993. Diagenetic formation of ferrimagnetic iron sulphide minerals in rapidly deposited marine sediments South Island, New Zealand, *Earth Planet. Sci. Lett.*, 115, 257-273.

Roberts, A.P., Stoner, J.S. and Richter, C., 1999. Diagenetic magnetic enhancement of sapropels from the eastern Mediterranean Sea. *Mar. Geol.*, 153, 103-116.

Robertson, D.J. and France, D.E., 1994. Discrimination of remanence-carrying minerals in mixtures, using isothermal remanent magnetization acquisition curves. *Phys. Earth Planet. Inter.*, 82, 223-234.

Robinson, S.G., Sahota, J.T.S. and Oldfield, F., 2000. Early diagenesis in North Atlantic abyssal plain sediments characterised by rock-magnetic and geochemical indices. *Mar. Geol.*, 163, 77-107.

Rochette, P., Fillion, G., Mattéi, J.-L. and Dekkers, M.J., 1990. Magnetic transition at 30-34 Kelvin in pyrrhotite: insight into a widespread occurrence of this mineral in rocks, *Earth Planet. Sci. Lett.*, 98, 319-328.

Rohling, E.J. and Gieskes, W.W.C., 1989. Late quaternary changes in Mediterranean intermediate water density and formation rate, *Paleoceanography*, 4, 531-545.

Rohling, E.J. and Hilgen F.J., 1991. The eastern Mediterranean climate at times of sapropel formation: a review. *Geologie en Mijnbouw*, 70, 253-264.

Romero, O. and Hensen, C., 2002. Oceanographic control of biogenic opal and diatoms in surface sediments of the South Western Atlantic. *Mar. Geol.*, 186, 263-280.

Rossignol-Strick, 1985. Mediterranean quaternary sapropels, an immediate response of the African monsoon to variation of insolation. *Palaeogeogr., Palaeoclimat., Palaeoecol.*, 49, 237-263.

Rossignol-Strick, M., Nesteroff, W., Olive, P. and Vergnaud-Grazzini, C., 1982. After the deluge: Mediterranean stagnation and sapropel formation, *Nature*, 295, 105-110.

Rutten, A. and de Lange G.J., 2002a. A novel selective extraction of barite, and its application to eastern Mediterranean sediments. *Earth Planet. Sci. Lett.*, 198, 11-24.

Rutten, A. and de Lange, G.J., 2002b. Sequential extraction of iron, manganese and related elements in S1 sapropel sediments, eastern Mediterranean. *Palaeogeogr., Palaeoclimat., Palaeoecol.*, 190, 79-101.

Sachs S.D. and Ellwood, B.B., 1988. Controls on magnetic grain size variations and concentration in the Argentine Basin, South Atlantic Ocean. *Deep-Sea Res.*, 35, 929-942.

Sagnotti, L., Roberts, A.P., Weaver, R., Verosub, K.L., Florindo, F., Pike, C.R., Clayton, T. and Wilson, G.S., 2005. Apparent magnetic polarity reversals due to remagnetization resulting from late diagenetic growth of greigite from siderite. *Geophys. J. Int.*, 160, 89-100.

Sarmiento, J.L., Herbert, T. and Toggweiler, J.R., 1988. Mediterranean nutrient balance and episodes of anoxia, *Global Biogeochem. Cycles*, 2, 427-444.

Schippers, A. and Jørgensen, B.B., 2001. Oxidation of pyrite and iron sulphide by manganese dioxide in marine sediments. *Geochim. Cosmochim. Acta*, 65, 915-922.

Schmidt, A.M., von Dobeneck, T. and Bleil, U., 1999. Magnetic characterization of Holocene sedimentation in the South Atlantic. *Paleoceanography*, 14, 465-481.

Schneider, R., Probst, U. and Donner, B., 1991. Stratigraphie. Bericht und erste Ergebnisse der Meteor-Fahrt M16/2, Ricife-Belem 28.04-21.05.1991. Berichte, Fachbereich Geowissenschaften, Universität Bremen, 19, pp. 51-67.

References

Schoonen, M.A.A. and Barnes, H.L., 1991. Reactions forming pyrite and marcasite from solution: II. Via FeS precursors below 100ºC. *Geochim. Cosmochim. Acta*, 55, 1505-1514.

Schulz, H.D., 2000. Quantification of early diagenesis: Dissolved constituent in marine pore water. In: *Marine Geochemistry*, Schulz H.D. and Zabel M. (Eds.), Springer-Verlag, Berlin Heidelberg New York Tokyo, pp. 85-128.

Schulz, H.D., Dahmke, A., Schinzel, U., Wallmann, K. and Zabel, M., 1994. Early diagenetic processes, fluxes, and reaction rates in sediments of the South Atlantic. *Geochim. Cosmochim. Acta*, 58, 2041-2060.

Schulz, H.D., et al., 2001. *Report and preliminary results of Meteor Cruise M 46/2*. Berichte, Fachbereich Geowissenschaften, Universität Bremen, 184, 107 pp.

Schwertmann, U., 1988. Some properties of soil and synthetic iron oxides, In: *Iron in Soils and Clay Minerals*, Stucki, J.W., Goodman, B.A. and Schwertmann, U. (Eds.), Dordrecht, Reidel Publishing, pp. 203-250.

Sigl, W., Chamley, H., Fabricius, F., Giroud d'Argoud, G. and Mueller, J., 1978. Sedimentology and environmental conditions of sapropels. *Init. Rep. Deep-Sea Drill. Proj.*, 42, 445-465.

Snowball, I. and Torii, M., 1999. Incidence and significance of magnetic iron sulphides in Quaternary sediments and soil, In: *Quaternary climates, environments and magnetism*, Maher, B.A. and Thompson, R. (Eds.), Cambridge, University Press, pp. 199-230.

Stacey, F.D. and Banerjee, S.K., 1974. *The Physical Principles of Rock Magnetism.* Elsevier, Amsterdam, 95 pp.

Stevenson, F.J. and Cheng, C.-N., 1969. Amino acid levels in the Argentine Basin sediments: correlation with Quaternary climatic changes. *J. Sediment. Petrol.*, 39, 345-349.

Stoner, J.S., Channell, J.E.T. and Hillaire-Marcel, C., 1996. The magnetic signature of rapidly deposited detrital layers from the deep Labrador Sea: relationship to North Atlantic Heinrich layers. *Paleoceanography*, 11, 309-325.

Sun, Y., Clemens, S.C., An, Z. and Yu, Z., 2005. Astronomical timescale and paleoclimatic implication of stacked 3.6-Myr monsoon records from the Chinese Loess Plateau, *Quatern. Sci. Rev.*, in press.

Tamrat, E. and Ernesto, M., 1999. Magnetic fabric and rock-magnetic character of the Mesozoic flood basalts of the Parana Basin, Brazil, *J. Geodynam.*, 28, 419-37.

Tarduno, J.A. and Wilkison, S.L., 1996. Non-steady state magnetic mineral reduction, chemical lock-in, and delayed remanence acquisition in pelagic sediments. *Earth Planet. Sci. Lett.*, 144, 315-326.

Tarduno, J.A., Tain, W. and Wilkinson, S., 1998. Biogeochemical remanent magnetisation in pelagic sediments of the western equatorial Pacific Ocean. *Geophys. Res. Lett.*, 25, 3987-3990.

Tauxe, L., 1993. Sedimentary record of relative paleointensity of the geomagnetic field: theory and practice, *Rev. Geophys.*, 31, 319 - 354.

Thompson, R., Batterbee, R.W., O'Sullivan, P.E. and Oldfield, F., 1975. Magnetic susceptibility of lake sediments, *Limnol. Oceanogr.*, 20, 687-698.

Thompson, R. and Oldfield, F., 1986. *Environmental Magnetism.*, Allen and Unwin, London, 227 pp.

Thomson, J., Jarvis, I., Green, D.R.H., Green, D.A. and Clayton, T., 1998. Mobility and immobility of redox-sensitive elements in deep-sea turbidites during shallow burial. *Geochim. Cosmochim. Acta*, 62, 643-656.

Thouveny, N., de Beaulieu, J.-L., Bonifay, E., Creer, K.M., Guiot, J., Icole, M., Johnsen, S., Jouzel, J., Reille, M., Williams, T. and Williamson, D., 1994. Climate variation in Europe over the past 140 kyr deduced from rock magnetism, *Nature*, 371, 503-506.

Thunell, R.C., Williams, D.F. and Belyea, P.R., 1984. Anoxic events in the Mediterranean Sea in relation to the evolution of late Neogene climates. *Mar. Geol.*, 59, 105-134.

van Santvoort, P.J.M., de Lange, G.J., Thomson, J., Cussen, H., Wilson, T.R.S., Krom, M.D. and Ströhle, K., 1996. Active post-depositional oxidation of the most recent sapropel (S1) in sediments of the eastern Mediterranean Sea. *Geochim. Cosmochim. Acta*, 60, 4007-4024.

Vergnaud-Grazzini, C., Ryan, W.B.F. and Cita, M.B., 1977. Stable isotopic fractionation, climate change and episodic stagnation in the eastern Mediterranean during the late Quaternary**.** *Mar. Micropaleont.*, 2, 353-370.

Vogt, C., Lauterjung, J. and Fisher, R.X., 2002. Investigation of the clay fraction (<2µm) of the Clay Minerals Society reference clays. *Clays Clay Minerals*, 50, 388-400.

von Dobeneck, T., 1996. A systematic analysis of natural magnetic mineral assemblages based on modeling hysteresis loops with coercivity-related hyperbolic basis functions. *Geophys. J. Int.*, 124, 675-694.

von Dobeneck, T., Petersen, N. and Vali, H., 1987. Bakterielle magnetofossilien - Paläomagnetische und paläontologische Spuren einer ungewöhnlichen Bakteriengruppe, *Geowisschenschaften in unserer Zeit*, 5, 27-35.

Wang, Q. and Morse, J.W., 1996. Pyrite formation under conditions approximating those in anoxic sediments I. Pathway and morphology. *Mar. Chem.*, 52, 99-121.

Weissenborn, P.K., Warren, L.J. and Dunn, J.G., 1995. Selective flocculation of ultrafine iron ore. 1. Mechanism of adsorption of starch onto hematite, *Coll. Surfaces*, 99, 11-27.

Wilkin, R.T. and Barnes, H.L., 1996. Pyrite formation by reactions of iron monosulfides with dissolved inorganic and organic sulfur species. *Geochim. Cosmochim. Acta*, 60, 4167-4179.

Wilson, T.R.S., Thomson, J., Hydes, D.J., Colley, S., Culkin, F. and Sørensen, J., 1986. Oxidation fronts in pelagic sediments: Diagenetic formation of metal-rich layers. *Science*, 232, 972-975.

Wilkin, R.T. and Barnes, H.L., 1997. Formation processes of framboidal pyrite. *Geochim. Cosmochim. Acta*, 61, 323-339.

Yamazaki, T., Abdeldayem, A.L. and Ikehara, K., 2003. Rock-magnetic changes with reduction diagenesis in Japan Sea sediments and preservation of geomagnetic secular variation in inclination during the last 30,000 years. *Earth Planets Space*, 55, 327-340.

Zabel, M. and Schulz, H.D., 2001. Importance of submarine landslides for non-steady state conditions in pore water systems. *Mar. Geol.*, 176. 87-99.

References

Samenvatting

Een belangrijke bron van informatie in paleomagnetische studies van het geomagnetisch veldgedrag en in 'environmental' magnetische studies zijn sedimenten en sedimentaire gesteenten. Daar deze studies in hoge mate afhankelijk zijn van de meting van het detritisch magnetisch signaal, is verandering van dit signaal door reducerende diagenetische processen, waarbij ijzerhoudende mineralen verdwijnen en secundaire (magnetische) zwavel houdende mineralen worden gevormd, een groot gevaar met betrekking tot de betrouwbaarheid van dit soort studies. Het is daarom noodzakelijk de mogelijke aanwezigheid van diagenetische c.q. autogene magnetische fasen (b.v.b. greigiet) zo snel mogelijk te herkennen en hun eventuele invloed op het paleomagnetisch signaal vast te stellen. Een 'chemical remanent magnetisation' (CRM) als gevolg van de aanwezigheid van deze fasen, kan in sommige gevallen het detritisch magnetisch signaal overtreffen. Het moet nog worden aangetoond hoe de voornaamste detritische mineralen onder deze sterk reducerende omstandigheden kunnen overleven en door welke mechanismen secundaire (magnetische) zwavel houdende mineralen worden gevormd.

Geochemische, 'environmental' magnetische en optische methoden, of een combinatie hiervan, kunnen worden toegepast, met als doel het onderzoeken van de aanwezige magnetische mineralen in mariene sedimenten en in het ideale geval het vaststellen van de primaire of secundaire oorsprong van deze mineralen.

Het toepassen van sequentiële chemische extractie methoden van (magnetische) mineraalfasen wordt herhaaldelijk gebruikt bij het zoeken naar een antwoord op deze vraag (Hounslow and Maher, 1996; van Oorschot and Dekkers, 1999; Rutten and de Lange, 2002a; 2002b). De destructieve aard van deze methode maakt hem echter minder toepasbaar in studies, waarbij de specifieke mineraal compositie van de magnetische fractie van centraal belang is.

'Environmental' of mineraal magnetische methoden zijn niet destructief, maar evenals bij de sequentiële extractie wordt alleen het totale magnetische signaal gemeten. Ratio's van de verschillende magnetische parameters zijn wel specifiek voor onder andere magnetische korrelgrote, mineralogie en/of concentratie. Met behulp van de coercitieve kracht kunnen verschillende magnetische mineralen van elkaar worden onderscheden (Robertson and France, 1994; Kruiver *et al.*, 2001). Het vergelijken van magnetische eigenschappen van verschillende studies, waarbij verschillende criteria gebruikt werden, is echter niet verstandig.

Raster en transmissie elektronenmicroscopie wordt tevens herhaaldelijk toegepast in (magnetisch) mineralogische studies. Bij de identificatie van de mineralen is 'energy

dispersive spectroscopy' (EDS) in combinatie met REM een krachtig hulpmiddel. Om de identificatie te vereenvoudigen kunnen voorafgaand fysische scheidingstechnieken worden toegepast. Naast zware vloeistof scheiding kan magnetische mineraalextractie toegepast worden. Conventionele mineraal magnetische scheiding technieken onttrekken relatief grove magnetische deeltjes (>20μm). Daar bacterieel magnetiet in sommige gevallen significant bijdraagt aan de sedimentaire NRM, werd een nieuwe manier van extractie ontwikkeld door Petersen *et al.* (1986) and von Dobeneck *et al.* (1987).

In de manuscripten, die tijdens deze promotie zijn vervaardigd, worden met betrekking tot de wetenschappelijk gestelde vraag combinaties van de bovengenoemde methoden besproken. In de volgende paragraven wordt een samenvatting gegeven van deze manuscripten met aanvullende achtergrondinformatie van de verschillende onderzoeks-gebieden.

De verandering van de magnetische parameters in sapropel S1 sedimenten na sequentiële ijzerfase extractie, worden onderzocht in **hoofdstuk 2.1**. Sapropelen in het oostelijke Mediterrane gebied vinden hun oorsprong in een toegenomen accumulatie/preservatie van organisch materiaal (OM). Verscheidene theorieën met betrekking tot het ontstaan van deze lagen zijn door verschillende autoren voorgesteld: b.v. een verbeterde preservatie door Bradley (1938) en Olausson (1961); een tragere circulatie door Rossignol-Strick *et al.* (1982); en een omgekeerde circulatie door Calvert (1983), Sarmento *et al.* (1988) en Rohling and Gieskes (1989).

De opeenvolging van organisch rijke lagen (sapropelen) en organische arme sedimenten, resulteert in een unieke sediment samenstelling om de diagenetische wisselwerkingen te bestuderen die plaatsvindt wanneer (anoxische) organisch rijke lagen en (sub)oxische organisch arme lagen elkaar afwisselen. De meest recente sapropel (S1, 8-10 kjaar) in de oostelijke Middellandse Zee is in het laatste decennia zeer intensief onderzocht met behulp van geochemische en mineraal magnetische technieken. Met de tijd worden de sedimenten blootgesteld aan verschillende redox condities die leiden tot de formatie van diagenetische c.q. autogene magnetische mineralen. De toegepaste sequentiële ijzerfase extractie toont aan dat in de geoxideerde S1 sedimenten ijzer hoofdzakelijk aanwezig is in silicaten en 'amorphe' oxides. In de gereduceerde sedimenten daarentegen zit het ijzer hoofdzakelijk in pyriet en silicaten. Drie verschillende magnetische mineralen kunnen worden geïdentificeerd met behulp van component analyse van de 'Isothermal remanent magnetisation' (IRM) acquisitie curven. Respectievelijk worden 'detritisch' magnetiet, biogeen magnetiet en hematiet gevonden. De formatie van in-situ magnetiet, als gevolg van de activiteit van magnetotactische

bacteriën, bevestigd eerdere resultaten, dat de hoge coercitieve krachten die in sommige sedimenten vlak bij het actieve oxidatiefront gevonden worden, hoogstwaarschijnlijk van diagenetische oorsprong zijn.

Geochemische en mineraal magnetische methoden worden tevens toegepast op sedimenten van de continentale helling nabij de monding van de Rio de la Plata. In de subtropische zuid Atlantische Oceaan worden significante hoeveelheden eolisch (Patagonische vlakte) en fluviatiel (Rio de la Plata) materiaal aangevoerd. Een plausibel model voor de recente sedimentatie patronen in de westelijke zuid Atlantische Oceaan is ontwikkeld door Frenz *et al.* (2004). De sedimenten van de continentale helling kunnen gesplitst worden in twee gebieden, een grof en carbonaat arm zuidwestelijk deel en een fijner, carbonaat rijk noordoostelijk deel. De scheiding ligt bij de 'Brasil Malvinas Confluence' (BMC), die gesitueerd is voor de monding van de Rio de la het Plata. Hier treffen de noordwaarts stromende 'Malvinas current' (MC) en de naar het zuiden stromende 'Brasil current' (BC) elkaar. De sedimenten onder de BMC worden gekarakteriseerd door hoge concentraties van organische koolstof (OC), laag carbonaat gehalte en een hoge concentratie van middelgrote sediment deeltjes. De fluviatiele lading van de Rio de la Plata is in dit model duidelijk zichtbaar in de vorm van een grove zand tong. De fijne fluviatiele fractie wordt op grotere diepte noordwaarts getransporteerd.

In **hoofdstuk 2.2** worden de resultaten van geochemische analyses, die als doel hebben de diagenetische processen op drie verschillende plaatsen op de continentale helling te bestuderen, beschreven. Het voorkomen van 'anaerobic oxidation of methane' (AOM) op enkele meters diepte, is een typisch kenmerk van de sedimenten. Het proces van AOM veroorzaakt een sterk reducerende (sulfidische) omgeving en versterkt de oplossing van oxische magnetische dragers en de vorming van ijzersulfiden, hoofdzakelijk pyriet. Dit resulteert uiteindelijk in een duidelijk herkenbaar minimum in susceptibiliteit rond de 'sulphate methane transition' (SMT). Modelmatige verwerking van de geochemische gegevens toonde aan dat een drastische veranderingen in de sedimentatie snelheid nodig is om de SMT op een zekere diepte voor langere tijd te fixeren en het duidelijk zichtbare minimum in de susceptibiliteit te veroorzaken. Het wordt aangenomen dat een sterke afname zoals bij de meest recente glaciaal/interglaciaal overgang verantwoordelijk is voor de fixatie van de SMT in de onderzochte sedimenten.

De resultaten van een gedetailleerde studie van de mineraal magnetische parameters worden beschreven in **hoofdstuk 2.3**. Hier wordt geconcludeerd dat minder dan 10% van de laag coercitieve ferrimagnetische (titaan-)magnetiet fractie overblijft na blootstelling aan de sulfidische omstandigheden die de SMT omringen. Bij de ijzer redox grens, in de bovenste meter van de sedimenten, verdwijnt al ongeveer 60% van de fijnere

magnetische fractie. De hoog coercitieve mineralen (o.a. hematiet) overleven deze overgang relatief goed, echter in de sulfidische zone worden grote gedeelten (>40%) diagenetisch opgelost. Afwijkend van eerdere waarnemingen lijkt de magnetische korrelgrootte af te nemen in de sulfidische zone. Verschillende factoren kunnen aan dit resultaat bijdragen. REM analyse in combinatie met EDS heeft kleine (titaan-)magnetiet deeltjes geïdentificeerd in de sulfidische zone, welke aanwezig zijn als insluitingen in silicaten en als 'vergroeiing' met hoog Ti houdende titaanhematiet lamellen. Een andere mogelijkheid en waarschijnlijk van zeer groot belang, is de 'versplintering' van grotere (titaan-)magnetiet deeltjes als gevolg van maghemitisering. Het enige secundaire ijzersulfide mineraal geïdentificeerd door thermomagnetische analyse en REM is pyriet. Het is aanwezig in de vorm van euhedrische kristal clusters of het vervangt rechtstreeks (titaan-)magnetiet.

Magnetische eigenschappen bij lage temperaturen van de 'vergroeide' mineralen die de sterke diagenetische processen overleven, zoals beschreven in **hoofdstuk 2.3**, worden in **hoofdstuk 2.4** besproken. Het cyclisch onderzoeken van een bij kamer temperatuur geïnduceerde 'saturation isothermal remanent magnetisation' (RT-SIRM; 5 T), van de magnetische extracten, naar 5 Kelvin en terug, maakt een scherpe afname van het remanente magnetische signaal zichtbaar bij ~210 K. Hiernaast is ook de Verwey overgang duidelijk zichtbaar, welke kenmerkend is voor magnetiet. De titaanhematiet lamellen, met behulp van REM zichtbaar gemaakt, zijn hoogst waarschijnlijk het resultaat van oxidatie op hoge temperatuur ('deuteric' oxidatie) en hebben een compositie van ongeveer TH85 tot ilmenite. Beneden de 210 K wordt het mineraal titanohematiet (TH85) ferrimagnetisch, echter het magnetische moment oriënteert zich antiparallel aan het magnetische moment van de (titaan-)magnetiet, welke het remanent magnetisch signaal bij kamertemperatuur draagt. Het mechanisme dat verantwoordelijk is voor deze ogenschijnlijke magnetische zelf omkering wordt gezocht in 'magnetostatic interaction'. Dit mechanisme verklaard ook de afwezigheid van een anomalie bij het opwarmen van een bij lage temperatuur geïnduceerde SIRM (LT-SIRM; 5T) naar kamer temperatuur.

Additioneel onderzoek van de magnetische extracten met behulp van 'electron backscatter diffraction' (EBSD) wordt in **hoofdstuk 2.5** beschreven. Deze methode is in staat om de chemisch identieke maar mineralogisch verschillende fasen titaanmagnetiet en titaanhematiet van elkaar te onderscheiden. Deze methode bevestigde in de sedimenten van de continentale helling nabij de monding van de Rio de la het Plata de aanwezigheid van hoog Ti houdende titaanhematiet lamellen evenals ilmeniet en titaanmagnetiet. De toepassing van deze techniek op sedimenten en magnetische extracten is relatief nieuw, maar heeft zich zeker bewezen als het gaat om de identificatie van magnetische 'vergroeiingen'.

Kurzfassung

Sedimente und Sedimentgesteine sind aufschlußreiche Informationsträger für die Rekonstruktion sowohl des erdmagnetischen Feldes als auch von Umweltszenarien der Vergangenheit. Ein Hauptproblem bei Untersuchungen mit den Methoden der Paläo- und Umweltmagnetik ist die Trennung des primären detritischen Signals - dem in der Regel das eigentliche Interesse gilt - von Veränderungen des magnetischen Mineralinventars durch sekundären diagenetische Prozesse. Dabei werden Eisen(hydr)oxide aufgelöst und (teilweise magnetische) Sulfidminerale gebildet, was die Zuverlässigkeit von Aussagen über die ursprünglichen magnetischen Charakteristika der Ablagerungen erheblich beeinträchtigen kann. Durch eine chemische remanente Magnetisierung (CRM) neu gebildeter diagenetischer/autogener Minerale, vielfach Greigit, wird etwa die originäre detritische Remanenz (DRM) weitgehend bis völlig überlagert. Im Detail ungeklärt ist bisher aber, wie detritische Fe-Oxide trotz aggressiver Lösungsbedingungen (zum Teil) erhalten bleiben und welche Mechanismen zur Bildung der sekundären magnetischen Sulfide führen.

Mit Hilfe von geochemischen, umweltmagnetischen und optischen Analysen oder ihren Kombinationen kann ermittelt werden, welche magnetischen Minerale in marinen Ablagerungen vorliegen. Im idealen Fall läßt sich feststellen, ob sie primären oder sekundären Ursprungs sind.

Im Rahmen dieser Fragestellung wird oft das Verfahren der sequenziellen chemischen Extraktion zur Trennung der Mineralphasen herangezogen (Hounslow und Maher, 1996; van Oorschot und Dekkers, 1999; Rutten und de Lange, 2002a; 2002b). Da die Minerale dabei weitgehend zerstört werden, ist diese Technik weniger für Untersuchungen geeignet bei denen nicht der gesamte Mineralbestand, sondern spezifisch die magnetischen Mineralfraktionen von zentraler Bedeutung sind.

Umweltmagnetische Analysen sind zerstörungsfrei, jedoch wird dabei, wie bei der chemischen Extraktion, nur die pauschale Zusammensetzung einer Probe ermittelt. Das Verhältnis verschiedener magnetischer Parameter kennzeichnet zum Beispiel die mittlere magnetische Korngröße oder Anteile verschiedener Magnetominerale. Die Verteilung der Koerzitivfeldstärken ermöglicht es, magnetische Mineralkomponenten genauer zu erfassen (Robertson und France, 1994; Kruiver *et al.*, 2001). Es sei darauf hingewiesen, daß hierbei ein Vergleich von Studien, bei denen nicht identische Meßkriterien angewandt wurden, zumeist wenig sinnvoll ist.

Raster- (REM) und Transmissions- (TEM) Elektronenmikroskopie werden häufig auch zur Identifizierung von magnetischen Mineralen verwendet. Besonders erfolgreich ist die

Kombination von REM mit 'Energie dispersiver Spektroskopie (EDS)'. Anreicherungen über Schwereflüssigkeiten oder auf magnetischem Wege erleichtern diese optischen Analysen erheblich. Das konventionelle magnetische Trennungsverfahren ist nur bei einer verhältnismäßig groben Korngrößenfraktion (>20 µm) erfolgreich. Da jedoch extrem feinkörniger bakterieller Magnetit beträchtlich zur sedimentären Remanenz beitragen kann, ist von Petersen *et al.* (1986) und von Dobeneck *et al.* (1987) eine verbesserte Technik der magnetischen Extraktion entwickelt worden.

In den Manuskripten, die im Rahmen dieser Dissertation erarbeitet wurden, werden die Ergebnisse der genannten Methoden in Beziehung zu den verschiedenen wissenschaftlichen Fragestellungen diskutiert. Die folgenden Abschnitte referieren diese Studien zusammen mit zusätzlichen Hintergrundinformationen über die Arbeitsgebiete und untersuchten Sedimente.

Kapitel 2.1 behandelt die nach sequenzieller Extraktion der Eisenphasen resultierenden Veränderungen der magnetischen Parameter im Sapropel S1 aus dem östlichen Mittelmeer. Die Sapropele stehen dort in enger Beziehung zu erhöhten Akkumulations-/Erhaltungsraten organischen Materials (OM). Verschiedene Autoren haben hierfür alternative Ursachen postuliert: Bradley (1938) und Olausson (1961) eine verbesserte Erhaltung, Rossignol-Strick *et al.* (1982) eine reduzierte Zirkulation und Calvert (1983), Sarmento *et al.* (1988) sowie Rohling und Gieskes (1989) eine Zirkulationsumkehr.

Die Abfolge von organisch reichen Horizonten (Sapropele) und Schichten mit geringen organischen Anteilen führt zu der ungewöhnlichen Situation, diagenetische Wechselwirkungen von anoxischen und (sub-)oxischen Lagen untersuchen zu können. Der jüngste Sapropel (S1, 8-10·10^3 Jahre) im östlichen Mittelmeer ist im letzten Jahrzehnt intensiv mit geochemischen und mineral-magnetischen Verfahren untersucht worden. Unterschiedliche Redox-Bedingungen im Verlauf der Ablagerung haben zur Bildung authigener magnetischer Phasen im oxischen und auch anoxischen Milieu geführt. Die sequenzielle Extraktion der Eisenphasen ergab, daß in den oxidierten S1 Sedimenten Eisen hauptsächlich in Silikaten und in 'amorphen' Oxiden gebunden ist, während in den anoxischen Lagen Pyrit neben Silikaten dominiert. Die Komponentenanalyse der isothermalen remanenten Magnetisierung (IRM) konnte drei Minerale identifizieren, 'detritischen' Magnetit, biogenen Magnetit und Hämatit. Die '*in situ*' Bildung von Magnetit spricht für die Aktivität von magnetotaktischen Bakterien. Damit sind Ergebnisse früherer Untersuchungen bestätigt, die eine hohe Koerzivität in den Sedimenten nahe der Oxidationsfront mit diagenetischen Prozessen erklärten.

Umfangreiche geochemische und mineralmagnetische Untersuchungen wurden auch an Sedimentkernen vom südamerikanischen Kontinentalhang vor der Rio de la Plata Mündung durchgeführt. In den südwestlichen subtropischen Südatlantik werden aeolisch große Mengen von Staub aus Patagonien sowie fluviatil die Schwebfracht des Rio de la Plata und zahlreicher kleinerer Flüsse eingetragen. Ein Modell der sich daraus bildenden Sedimentationsmuster ist von Frenz *et al.* (2004) entwickelt worden. Am Kontinentalhang können demnach zwei Gebiete unterschieden werden: grobkörnige und karbonatarme Sedimente im südwestlichen Teil und feinkörnige und karbonatreiche Ablagerungen im Nordosten. Die Grenze markiert die 'Brasil Malvinas Confluence (BMC)', wo der nordwärts fließende 'Malvinas Current' (MC) in der Nähe der Rio de la Plata Mündung auf den südwärts gerichteten 'Brazil Current (BC)' trifft. Im Bereich der BMC sind die Sedimente durch hohe Konzentrationen organischen Kohlenstoffs, niedrige Karbonatgehalte und eine dominierende Siltfraktion charakterisiert. Die Flußfracht des Rio de la Plata ist deutlich an grobkörnigen Sanden erkennbar, die sich auf dem Kontinentalabhang abgelagert haben, während der feinkörnige Anteil nordwärts in größere Tiefen transportiert wird.

Die gewonnenen geochemischen und mineralmagnetischen Ergebnisse werden in **Kapitel 2.2** diskutiert. Mit dem Ziel diagenetische Prozesse zu studieren, wurden drei Kernstationen auf dem Kontinentalhang ausgewählt, wo in wenigen Metern Tiefe die Zone der 'anaerobic oxidation of methane' (AOM) erreicht wird, typisch für die Sedimente vor der Rio de la Plata Mündung. Die AOM verursacht ein stark reduzierendes (sulfidisches) Milieu mit intensiver Lösung von oxidischen magnetischen Mineralen und der Bildung von Eisensulfiden, hauptsächlich von Pyrit. Infolgedessen resultiert ein charakteristisches Minimum der magnetischen Suszeptibilität im Bereich der 'sulphate methane transition (SMT)'. Die numerische Modellierung der geochemischen Daten hat gezeigt, daß ausgeprägte Änderungen der Sedimentationsraten notwendig sind, um die SMT in einer bestimmten Tiefe für längere Zeitspannen stationär zu halten und damit das beobachtete Minimum der Suszeptibilität zu erzeugen. Es wird angenommen, daß in den untersuchten Sedimenten die drastische Abnahme der Sedimentationsrate am letzten Wechsel von glazialen zu interglazialen Bedingungen verantwortlich ist für die Fixierung der SMT.

In **Kapitel 2.3** sind Ergebnisse detaillierterer mineralmagnetischen Untersuchungen dargestellt. Weniger als 10% der niedrig koerzitiven ferrimagnetischen (Titano-) Magnetitkomponente bleibt am Übergang zum sulfidischen Milieu erhalten. Ungefähr 60% dieser Fraktion wird bereits an der Eisen-Redox-Grenze im obersten Meter der sedimentären Sequenz aufgelöst. Die hoch koerzitiven Minerale sind dort verhältnismäßig weniger beeinflußt, werden jedoch im sulfidischen Bereich in großem Umfang (>40%) diagenetisch zerstört. Im Gegensatz zu vielen Beobachtungen an der Eisen-Redox-Grenze nimmt die magnetische Korngröße in der sulfidische Zone ab. Verschiedene Faktoren können dazu

beitragen. Anhand von REM- in Kombination mit EDS-Analysen wurde feinkörniger (Titano-)Magnetit auch in der sulfidischen Zone identifiziert, entweder gut erhalten in einer silikatischen Matrix oder als Relikt innerhalb der Lamellenstruktur von Titanohämatiten mit hohen Titangehalten. Eine andere Möglichkeit, die wahrscheinlich größere Bedeutung hat, ist die weitgehende Zergliederung größerer Minerale im Laufe der Maghemitisierung. Das einzige sekundäre Eisensulfidmineral, das mit thermomagnetischen Messungen und SEM bestimmt werden konnte, ist Pyrit in Agglomeraten euhedrischer Kristalle oder direkt (Titano-)Magnetit ersetzend.

Tieftemperaturmessungen an den nach zweistufiger Diagenese noch verbliebenen magnetischen Mineralen werden in **Kapitel 2.4** diskutiert. Eine bei Raumtemperatur im Feld von 5 Tesla magnetischen Extrakten aufgeprägte 'saturation isothermal remanent magnetization' (RT-SIRM; 5 T) nimmt während der Abkühlung im Temperaturintervall um etwa 210 K sehr stark ab. Daneben konnte auch der für Magnetit spezifische Verwey-Übergang bei etwa 110 K nachgewesen werden. Die in den REM Analysen identifizierten Titanohämatite haben Ilmenitanteile von 85 bis nahezu 100%. Ihre Lamellenstruktur ist durch Hochtemperaturoxidation ('deuteric oxidation') vulkanogen in den ursprünglichen Laven entstanden. Bei Raumtemperatur sind Titanohämatite dieser Zusammensetzung paramagnetisch, sie werden unterhalb von Curie Temperaturen um 210 K und weniger ferrimagnetisch. Ihr sich dann bildendes magnetisches Moment ist antiparallel orientiert zum magnetischen Moment der mit ihnen verwachsenen (Titano-)Magnetite, die Träger der Remanenz bei Raumtemperatur sind. Als Mechanismus, der für diese partielle magnetische Selbstumkehrung verantwortlich ist, wird eine relativ schwache 'magneto-static interaction' postuliert. Dies würde auch erklären, daß keine analoge Anomalie während der Erwärmung von Remanenzen beobachtet wird, die bei tiefen Temperaturen (5 K) aufgeprägt wurden (LT-SIRM, 5 T).

Kapitel 2.5 faßt knapp weitere mittels 'Electron Backscatter Diffraction (EBSD)' an magnetischen Extrakten durchgeführte Untersuchungen zusammen. Die EBSD Methode erlaubt es, chemisch identische mineralogisch aber verschiedene Phasen von Titano-magnetit und Titanhämatit zu unterscheiden. In den Sedimenten vom südamerikanischen Kontinentalrand konnte so neben Titanohämatit mit hohen Titangehalten verbreitet auch Ilmenit und Titanomagnetit bestätigt werden. Die Anwendung von EBSD auf Sedimente und auf magnetische Extrakte ist neu und hat sich vor allem bei der Analyse von magnetischen Verwachsungen als erfolgreich erwiesen.

Acknowledgements

A special thanks goes to Prof. Dr. Georg Irion and his family for supporting me during my promotion and providing a second home in Germany. The 'expedition' to the Amazon in 2005 was an unforgettable experience.

A personal thanks goes to my friends in Bremen for their motivation and support and the countless evenings spent actively and afterwards eating 'käsekuchen' or burgers, or just enjoying the good life.

Last but not least I want to give a big thank you to my family for constantly supporting me and for just being there.

Curriculum Vitae

Johanna Fredrika Lukina Garming was born on May 1, 1977 in Emmen, the Netherlands. In 1989 she started her secondary education at the 'Gemeentelijke Scholen Gemeenschap' in Emmen. After receiving her 'V.W.O.' diploma in 1995, she started in the same year with the study Chemistry/Biology (Hogere Laboratorium Opleiding) in Emmen. After receiving her first year's certificate in 1996, she changed to the study of Biotechnology at the 'Noordelijke Hogeschool Leeuwarden'. In 1999 she received her Bachelor's degree in Environmental Biotechnology (Milieubiotechnologie). In same year she started the short program of Environmental Geochemistry (Milieugeochemie) at the University of Utrecht. This study was successfully completed in 2001 with a degree (Marine Geochemistry).

From November 2001 until January 2005 she worked as a PhD student at the marine geophysics department of the University of Bremen, in the European Graduate College 'Proxies in Earth History' (EUROPROX), funded by the NWO (Nederlandse Organisatie voor Wetenschappelijk Onderzoek) and the DFG (Deutsche Forschungs Gemeinschaft). She completed and defended her thesis in 2006.